STREAMLINE TRACING AND SENSITIVITY CALCULATION IN FRACTURED RESERVOIR WITH COMPLEX GEOMETRY: FIELD APPLICATION TO HISTORY MATCHING AND FLOOD OPTIMIZATION

A Dissertation

by

HONGQUAN CHEN

Submitted to the Office of Graduate and Professional Studies of
Texas A&M University
in partial fulfillment of the requirements for the degree of

DOCTOR OF PHILOSOPHY

Chair of Committee,	Akhil Datta-Gupta
Committee Members,	Michael J. King
	Eduardo Gildin
	Debjyoti Banerjee
Head of Department,	Jeff Spath

December 2018

Major Subject: Petroleum Engineering

ABSTRACT

The popularity of streamline application mainly depends on two aspects: efficient tracing algorithm to generate streamline, and effective flow and transport analysis along streamline. Previous studies proved its applicability for conventional resources such as waterflood in single and dual porosity models. Streamline technology has limited success in extension to fractured reservoir with discrete fracture networks due to lack of efficient tracing method in the complex porous media geometry. Streamline based application such as history matching and rate optimization also has limitation to gas reservoir depletion or fractured reservoir waterflood due to lack of effective streamline-based flow and transport analysis for highly compressible fluid and highly contrasted porous media.

In this study, we first develop streamline tracing method in complex geometry such as faults and discrete fractures. The discrete fractures here are depicted by embedded discrete fracture model (EDFM). We are going to propose novel methods to construct boundary layers for fault non-neighbor connections and EDFM non-neighbor connections. The novel methods reduce the treatment of complex grid geometry to a minimum level and honor the flux of each connection. The utility and validity of this proposed approach is demonstrated using both 2D and 3D examples.

Second, we propose an amended streamline-based travel time sensitivity formulation. This novel sensitivity formulation has improved accuracy than the legacy one when compared to numerical perturbed sensitivity, thus results in faster data misfit reduction. We also develop general streamline-based bottom hole pressure sensitivity

calculation method suitable for highly compressible fluids or complex geometry caused by non-neighbor connections. The bottom hole pressure sensitivity calculation is validated by a successful history matching application to a high pressure high temperature gas reservoir.

Finally, we develop a rate allocation optimization method based on fast estimation of oil recovery, which also applies to fractured reservoirs. The oil recovery is estimated along streamline within the drainage volume by the end of optimization period. The injection/production rates are updated to maximize the field oil recovery. The novel optimization method results in better performance than equalizing well pair injection efficiency or equalizing well pair time of flight when applying to a waterflood case in fractured reservoir. Its validation is further established by the waterflood optimization application to a field scale EDFM reservoir.

We concluded that our proposed approach of streamline tracing, inversion and optimization algorithm extends streamline technology application to fractured media represented by discrete fracture networks and highly compressible fluid, leading to a highly effective reservoir management tool.

ACKNOWLEDGEMENTS

I would like to express my sincere gratitude to my committee chair, Dr. Datta-Gupta for his academic guidance and financial support throughout the course of this research. I would also like to extend my sincere appreciation to Dr. King, for the kind advice to advance and improve my research. I would also like to extend my appreciation to Dr. Gildin, and Dr. Banerjee for their thoughtful discussions and suggestions that improved the contents of this dissertation.

Thanks also go to MCERI alumni and current students for their mentorship, partnership and friendship throughout my study life.

Finally, thanks to my family for their support.

CONTRIBUTORS AND FUNDING SOURCES

Contributors

This work was supported by a dissertation committee consisting of Professor Akhil Datta-Gupta [advisor], Michael J. King, and Eduardo Gildin of the Harold Vance Department of Petroleum Engineering, and Professor Debjyoti Banerjee of the Department of Mechanical Engineering.

The validation of the novel streamline tracing method depicted in Chapter II were conducted in part by Tsubasa Onishi and Feyisayo Olalotiti-Lawal of the Department of Petroleum Engineering and were published in 2018.

All other work conducted for the dissertation was completed by the student independently.

Funding Sources

Graduate study was supported by the Research Assistantship funded by the research project under Dr. Datta-Gupta from Texas A&M University.

TABLE OF CONTENTS

Page

LIST OF FIGURES

Page

LIST OF TABLES

Page

CHAPTER I

INTRODUCTION AND STUDY OBJECTIVES

Streamline technology has achieved remarkable success in conventional reservoirs including flow visualization, model calibration and optimization. In this chapter, we will discuss current streamline technology, how we can improve it, and most importantly, how we can extend its application to the unconventional resource such as fractured reservoirs or tight oil and tight gas.

1.1 Statement of the Problem and Challenges

Recently, unconventional resources, such as fractured reservoirs, tight oil and tight gas, have become more and more important in the oil and gas industry. They have also placed several challenges in the area of academic research and study, including flow diagnostics in fractured reservoirs, history matching for gas reservoirs, and well rate allocation optimization in fractured reservoirs.

Streamline tracing is the starting point of any streamline application. It is usually limited to structured grids especially in the field-scale applications. The rock media becomes much more complex due to the common existence of natural and hydraulic fractures and faults, which make the grid geometry highly unstructured and grid property highly contrasted. Streamline tracing relies on an interpretation of a continuum velocity field, which is not easy in such an unstructured grid for a fractured reservoir. The velocity interpretation in unstructured grid has been studied by several authors, mainly focusing on triangular grids (Cordes and Kinzelbach 1992; Pr´evost et al. 2002; E. Jimenez, M. J. King,

and A. Datta-Gupta 2008) and PEBI grids (Y. Zhang, M. J. King, and A. Datta-Gupta 2012). The solution was applied to some synthetic fractured reservoirs depicted by triangular girds (Hægland 2009). However, the study still remains in 2D and lacks 3D field-scale applications due to the complexity in building unstructured grids and significant computation cost of flow simulation and velocity interpretation in unstructured grids.

Geological model calibration is also commonly known as history matching. Over decades, various methods have been developed, mainly categorized in gradient and non-gradient (derivative-free) methods. Streamline-based method is one of the gradient methods which has been successfully applied to history matching dynamic data of individual wells, such as water cut and flowing bottom hole pressure (Rey et al. 2009; Hohl et al. 2006; Cheng et al. 2004; S. Tanaka and D. Kam 2014). This approach has many advantages in terms of computational efficiency and applicability (Datta-Gupta and King 2007). In order to improve the performance of streamline-based history matching, the nonlinearities of different variations of streamline-based methods have been discussed and tested (H. Cheng, A. Datta-Gupta, and Z. He 2005). For the same purpose, the improvement of streamline-based sensitivity is another aspect requiring further study. Tight oil or tight gas is usually developed by multi-fractured horizontal wells, and its recovery mainly relies on depletion of fluid energy rather than fluid displacement. Previous streamline-based history matching applications are mainly applied to waterflood cases. A novel derivation and implementation of streamline-based sensitivity is needed to extend streamline based history matching to a reservoir mainly developed by depletion.

The allocation optimization of the flow rate of the injector and producer is another important application of streamline technology. A streamline-based rate optimization usually balances the time of flight or injection efficiency between different injector-producer pairs. They normally perform well in conventional resources. However, both approaches have application restrictions: injection efficiency optimization is valid after water breakthrough, and time of flight equalization is valid before water breakthrough. In addition, the rate allocation optimization is far more challenging in a fractured reservoir with highly contrasted grid properties. The well connections in a fractured reservoir could be far more complicated. Any producer can be connected to any injector by a highway network of fractures regardless of the distance between two wells. What's more, the water break through time and injection efficiency mainly reflect the oil recovery along fractures but ignore the resources remaining in the matrix. Such balancing strategy might lead to quite limited oil recovery improvements. A more general streamline based optimization algorithm is needed to apply to the fractured reservoirs at any time in the life of the reservoir.

1.2 Study Objective and Thesis Outline

This research focuses on a robust implementation of a streamline software to improve the efficiency and effectiveness of streamline applications and to extend streamline-based technology to unconventional resources. Main objectives and corresponding chapters of this dissertation are as follows.

- Chapter II: *Development of novel streamline tracing workflow in fractured reservoir with complex geometry*. In this chapter, a boundary layer method will be developed to trace streamlines in embedded discrete fracture models with faults. Fractured reservoir flow visualizations will then be generated both in 2D and 3D cases.
- Chapter III: *Amended streamline-based sensitivity calculation and field application*. In this chapter, an amended streamline-based travel time sensitivity will be proposed for a better water cut history matching performance, the streamline-based bottom hole pressure sensitivity will be extended to gas reservoir depletion, and the novel bottom hole pressure sensitivity will be applied to a history matching field application of high pressure high temperature tight gas reservoir.
- Chapter IV: *Rate allocation optimization in fractured reservoirs based on fast estimation of oil recovery*. The proposed approach is demonstrated using a synthetic embedded discrete fracture model. The results are compared with the optimization cases by equalizing injection efficiency and equalizing time of flight. A field-scale application is performed to further test the novel method.
- Chapter V: *Conclusions and future work.*

1.3 Software Prototype

The primary product of this work will be a software prototype called "DESTINY" for streamline tracing, streamline-based history matching, and well rate allocation optimization. All of the proposed methods are implemented in this software. The applications in this dissertation have been carried out using DESTINY (Appendix A).

CHAPTER II

DEVELOPMENT OF NOVEL STREAMLINE TRACING WORKFLOW IN FRACTURED RESERVOIR WITH COMPLEX GEOMETRY*

2.1 Chapter Summary

Unstructured grids are commonly used for modeling fractured reservoirs, and multiple streamline tracing methods have been developed for unstructured grids. However, the construction of unstructured grids is much more complex than structured grids such as shoe-box type and corner point grids. And the corresponding streamline tracing algorithms are also more tedious and less efficient than the regular ones. Recent research proposed an embedded discrete fracture models (EDFM) for modeling the complex geometries of fractured reservoirs. Due to its simplicity and efficiency, it has gained popularity. EDFM uses non-neighbor connections to embed discrete fracture grids into the matrix grid, and can be simply realized in most of the commercial simulators by the user specifying grid geometry and non-neighbor connections in the input deck, and there is no need for a simulator developer to hard code additional modules. What's more, in most situations the connections through faults are also constructed by non-neighbor connections. Thus the development of general streamline tracing method through non-

* Part of data reported in this chapter is reprinted with permission from "Streamline Tracing and Applications in Naturally Fractured Reservoirs Using Embedded Discrete Fracture Models" by Chen, H., Onishi, T., Olalotiti-Lawal, Feyisayo, and Datta-Gupta, A. 2018, Paper SPE-191475-MS Presented at the SPE Annual Technical Conference and Exhibition 2018, 24-26 September, Dallas, Texas, U.S.A. Copyright 2018 Society of petroleum Engineers

neighbor connections will greatly push forward the streamline applications in faulted and fractured reservoirs.

For a faulted and fractured reservoir characterized by an embedded discrete fracture model, each face of a cell may be connected to two or more cells, and the velocity across faces of a cell is unevenly distributed and not clear according to the non-neighbor fluxes. In contrast, the standard flux based streamline tracing method (Pollock's scheme) assumes that the flux is evenly distributed on cell faces and thus giving a clear velocity field. To trace streamlines in faulted reservoirs with non-neighbor connections, a boundary layer method (E. Jimenez, M. J. King, and A. Datta-Gupta 2008) was previously proposed to interpret the velocity field of non-neighbor fluxes. This method constructs boundary layers via local grid refinement, and solves flux between local refined cells by mass balance equations with non-neighbor connection fluxes as boundary conditions. However, local grid refinement requires tedious grid subdivision and is hard to generalize to 3D case, especially for embedded discrete fracture model. What's more, local grid refinement method is geometry-based and cannot deal with non-neighbor connections whose connected cells are not physically contacted.

In this chapter, we are going to propose novel methods to construct boundary layers for fault non-neighbor connections and discrete fracture non-neighbor connections. The novel methods construct boundary layers as extended grids on cell faces, reduce the treatment of complex grid geometry to a minimum extent, and honor the fluxes distributions in space. This method is flux-based and can deal with arbitrary fault geometry

or fracture geometry. The utility and validity of this proposed approach is demonstrated using both 2D and 3D examples.

2.2 Introduction of Streamline Tracing and Embedded Discrete Fractured Model

The streamline-based methods have been recognized for their effectiveness for subsurface fluid flow imaging and flow diagnostics through variety of field-scale applications (Datta-Gupta and King 2007; Yin et al. 2010; Bhark et al. 2011; Kam and Datta-Gupta 2016; Olalotiti et al. 2017; Hetz et al. 2017). Based on the flow paths denoted by streamlines in classical finite volume models, further applications can be done in rapid screening and ranking 3D reservoir models (Idrobo et al. 2000; Ates et al. 2005) and in fast flow simulations, which account for realistic flow physics including gravity, capillary pressure, compressibility, and multicomponent phase behavior (Bratvedt et al. 1996; Blunt et al. 1996; Jessen and Orr 2002; Chen et al., 2006; Osako and Datta-Gupta 2007; Tanaka et al. 2013). A streamline is defined as the instantaneous curve in space along which every point is tangent to the local velocity vector. Tracing streamlines from injectors to producers is based on the analytical description of a streamline path within a grid-block as outlined by Pollock (1988). The underlying assumption is that the velocity of fluid particals in each coordinate direction varies linearly and is independent of the velocities in the other directions. The Pollock's method is attractive because it is analytical and consistent with the governing material balance equation. Although original Pollock's equation are assuming orthogonal grid blocks, it can be extended into general corner point grids (Cordes and Kinzelbach 1992, Prevost, Edwards, and Blunt 2002).

Modeling of fractured media has been an active area of research as a response to the significant hydrocarbon reserves in naturally fractured reservoirs (NFRs) (Allan and Sun 2003). Development of NFRs, however, poses certain challenges arising from

complex fracture networks and inherent uncertainties in their structures. One practical implication of this challenge is premature water or gas breakthrough and consequently, poor secondary or tertiary recovery performance (Gilman 2003). It is therefore important to perform careful reservoir management and uncertainty assessment in NFRs. For NFRs, current streamline models are well suited for dual porosity single permeability (DPSP) systems because streamlines need to be traced only for the fracture system. Several authors have presented streamline-based simulation and applications in DPSP systems (Di Donato and Blunt 2003; Al-Huthali and Datta-Gupta 2004; Myasnikov et al. 2006). However, for dual porosity dual permeability (DPDP) systems, the assumptions underlying the DPSP construction are no longer hold. In fact, since the matrix contributes to both flow and storage in DPDP systems, streamlines need to be traced for both fracture and matrix systems. As shown in prior attempts made at solving the problem, an aberration of appearing and disappearing streamlines in both fracture and matrix media can be noticed especially as the two media closely interact. As a result, the streamline model does not only loses its visual appeal, the model also easily becomes intractable, especially with high concentration of wells.

In this paper, we present a robust streamline tracing framework for use in the DPDP models via an Embedded Discrete Fracture Model (EDFM) framework. In EDFM models, the reservoir grid system is used to represent the matrix domain, while dominant fractures are explicitly described within the matrix domain as 2D planes with specific 3D orientation. Matrix-fracture interactions are described by a local flow assumption with appropriate transmissibility (Li and Lee 2008; Moinfar et al. 2014) which typically

employs non-neighbor connections (NNCs) in the implementation. With the explicit fracture representations and regular finite volume grids for the matrix domain, EDFM models can overcome drawbacks of the dual continuum models (Warren and Root 1963; Kazemi, et al. 1976; Blaskovich et al. 1983) and also can mitigate the gridding challenges in unstructured discrete fracture models (Noorishad and Mehran, 1982; Karimi-Fard and Firoozabadi 2001; Monteagudo and Firoozabadi, 2004; Mallison et al. 2010; Hyman et al. 2015). EDFM is currently recognized as a promising alternative to classical fracture modeling approaches in subsurface models. Many extensions and applications of EDFM models are available (e.g., Fumagalli et al. 2016; Tene et al. 2017; Du et al. 2017; Hui et al. 2018; Chai et al. 2018), however, these are beyond the scope of this paper.

Accurate streamline tracing and time-of-flight (TOF) calculations play a significant role in streamline-based methods. The linear velocity interpolation model (Pollock 1988) is by far the most commonly used in current streamline based methods. While Pollock's algorithm is suitable for Cartesian grid systems, special treatments are required to account for the complex grid systems in EDFM models associated with fractures and NNCs. Also, modern reservoir models routinely employ a much richer set of grid systems. Consequently, extensions of streamline tracing to irregular grid systems have been introduced (e.g., Prevost et al. 2002; Jimenez et al. 2008, 2010; Rasmussen 2010. In our approach, we generalize our previously proposed streamline tracing algorithms for local grid refinements (LGR) and faulted systems with NNCs (Jimenez et al. 2010) to discrete fracture network models where a fracture grid block in EDFM is treated as a boundary layer for flux continuity and streamline tracing. Our strategy is based

on a boundary layer method that can be used to honor the fluxes at the matrix-fracture interface during streamline tracing. A simple and powerful streamline tracing framework allows our approach to be coupled with existing reservoir simulators and used in field scale reservoir models.

It is worth mentioning that Shahvali et al. (2012) and Moyner et al. (2015) introduced an alternative flow diagnostics approach in which the steady-state transport equations for a neutral tracer and TOF are solved in finite-volume framework. Their framework can be used in any grid systems without tracing streamline. We will discuss comparisons between our streamline based method and the grid based method in the following sections.

This chapter is organized as follows. First we provide a description of the boundary layer method that has been implemented in our streamline tracing framework (Fig. 2.1) as a post processing tool for a commercial simulator. The implementation is validated by comparing streamline trajectories, TOF and tracer responses with a semi analytical solution based on complex variable boundary element method (CVBEM) (Sato and Abbaszadeh 1994; Nakashima et al. 2000). Then we will present applications of our approach to flow diagnostics and rate allocation optimization with a series of numerical examples encompassing different levels of geologic and geometrical complexity to illustrate the robustness of the approach. Finally, we will give summary and conclusions.

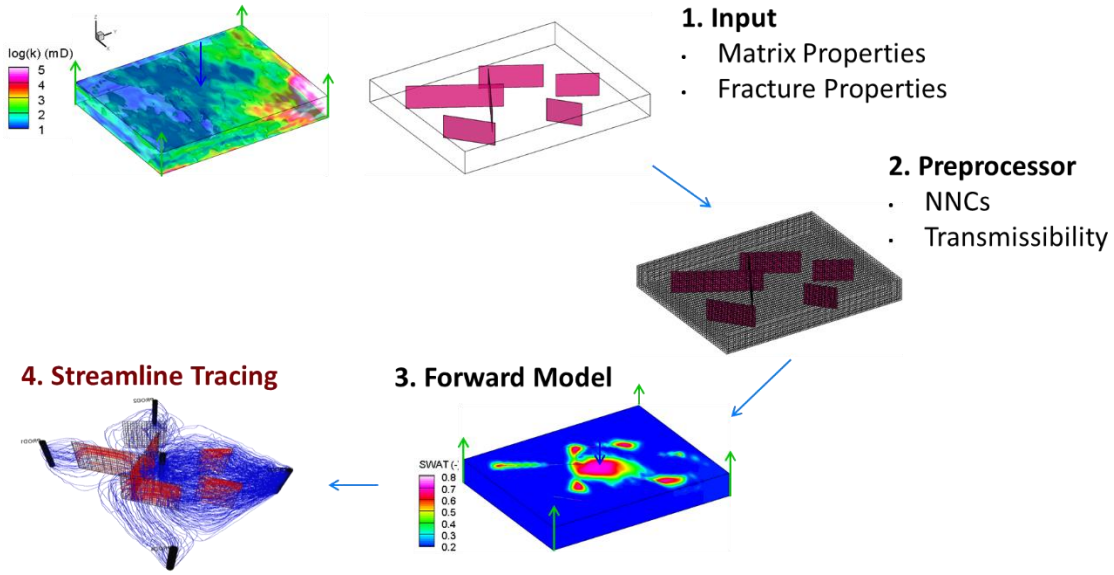

Figure 2.1: Streamline tracing framework via EDFM

2.3 Methodology

Our strategy is based on a boundary layer method that can be used to honor the fluxes at the matrix-fracture interface during streamline tracing. In the EDFM framework, multiple fracture grid blocks may exist within a matrix grid block and thus the subdivisions and local flux calculations can be intractable and challenging to generalize for field scale applications. In this session, we present an efficient method to construct boundary layers for the EDFM framework whereby the treatment of irregular grid system is simplified while honoring the flux continuity at each connection.

2.3.1 Background: Streamline Trajectories and Time of Flight Formulation

Streamline trajectories calculation by Pollock method relies on the calculation of time of flight. Time of flight is a term which refers to the transit time of a neutral tracer under the influence of a defined velocity field (Datta-Gupta and King, 2007). The time of flight τ along an arbitrary flow path or streamline ξ defined by Darcy velocity $u(\xi)$ can be mathematically expressed as:

$$\tau = \int_{\xi} \frac{\phi(\xi) d\xi}{u(\xi)} \tag{2.1}$$

In the calculation of streamline trajectories and time of flight by Pollock method, each grid block is rectangular cell, and the transit time form an initial point in space is built up one cell at a time and single uniform velocity is applied to each face. This approach is generalized for corner point grids by Cordes and Kinzelbach (1992), and

further simplified by Jimenez et al. (2007) by introducing a pseudo time of flight T in corner point grids,

$$dT = \frac{1}{\phi}\frac{d\tau}{J(\alpha,\beta,\gamma)} = \frac{d\alpha}{Q_1(\alpha)} = \frac{d\beta}{Q_2(\beta)} = \frac{d\gamma}{Q_3(\gamma)} \tag{2.2}$$

Where τ is the time of flight, (α,β,γ) are unit space coordinates, J is Jacobian matrix of isoparametric mapping from physical space (x,y,z) to unit space(α,β,γ), and $Q_1(\alpha)$, $Q_2(\beta)$, $Q_3(\gamma)$ are the fluxes along three directions.

These sets of equations can be independently integrated along each direction. The integral solution of the exit pseudo time in α direction is

$$\Delta T_\alpha = \int_{\alpha_0}^{\alpha=1} \frac{d\alpha}{Q_1(\alpha)} = \int_{\alpha_0}^{\alpha=1} \frac{d\alpha}{a_1 + c_1\alpha} = \frac{1}{c} ln\left[\frac{a_1 + c_1}{a_1 + c_1\alpha_0}\right] \tag{2.3}$$

Where a_1 is flux on left face ($\alpha = 0$) of cell, c_1 is the flux gradient in α direction.

Similar solution will also apply in β and γ directions. The final pseudo time of flight at the exit point of cell is given by minimum positive value among the exit pseudo times in all three directions,

$$\Delta T = Min\ Positive\{\Delta T_\alpha, \Delta T_\beta, \Delta T_\gamma\} \tag{2.4}$$

After the exit time is determined inside the cell, the exit point coordinates can be easily calculated. The α coordinate of the exit point is

$$\alpha_e = \alpha_0 + (a_1 + c_1\alpha_0)\left(\frac{e^{c_1\Delta T} - 1}{c_1}\right) \tag{2.5}$$

Similar solution also apply along β and γ directions. Knowing the unit space coordinates of the exit point, the corresponding physical space coordinates can be obtained via trilinear interpolation. A complete streamline trajectory is obtained by repeating this

single cell tracing procedure cell by cell until a termination point is met, such as a well cell, stagnation point, and so on.

2.3.2 Problem Description and General Tracing Steps for NNC

The faulted and fractured reservoir via EDFM has two kinds of non-neighbor connections: fault non-neighbor connections and discrete fracture non-neighbor connections.

Let's consider a scenario for fault in Fig. 2.2 involving a single matrix cell (Cell A), with another three matrix cells (Cell B, Cell C, and Cell D). The connections between Cell A and Cell B or Cell D are described by Non-Neighbor Connections (NNCs), and the connections between Cell A and Cell C are described by Natural Ordering Connection (NOC). Flux Q_{AB}, Q_{AC} , Q_{AD} quantifies the connection strength between matrix Cell A and Cell B, Cell C, and Cell D.

Let's consider another scenario for discrete fractures in Fig. 2.3 involving a single matrix cell (Cell A), with two fracture cells (Cell B and Cell C) embedded in it. The connections between these three cells are described by Non-Neighbor Connections (NNCs), so that flux Q_{AB} quantifies the connection strength between matrix Cell A and fracture Cell B, Q_{AC} between matrix Cell A and fracture Cell C, and Q_{BC} between fracture Cell B and fracture Cell C.

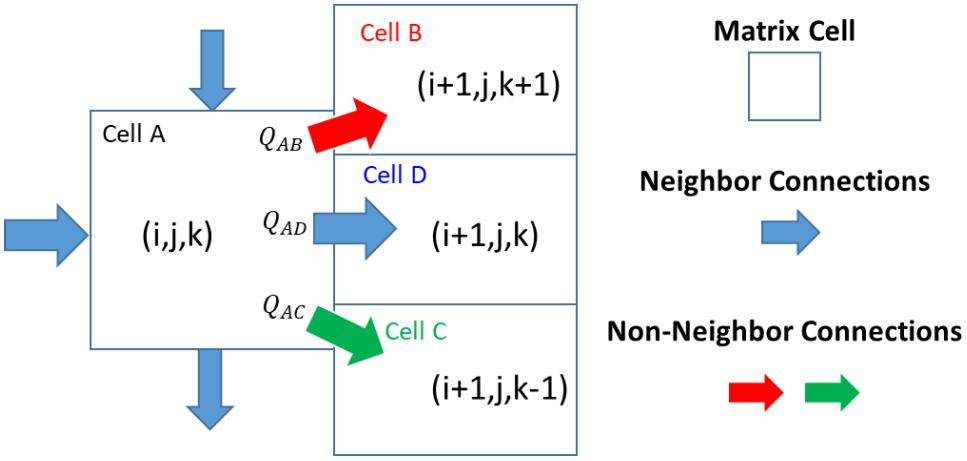

Figure 2.2: Matrix-matrix interaction (fault)

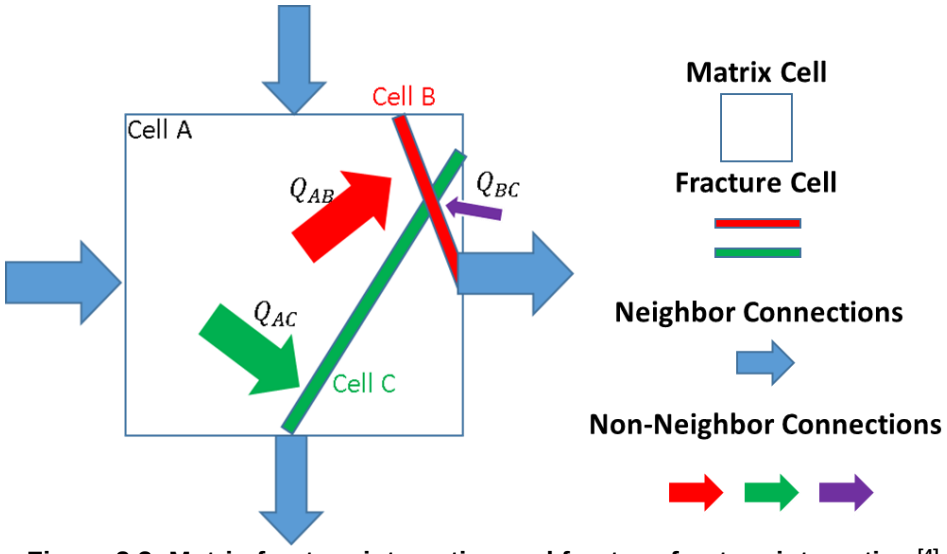

Figure 2.3: Matrix-fracture interaction and fracture-fracture interaction [4]

Unlike neighbor connection fluxes which are typically cell face properties, non-neighbor connection fluxes are not explicitly assigned to any cell face, and this causes a difficulty with applying most flux-based tracing methods which rely on structured flux assignment at cell faces. In this paper, we propose a robust tracing methodology which accurately handles both natural ordering and NNC fluxes in complex grid connection

systems. The general streamline tracing steps are summarized as below. Steps 1-4 discussed below are carried out for both upstream and downstream cells across each NNC. The illustration provided here focuses on the upstream side only since the downstream side follows a similar procedure. Also, only boundary layer on matrix cell face is shown although boundary layers should be constructed on faces of all related cells. All these simplification in Fig. 2.4 and Fig. 2.5 is to depict the overall work flow to readers first, all details will be revealed in the following sections.

1. NNC flux association to cell faces. Our flux-based tracing requires fluxes on cell faces as constraints, where defined NNCs connects two cells (matrix-matrix or matrix-fracture or fracture-fracture). For each cell, one of its faces is associated to the NNC on grid geometry, and a representative position for the NNC is mounted on the associated face (Fig. 2.4(b) and Fig. 2.5(b)).
2. Boundary layer construction. For a cell face with an associated NNC, a 2D Cartesian grid is generated to serve as the boundary layer for this face (Fig. 2.4(c) and Fig. 2.5(c)). The NNC fluxes and the neighbor connection flux will all be assigned to the boundary layer cells according to their representative positions on cell face.
3. Solve inter-cell flux within boundary layer. After the boundary layer grid is constructed, a pseudo pressure is assumed to control the Darcy flow within the boundary layer grid. With all the fluxes that are associated with single face as boundary conditions, mass conservation equations are constructed to solve for the pseudo pressure for all cells in boundary layer grid, and thus the inter-cell flux

(Fig. 2.4(d) and Fig. 2.5(d)) within boundary layer can be calculated by pseudo pressure difference and inter-cell transmissibility.

4. Tracing through boundary layers. As the boundary layer is simple Cartesian grid with all inter-cell fluxes already known, streamline tracing (Fig. 2.4(e) and Fig. 2.5(e)) through it can be easily done with Pollock method.
5. Map streamline back to original grid geometry. As boundary layer is an imaginary layer introduced to organize fluxes on a single cell face but not the real space where fluids flow, as long as the position for streamline to enter the downstream cell is determined, streamline can be mapped back to original grid geometry (Fig. 2.4(f) and Fig. 2.5(f)).

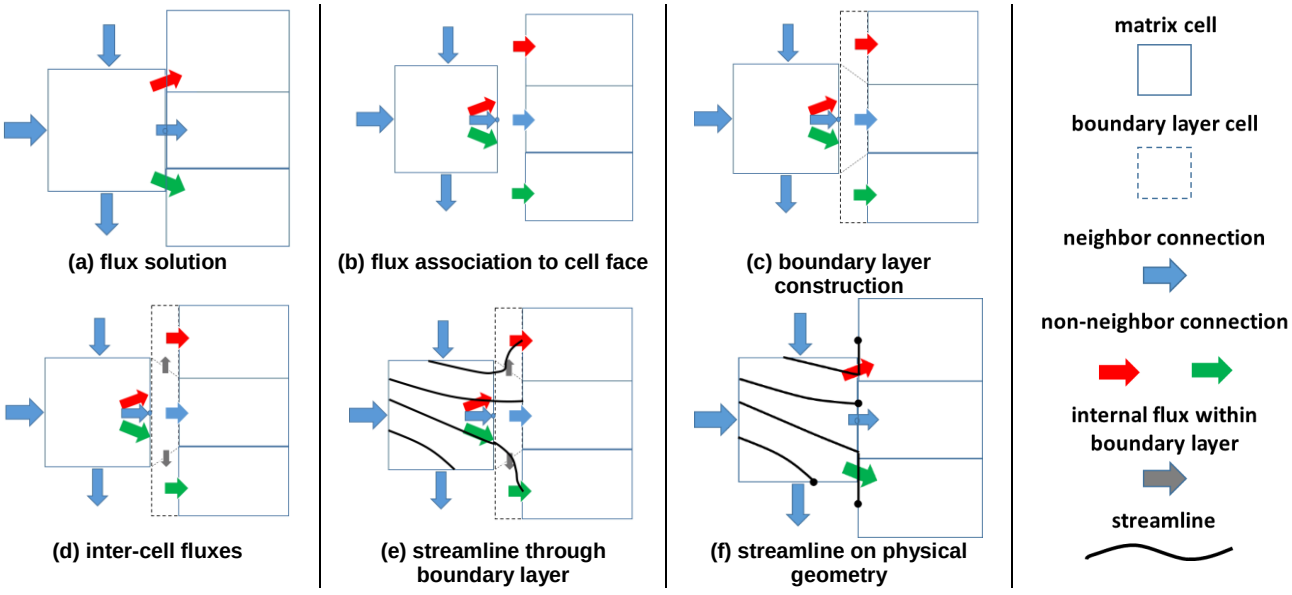

Figure 2.4: Illustration for streamline tracing in fault

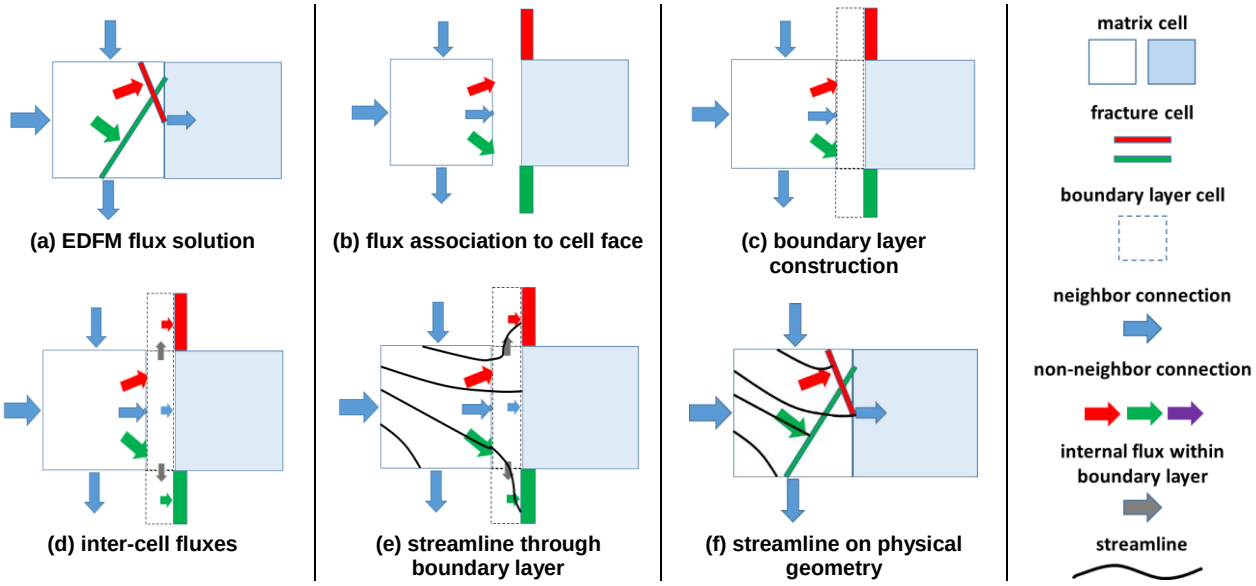

Figure 2.5: Illustration for streamline tracing to discrete fractures (EDFM) [4]

2.3.3 Flux Association with Cell Faces

Here we provide a discussion of the details involved with the geometrical treatment of NNCs during streamline tracing. The flux association for the fault scenario is quite intuitive, and the selection of flux associated cell face is determined by relative position of one cell to the other. A more sophisticated mechanism is provided for the discrete fracture scenario here. The entire process is described in Fig. 2.6. When an NNC connects an upstream cell A with a downstream cell B, flux association should be done for both A and B. To determine which face of A the NNC flux is associated with, one needs to compare the position of B relative to the position of each face of A. The position of B relative to A is defined by a position vector x_B, which is from the center of A to the center of B. The position of each face of A is defined by a face position vector x_{fi} which is from center of A to face center (i refers to face index within cell A). We will associate each

NNC flux with its closest face whose position vector x_{fi} has the smallest angle θ from position vector of B, and technically, it means to maximize $\{\frac{x_B \cdot x_{fi}}{|x_B||x_{fi}|}\}$.

After face i is associated with the NNC, one still needs to pick a position α_{BA} on face i to represent this NNC. This is necessary to roughly honor the flow geometry in situations of existing multiple connections linked to the same face. The representative position is selected by moving and projecting downstream cell position vector on cell face.

The same procedures are also needed for the downstream cell B. The size of cell B is exaggerated for a better illustration.

Flux association should be done for all the NNC fluxes before boundary layers are constructed.

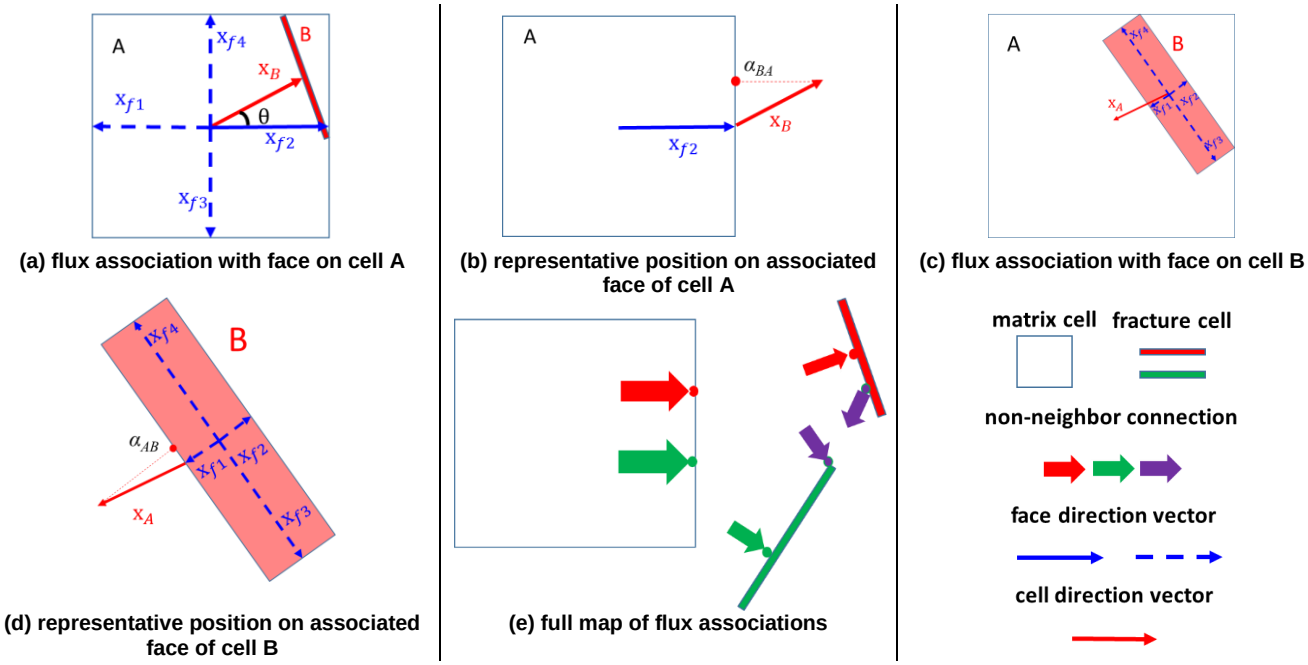

Figure 2.6: Illustration of flux association with cell faces[4]

2.3.4 Construction of Boundary Layers

A boundary layer is constructed for each cell face that is associated with one or more NNC flux. Let us take the right face of matrix cell A for example. As shown in Figs. 2.3 and 2.7, flow through the right face is associated with three fluxes: one neighbor connection flux (which connects cell A to the next natural neighbor to the right of A), and the other two NNC fluxes (that connect matrix cell A to fracture cells B and C). The total number of required boundary layer grids to handle this scenario equals to the amount of associated connections, which is three in this case. A boundary layer is a representation of the cell face (Fig. 2.7), one side connected to the study cell with summation of all fluxes, the other side connected to other cells with respective flux. The flux assignment guarantees that there is no accumulation inside boundary layer, based on which mass balance equation will be constructed to solve inter-cell flux within boundary layer.

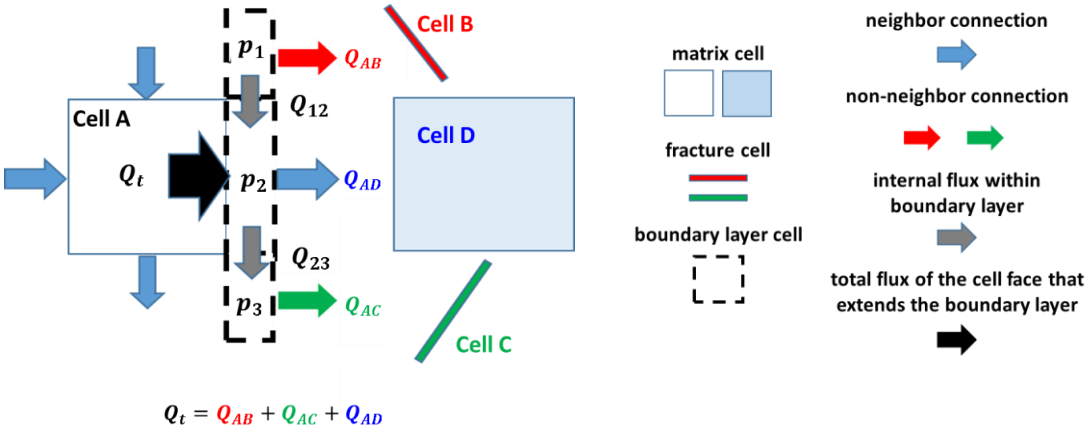

Figure 2.7: Boundary layer for the right face of cell A[4]

2.3.5 Solving Inter-cell Flux within Boundary Layer

To trace streamlines through the boundary layer grid, inter-cell flux within boundary layer should be known. According to the flux assignment during the construction of boundary layer grid, the boundary layer has no accumulation inside zero thickness. To establish the mass balance equations, a pseudo pressure p is used as the primary variable to describe the cell state, and inter-cell flux is directly calculated by the pseudo pressure difference, $q = \Delta p$. As an example, the mass balance equations for the specific case in figure 4 should be established as

$$\begin{cases} (-p_1 + p_2) = Q_{AB} \\ (p_1 - 2p_2 + p_3) = Q_{AD} - Q_t \\ (p_2 - p_3) = Q_{AC} \end{cases} \tag{2.6}$$

Where $Q_t = Q_{AB} + Q_{AC} + Q_{AD}$.

And inter-cell fluxes should be calculated as

$$\begin{cases} q_{12} = (p_1 - p_2) \\ q_{23} = (p_2 - p_3) \end{cases} \tag{2.7}$$

2.3.6 Tracing through Boundary Layers

For fracture cell B, boundary layer is also constructed on its face and inter-cell flux is also solved. As all the required information is ready, streamline from cell A to cell B is traced segment by segment as is shown in Fig. 2.8(a). Streamline tracing from boundary layer 1 to boundary layer 2 is not by Pollock method but by a direct mapping where point *a* and *a'* will overlap when the two corresponding cell faces are completely overlapped.

When the entrance point on cell B is determined, the streamline trajectory from cell A to cell B is then mapped to the original grid system. As shown in Fig. 2.8(b).

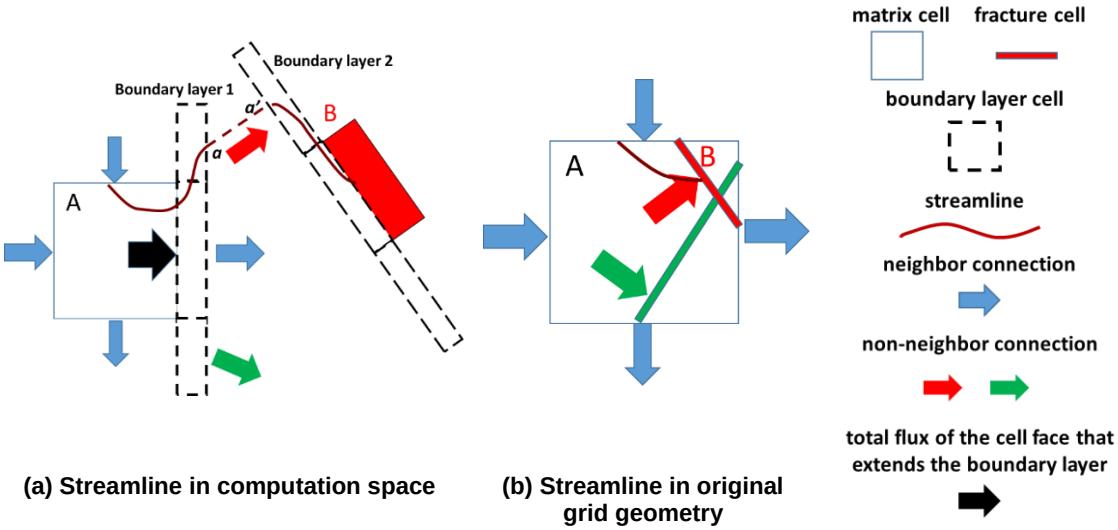

(a) Streamline in computation space **(b) Streamline in original grid geometry**

Figure 2.8: Streamline tracing from matrix cell A to fracture cell B[4]

2.4 Validation

In this section, we present cases of incompressible flow systems involving quarter five-spot injection patterns to validate our streamline tracing method. We compare our approach against a semi-analytical solution and finite volume grid-based scheme. In the semi-analytical solution, streamline trajectories and time-of-flight are computed using a complex variable boundary element method (CVBEM) (Sato and Abbaszadeh 1994; Nakashima et al. 2000). The approach is known to generate accurate flow trajectories for 2D problems with homogeneous flow parameters. For the direct computation of time-of-flight on the finite volume grid, we applied the single point upwind scheme in the solution of the differential form of Eq. (2.1) as proposed by Shahvali et al (2012). Since total fluxes within and across fractures are obtained as NNC fluxes, the numerical scheme can be directly applied without any modification for the time-of-flight calculation.

Simple 2D cases with different fracture configurations and fracture-matrix conductivity contrasts ($k_f\omega_f/k_m$) are used to demonstrate accuracy and robustness of our approach. We will show comparison between the semi-analytical solution, streamline-based method, and the grid-based method in terms of time-of-flight distributions in the flow domain. For a more quantitative comparison, plots of tracer concentration at the producer versus dimensionless time are compared. For the streamline-based method the tracer concentration at a threshold dimensionless time t_D is simply obtained as the proportion of the number of streamlines reaching the producer with arrival times less than or equal to t_D. For the grid-based method on the other hand, the tracer concentration curves identically results from an analytical manipulation of the respective diagnostic

Lorentz $(F-\Phi)$ curves (Møyner et al, 2015; Shahvali et al, 2012). The dimensionless sweep efficiency curve, which can be obtained directly from the corresponding Lorentz curve (Shook and Mitchell, 2009), shows the recovery factor E_V of the displaced fluid as a function of Pore Volumes Injected (PVI) under assumption of unit mobility piston-like displacement. The tracer concentration is therefore computed as $1-dE_V/dt_D$. In all the calculations presented, $F-\Phi$ and E_V curves are computed with high resolution of t_D to mitigate sharp fluctuations in the calculated tracer concentration profiles.

2.4.1 A Single Fracture, Two-dimensional Case

The first example is a simple 2D problem with a single diagonal fracture. The model comprises of a homogeneous square domain of length 1.0 (*ft*), discretized into 10,000 grid blocks, each having equal dimension of 0.01×0.01×0.2 (ft^3). The system is assumed to be single phase, isothermal and incompressible. Uniform permeability and porosity values of 1.0 (*md*) and 0.5 are assumed. The model consists of a single injection well at origin and a single producer located at top-right (1.0, 1.0) ft. A neutral tracer flow simulation is conducted with 3.0 pore volumes injected (PVI). The producer is open and thus, the initial pressure is maintained throughout the duration. We examined two cases with different fracture-matrix contrasts ($k_f\omega_f/k_m=0.10$ *and* $k_f\omega_f/k_m=100.0$).

Visual comparisons in terms of TOF are summarized in Fig. 2.9 (low contrast) and Fig. 2.10 (high contrast). For both cases of fracture conductivity considered, our model shows excellent agreement with the semi-analytical solution. Although a general

agreement in trend can be observed when compared to the grid-based time of flight calculations, a severe dispersion effect is apparent.

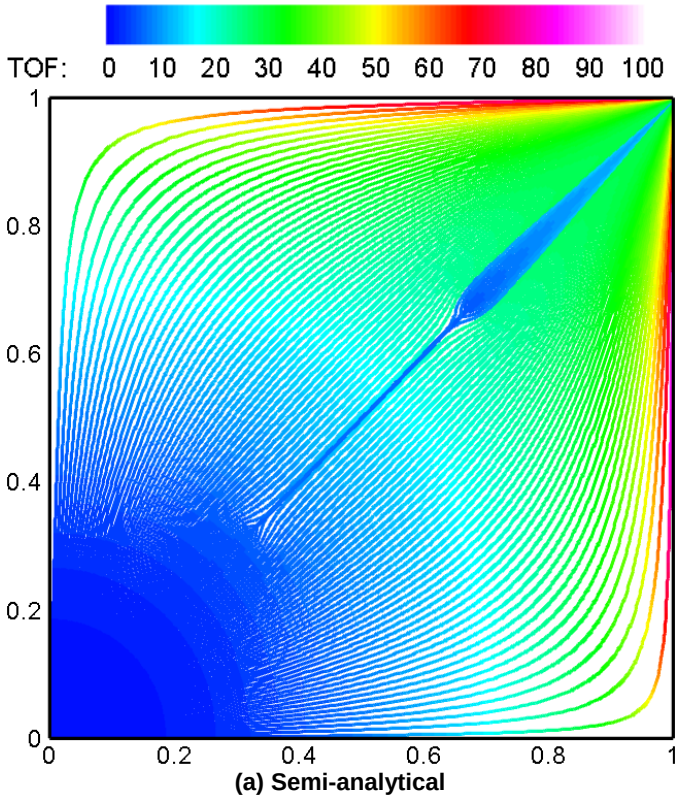

Figure 2.9: Comparison of time-of-flight (k_{fo}/k_m=0.10) [4]

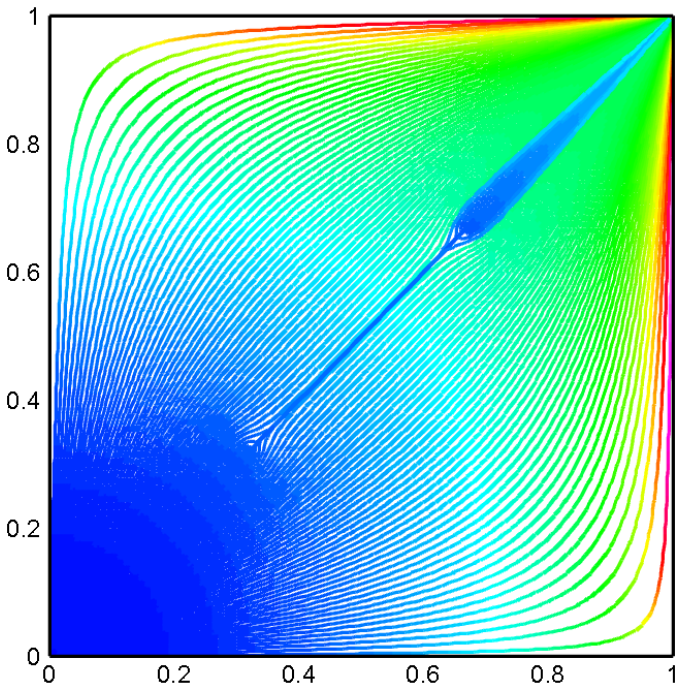

(b) Streamline-based

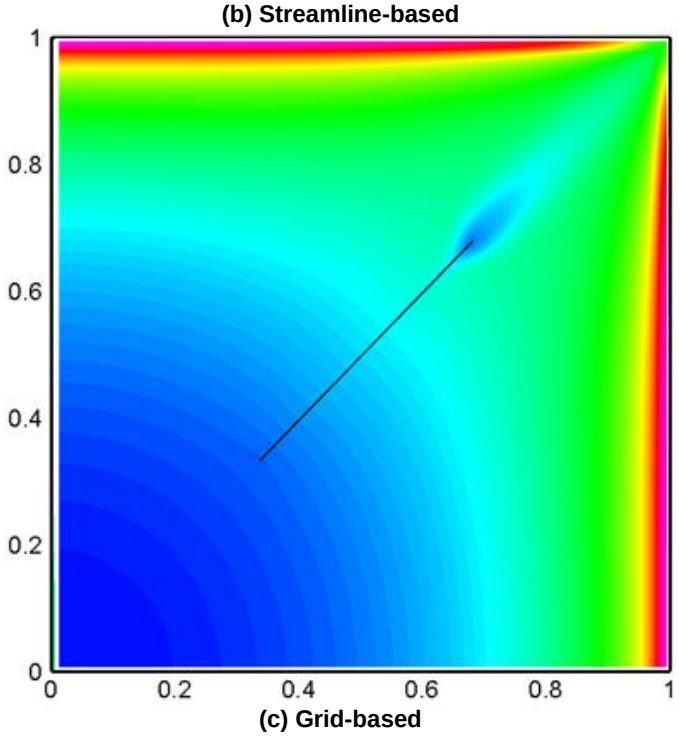

(c) Grid-based

Figure 2.9 Continued.

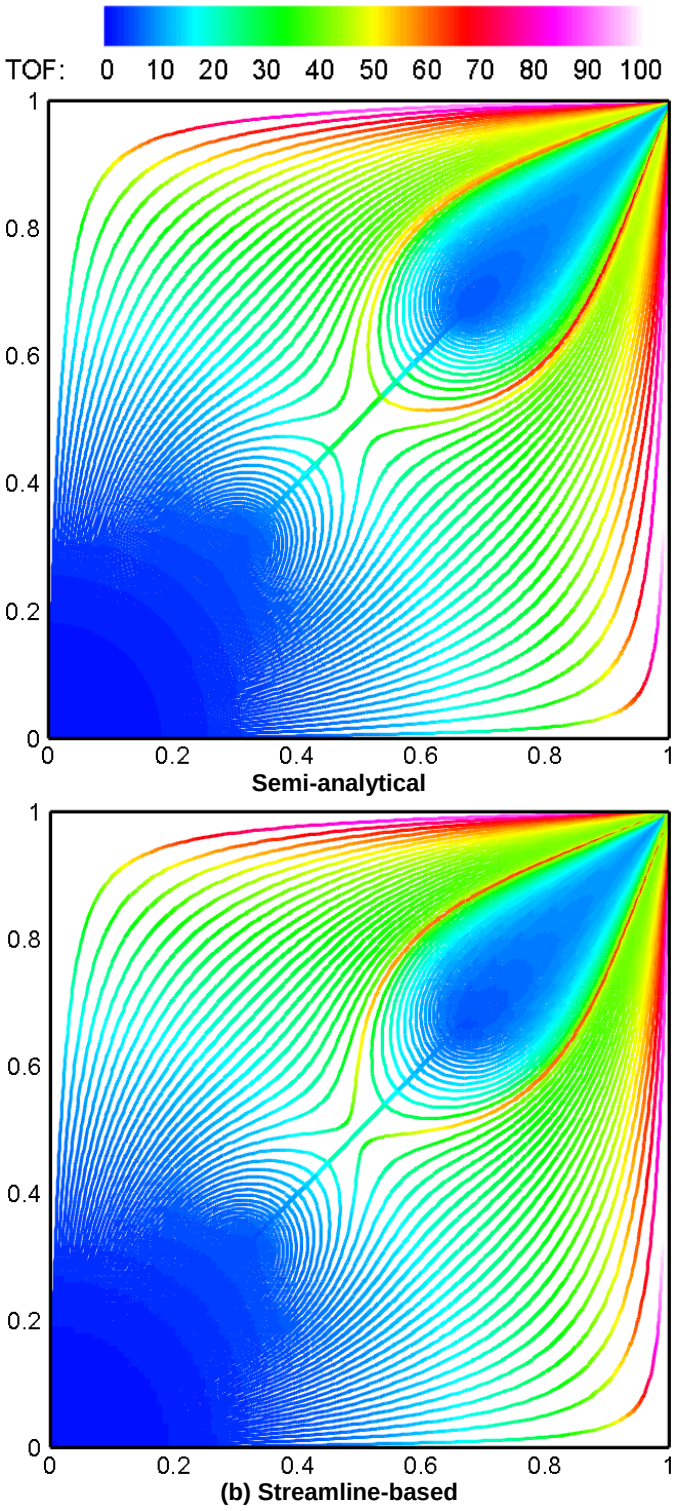

Figure 2.10: Comparison of time-of-flight ($k_f\varnothing/k_m$=100.0) [4]

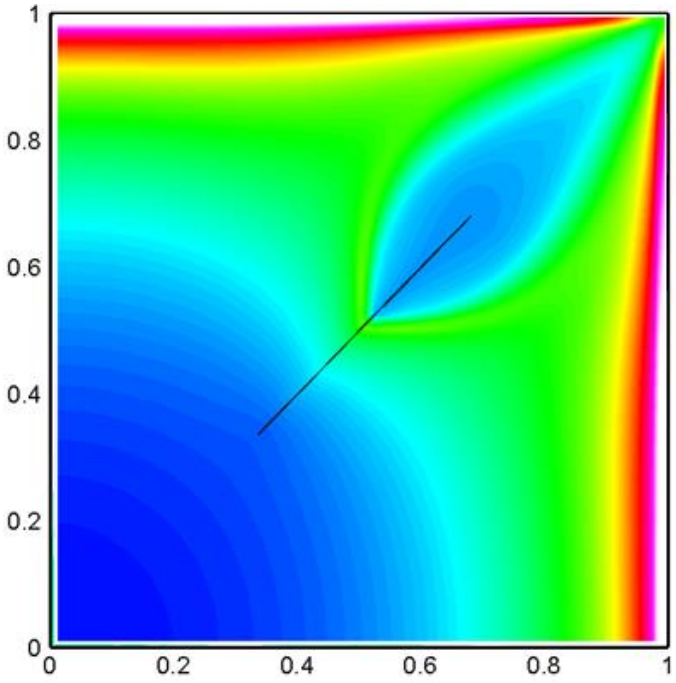

(c) Grid-based

Figure 2.10 Continued.

The interpretation of the comparative performances of the methods presented based on visual observations is reinforced by the tracer concentration responses shown in Fig. 2.11. For the case of low fracture conductivity, tracer breakthrough responses (due to the fracture and matrix) are smeared in the grid-based method. Furthermore in the high fracture conductivity case, the smearing effect results in the delay in first tracer breakthrough and slightly expedited second tracer breakthrough. The smearing effect observed results from two systemic inadequacies of the grid-based time of flight computations. First, the numerical scheme suffers from numerical dispersion effects which is tied with any grid-based methods (Lantz, 1971). Second, solving the differential form of Eq. 2.1 on a finite volume grid results in a time of flight computation on an average sense which tends to blur out direct interactions between sources and sinks in the flow

domain. This shortcoming was identified by Ibrahima et al (2017) who suggested a slightly more involving numerical scheme to mitigate the effect.

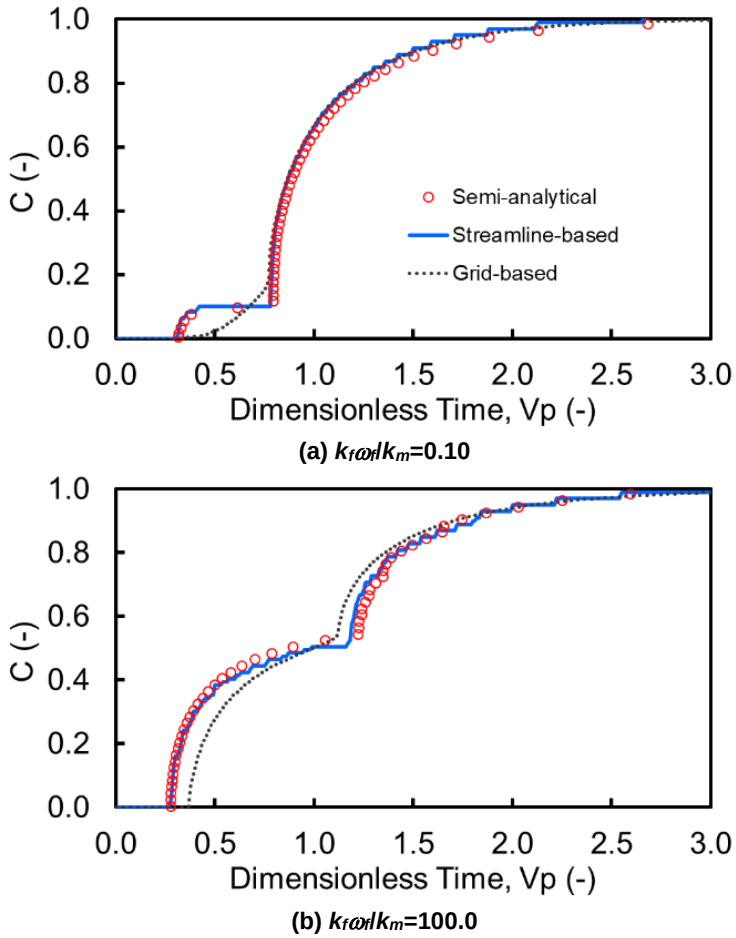

(a) $k_f\omega_f/k_m$=0.10

(b) $k_f\omega_f/k_m$=100.0

Figure 2.11: Comparisons of tracer responses (one fracture) [4]

2.4.2 Three Fractures, Two-dimensional Case

Next, we test our model with a 3 fractures case to demonstrate the ability of our method for multiple fracture scenarios. Fracture locations are illustrated in the Fig. 2.12. This case was set up using similar parameter set with example1. Note that special

treatments are required in CVBEM for intersected fractures and these are beyond the scope of this paper.

Simulation results are summarized in Fig. 2.12, Fig. 2.13, and Fig. 2.14. Again, good agreement in terms of TOF distributions and tracer responses is obtained between the semi-analytical solution and our model, whereas the grid-based method shows major deviations. As discussed earlier, these deviations are a result of the inherent shortcomings of the grid-based computations. The averaging effect of the grid-based time of flight calculations results in the smearing of the 4 distinct tracer breakthrough signatures observed in the low fracture conductivity case. Smearing effects similar to the single high conductivity fracture case is also observed here.

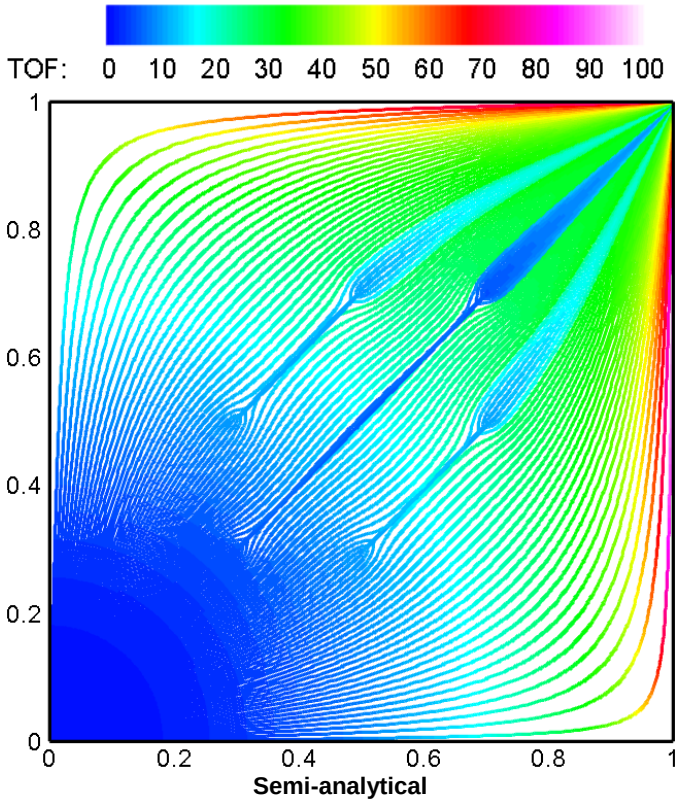

Figure 2.12: Comparison of time-of-flight ($k_f w/k_m$=0.10) [4]

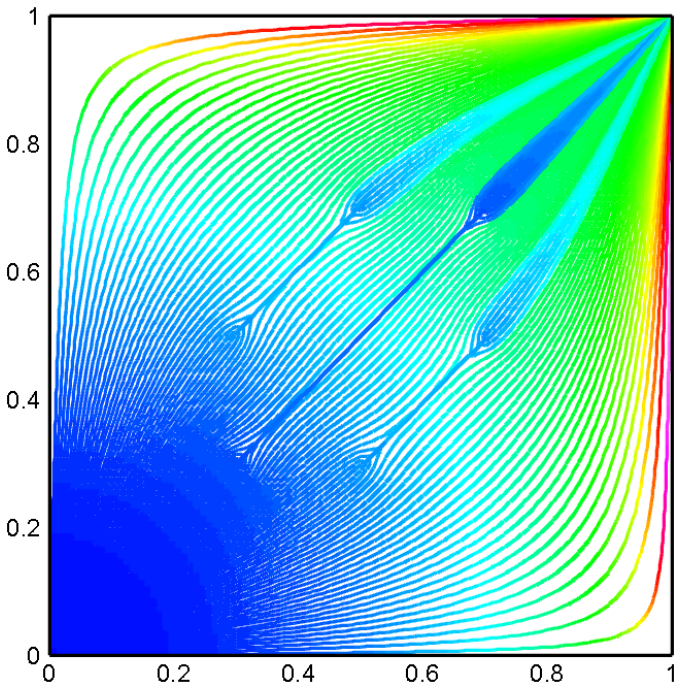

(b) Streamline-based

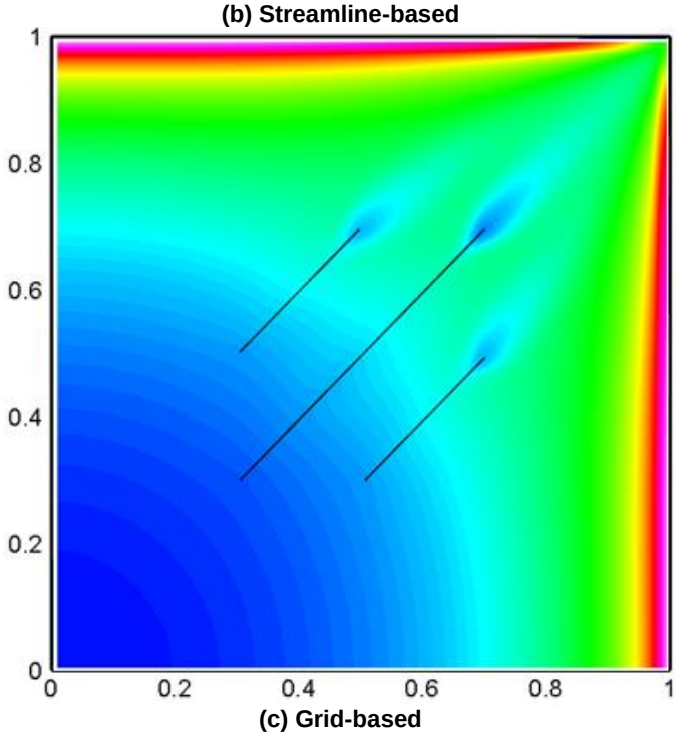

(c) Grid-based

Figure 2.12 Continued.

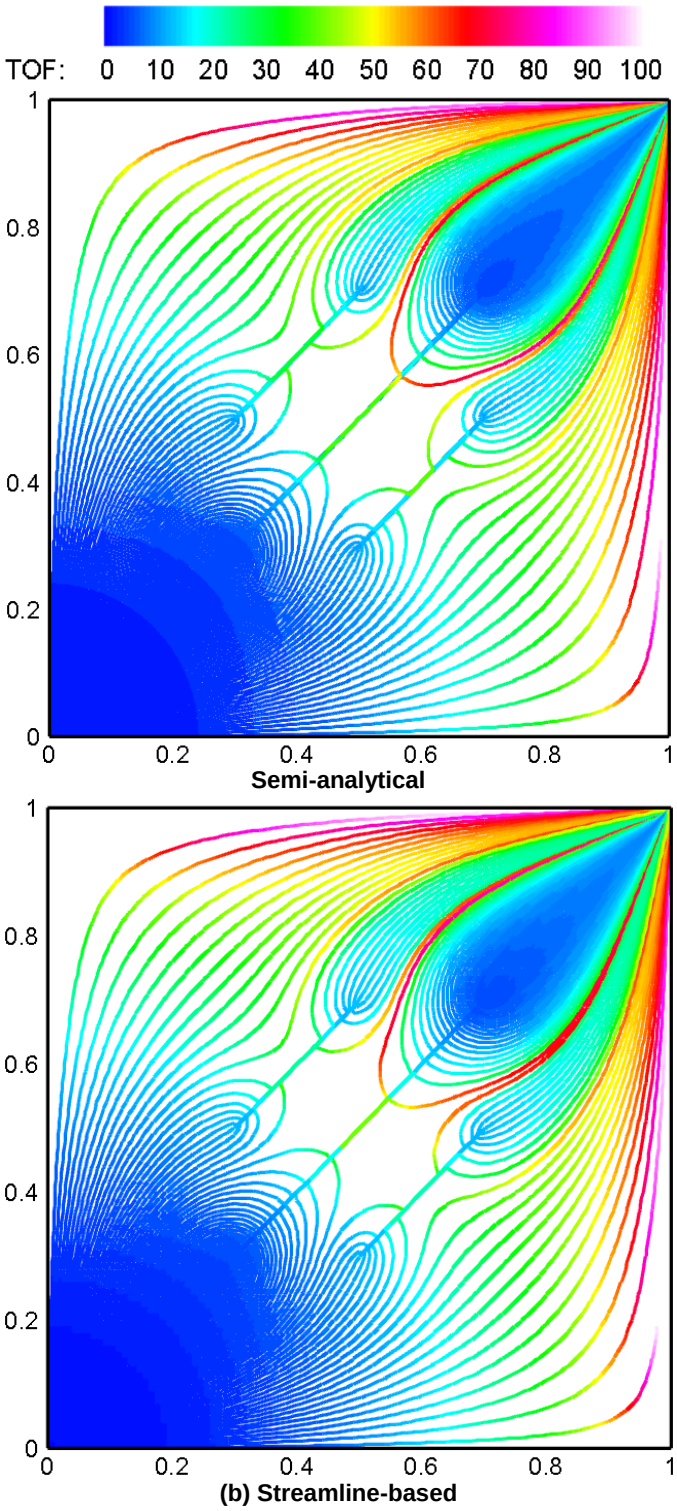

Figure 2.13: Comparison of time-of-flight ($k_f\omega_f/k_m$=100.0) [4]

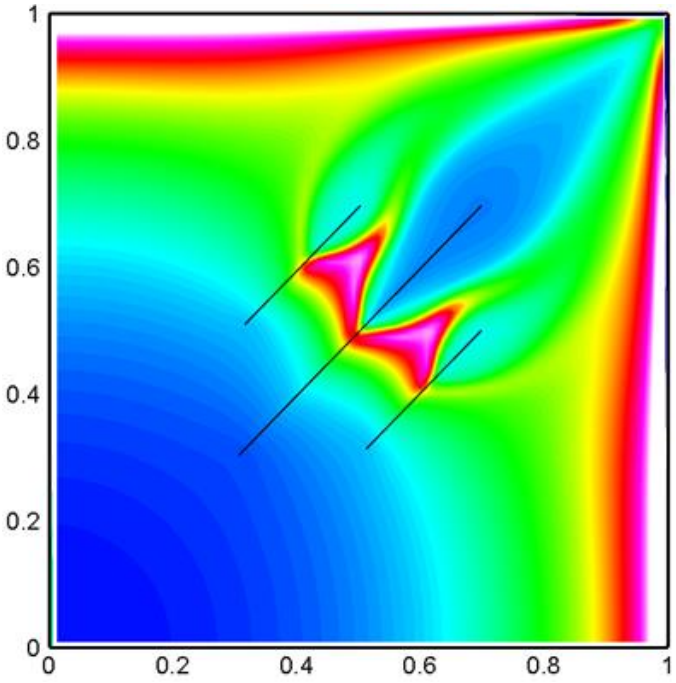

(c) Grid-based

Figure 2.13 Continued.

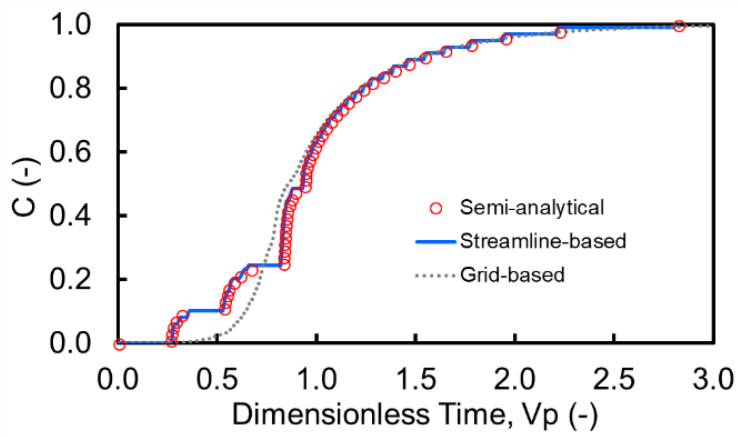

(a) k_{frac}/k_m=0.10

Figure 2.14: Comparisons of tracer responses (three fractures) [4]

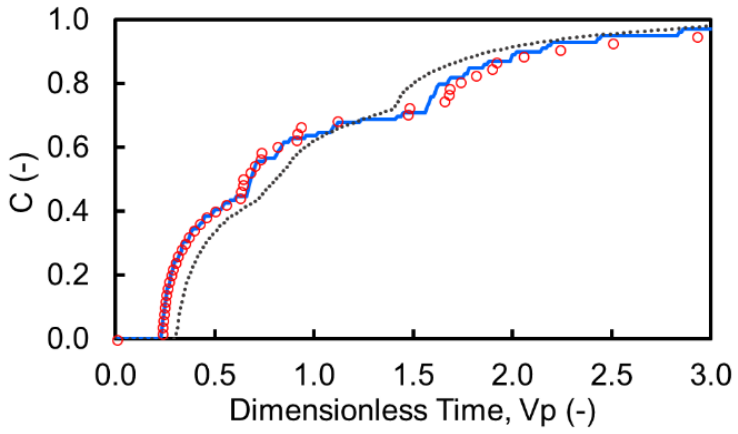

(b) $k_f\omega_f/k_m$=100.0

Figure 2.14 Continued.

Based on the observations from this section, it is found that our approach can capture the effect of fractures at different levels of geometry and conductivity contrasts, whereas, the grid-based method showed deviations due to the numerical artifacts. Although the grid-based method is simple and generally applicable to any grid system, the observed inadequacies of the grid-based method resulted in an averaging effect with results in smearing of the tracer concentration profiles. A direct implication of this is delayed breakthrough or wrong breakthrough signatures of displacing fluids (e.g. water or polymer). For such cases, our proposed approach therefore becomes a good option. We will present the applications of our model to field-scale examples to demonstrate the robustness in the following sections.

2.5 Field-scale Application of Flow Visualization

Streamline-based methods have been proven to be effective for reservoir management by providing injector-producer connection pairs and allocation factors for wells. The information obtained from streamlines is useful in understanding the fluid allocation patterns and can be utilized for a variety of applications. In this section, we introduce applications of our approach to flow diagnostics.

2.5.1 SAIGUP Model

We applied our streamline-based method to a field scale reservoir model generated by the Sensitivity Analysis of the Impact of Geological Uncertainties project (SAIGUP) (Manzocchi et al. 2008). This reservoir model includes features which enhances its geologic realism such as complex fault structure, channels, and inactive cells. Therefore, it is a good example to demonstrate the robustness of our streamline-based method.

The grid configuration and static properties are provided in Fig. 2.15 and the other properties are summarized in Table 2.1. Large natural fractures are generated using our in-house EDFM preprocessor and mapped onto the original grid (Fig. 2.15 (a)). The system is assumed to be isothermal and two phase, oil and water. Relative permeability curves for the reservoir domain and the fracture domain are provided in Fig. 2.16. The reservoir consists of 10 producers placed within the oil zone and 12 peripheral injectors (Fig. 2.15 (d)). While producers are connected to top 15 layers that cover the oil columns, injectors are fully penetrated and completed. In this application, all injectors are constraint by uniform water injection rates of 1000.0 STB/D, whereas all producers are constraint by

liquid production rates of 1200.0 STB/D. Using these settings, water injection simulation is conducted for 10 years.

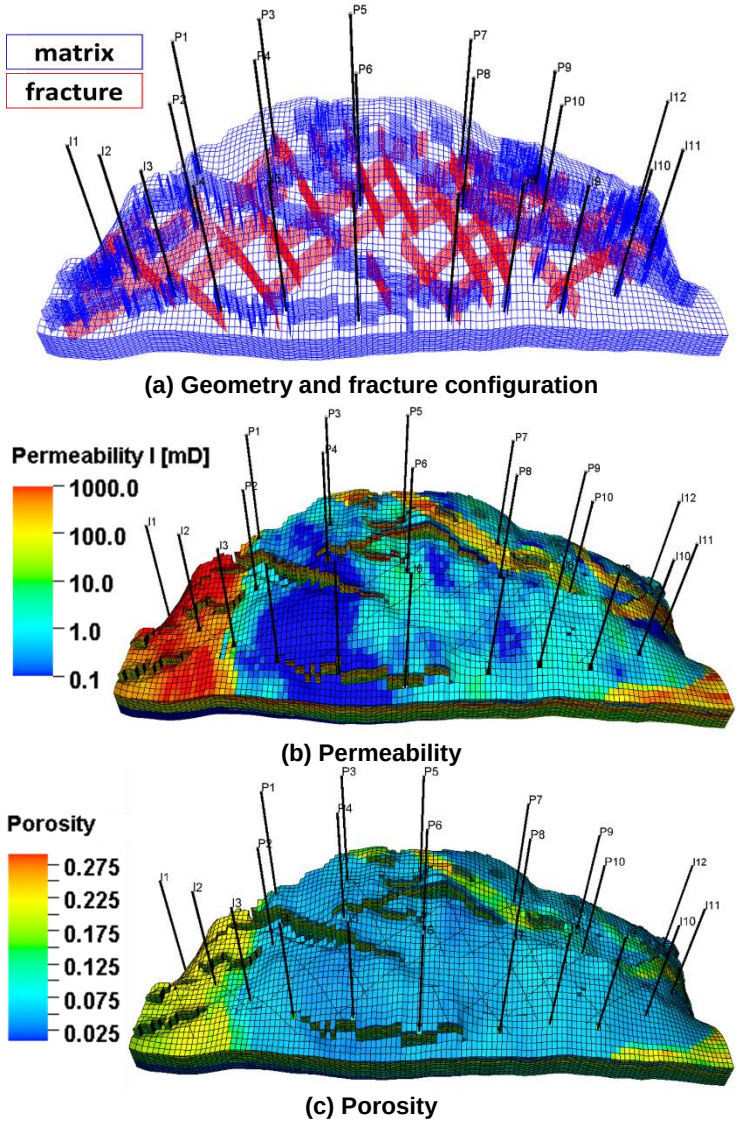

Figure 2.15: Summary of the SAIGUP model, static properties and initial water saturation distributions[4]

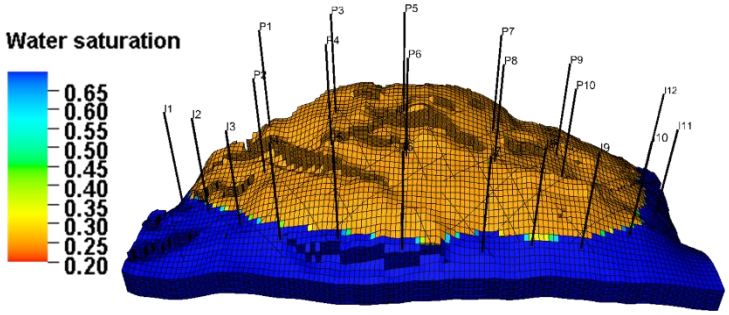

(d) Initial water saturation

Figure 2.15 Continued.

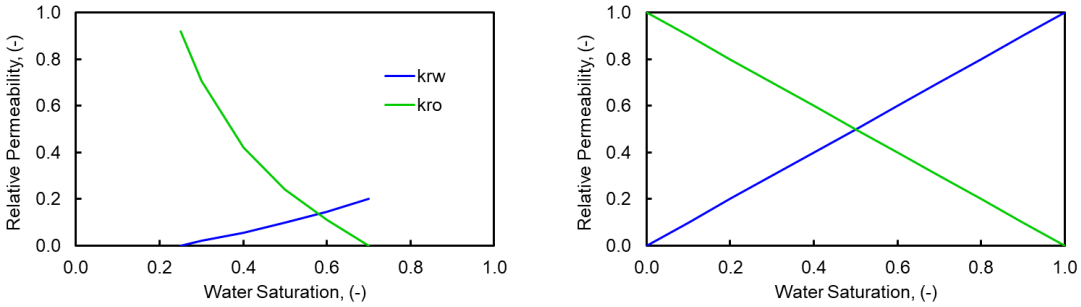

(a) Reservoir domain **(b) Fracture domain**

Figure 2.16: Relative permeability curves[4]

Table 2.1: Reservoir, fluid and rock properties for SAIGUP model[4]

Parameter	Symbol	Unit	Value
Grid size	*ni, nj, nk*	-	40, 188, 20
Oil density	ρ_o	lb/ft^3	52
Oil viscosity	μ_o	*cp*	2
Oil compressibility	*Co*	psi^{-1}	2.07E-2
Water density	ρ_w	lb/ft^3	64
Water viscosity	μ_w	*cp*	0.5
Water compressibility	*Cw*	psi^{-1}	6.9E-3
Rock compressibility	*Cr*	psi^{-1}	2.07E-2

2.5.2 Flow Diagnostic Plot based on Streamline

The results of the flow diagnostics are summarized in Fig. 2.17. Fig. 2.17(a) and Fig. 2.17(b) illustrate streamline TOF distributions at the end of the simulation period with

the τ contoured along each streamline. Flow partitions at the end of the simulation and different time periods are shown in Fig. 2.17(c) – (h). In addition, drainage volume and swept volume by a well and corresponding pie charts are shown in Fig. 2.17(i) – (j). Fig. 2.17(k) presents flux allocation between well pairs in which thickness of arrows represents the flux allocations. For these results, we see how the fluid allocation changes with the flood progression based on streamlines accounting for complex geometry and heterogeneity due to fractures. These are also useful to determine when and where to drill additional wells.

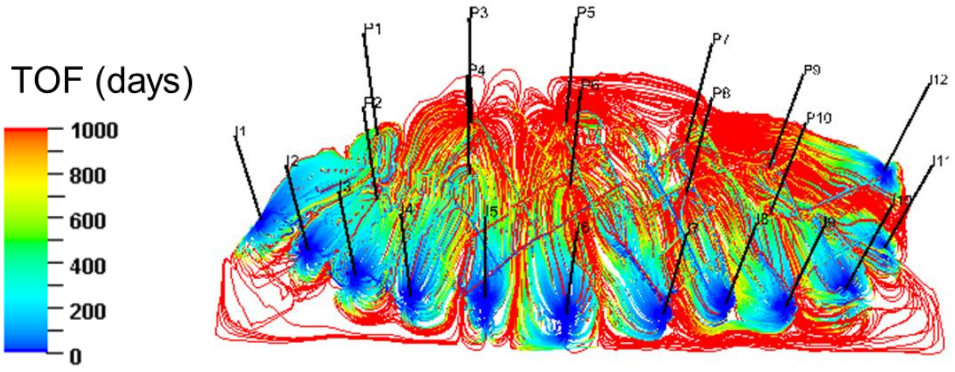

(a) TOF from Injectors

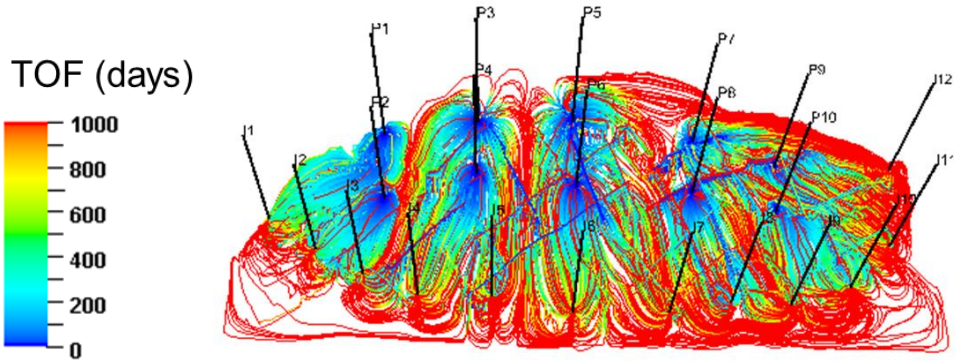

(b) TOF from producers

Figure 2.17: Flow diagnostics results, flow partitions and swept/drainage volumes[4]

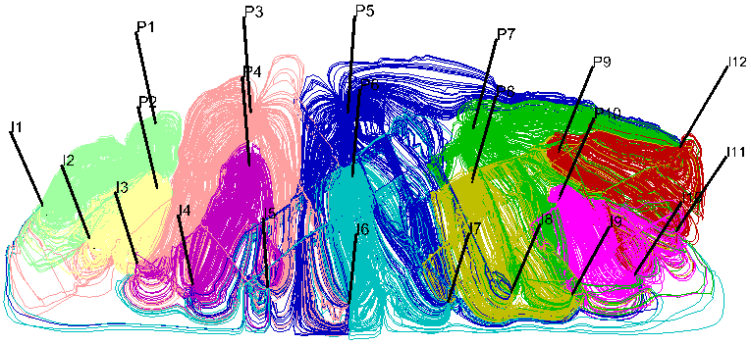

(c) Producer partitions

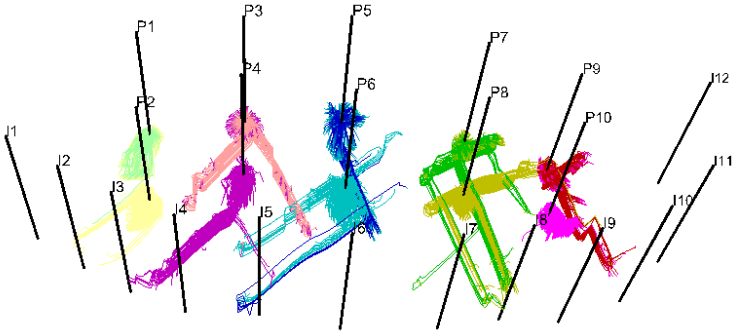

(d) Drainage volume at 60 days

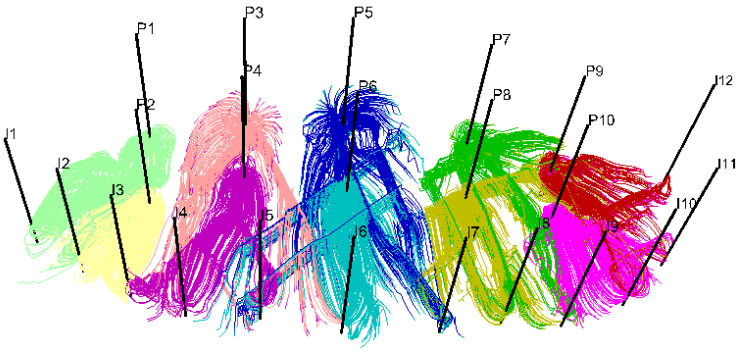

(e) Drainage volume at 600 days

Figure 2.17 Continued.

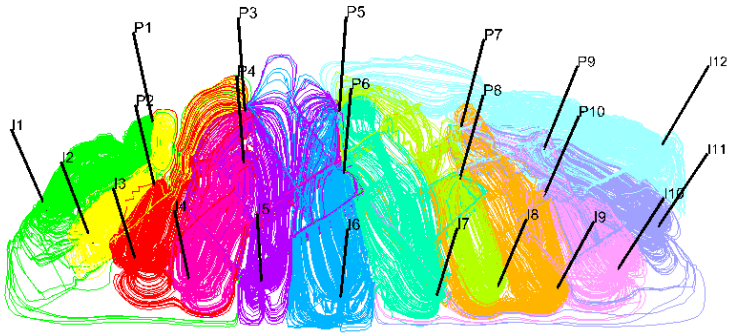

(f) Injector partitions

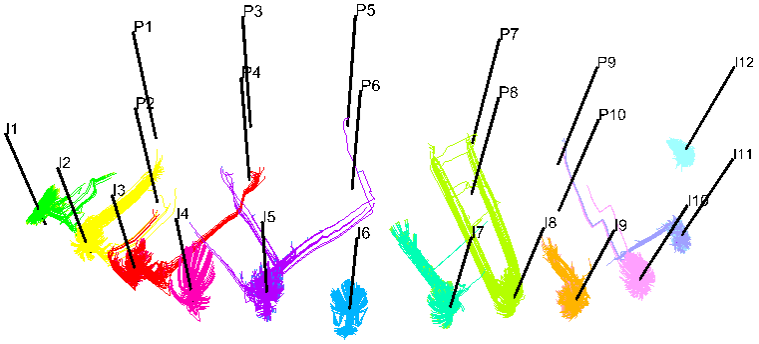

(g) Swept volume at 60 days

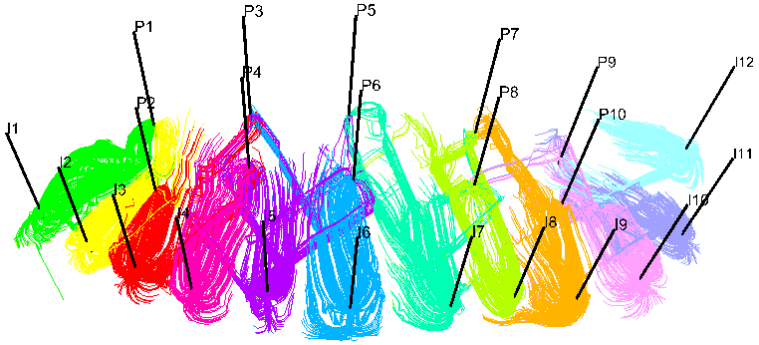

(h) Swept volume at 600 days

Figure 2.17 Continued.

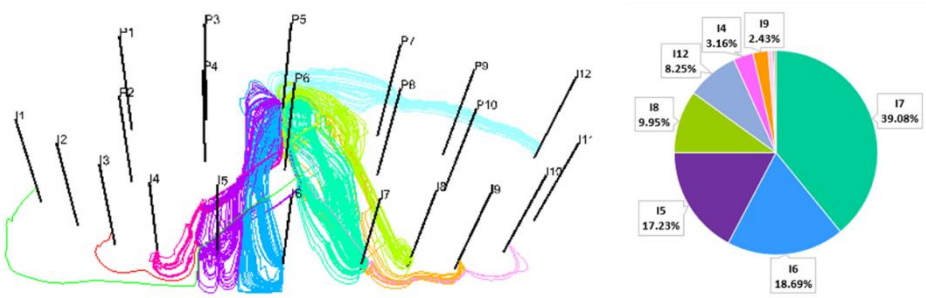

(i) Drainage region developed by P5 and corresponding pie chart

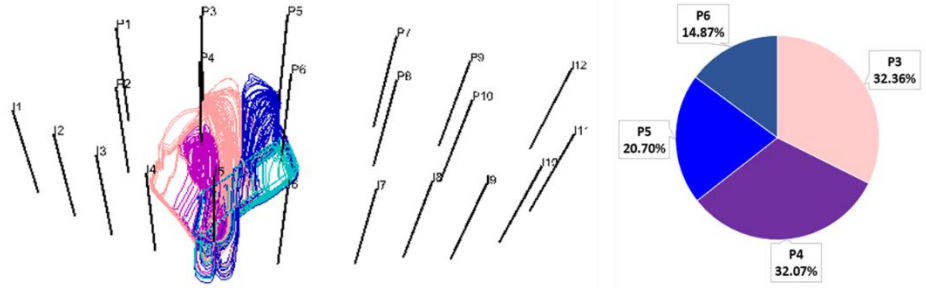

(j) Region swept by I5 and corresponding pie chart

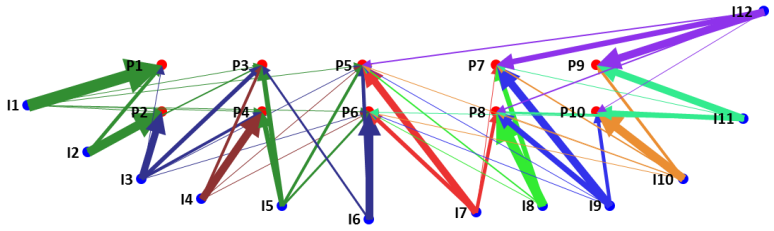

(k) Flux allocations between well-pairs

Figure 2.17 Continued.

2.6 Chapter Conclusions

We presented streamline tracing and applications in fractured reservoir with complex geometry, including faults and discrete fractures. The discrete fracture system is implemented via EDFM framework. The following conclusions are drawn from this study.

1. Streamline tracing algorithm on EDFM based on the boundary layer method has been successfully implemented. The implementation is validated comparing with a semi-analytical solution.
2. Comparisons between the semi-analytical solution, our model, and the grid-based model in terms of TOF distributions and tracer responses with 2D examples suggest that our model outperforms the grid-based model.
3. Our method has been applied to flow diagnostics for a field scale model, SAIGUP reservoir that includes realistic features such as faults, channels, and inactive cells, and is embedded with multiple intersected discrete fractures by our own in-house code. The results show how the fluid allocation changes with the flood progression based on streamlines accounting for complex geometry and heterogeneity due to fractures. Through this exercise, we demonstrated the robustness and utility of our streamline-based approach to a field scale application.
4. The proposed approach is simple and easy to implement. In our application, we coupled our model with a commercial simulator. The mathematical framework proposed here is capable of streamline tracing and applications in field-scale applications.

CHAPTER III

AMENDED STREAMLINE-BASED SENSITIVITY CALCULATION AND FIELD APPLICATION

3.1 Chapter Summary

Previous history matching with streamline-based approach has shown great promise for integrating field-scale water cut and bottom hole pressure data into high resolution geologic models.

In order to improve the performance of streamline-based history matching, the nonlinearities of different streamline-based methods have been discussed and tested (H. Cheng, A. Datta-Gupta, and Z. He 2005). For the same purpose, the robustness and accuracy of streamline-based sensitivity is another aspect requiring further study.

In this chapter, streamline-based travel time sensitivity is amended accounting for water flow fraction and time of flight distribution among the streamlines. The amended sensitivity is tested in a synthetic case. The sensitivity by the amended method shows better agreement with the perturbation sensitivity than the legacy sensitivity. The model calibration by the amended method reveals faster data misfit drop and more favorable final result than the model calibration by the legacy method.

Previously, the streamline-based history matching was used to integrate production data from oil reservoirs developed by waterflood (Cheng et al. 2007; Yin et al. 2010; Tanaka and Kam, 2014). Tight oil or tight gas is usually developed by multi-fractured horizontal wells, and its recovery mainly relies on the depletion of fluid elastic

energy rather than fluid displacement. In order to extend streamline based history matching to a reservoir mainly developed by depletion, a novel implementation of the streamline-based bottom hole pressure sensitivity is developed accounting for both incompressible and highly compressible fluid, and this method is also valid for grids with non-neighbor connections. The newly implemented bottom hole pressure sensitivity is first validated with a synthetic gas reservoir case, and then tested in a field application to history match the bottom hole pressure of a high pressure high temperature tight gas reservoir. The tight gas reservoir is faulted, naturally fractured, and developed by producers only.

3.2 Introduction of Streamline-based History Matching

Typically the history data means the observed data collected from oil or gas field during underground fluid production, and history matching is the process to minimize production history and calculated simulation results as

$$min\left\{\sum_{data}(d_{obs}-d_{cal})^2\right\} \tag{3.1}$$

There are gradient or non-gradient approaches to solve this problem. The stochastic methods are typically non-gradient methods because they try to search the whole solution space by evolutionary algorithms, Markov chain Monte Carlo (MCMC) methods, Ensemble Kalman Filter methods (Aanonsen *et al.* 2009; Tanaka *et al.* 2010), or Ensemble Smoother methods (Chen and Oliver 2012). These methods generally require multiple initial static models and generations of updates to find the global minimum of the solution space.

The streamline-based history matching is a gradient-based method. Analytically parameter sensitivities are computed along streamlines, and are utilized to calibrate high resolution geologic models. The approach has been developed to include water cut data (Vasco et al. 1999; Chen et al. 2005), bottom hole pressure data (Tanaka et al. 2015), and time-lapse seismic data (Watanabe et al. 2017) into high-resolution reservoir model calibrations.

A streamline-based model calibration is usually conducted within a hybrid history matching workflow to conduct stochastic and streamline-based inversion sequentially, where global parameter such as oil-water contact, fault permeability, or fluid PVT

properties are to be calibrated by a stochastic algorithm, and local permeability fields are calibrated by streamline-based sensitivity (Yin *et al.* 2010). The hybrid method is usually conducted with multiscale models, upscaled models for the global stage calibrations and fine models for local stage calibrations, to save the total time for the full process.

3.2.1 Streamline-based History Matching Workflow

The streamline-based history matching workflow (Fig. 3.1) starts with a given prior reservoir model and the history matching process proceeds in an iteration manner for model calibrations. For each iteration, first the data misfit between simulation results and observed data is checked. If the data misfit is beyond the preset tolerance or the iteration has not reached its maximum number, streamlines are traced based on velocity or flux information extracted from the simulation results, and then parameter sensitivities are calculated along streamline trajectories. Finally, the geological model is calibrated to minimize the objective function, and the updated model is run for simulation again. This iteration will keep going until the data misfit has fallen inside the tolerance range or the iteration reaches the maximum number. In this process, the key point of integrating the dynamic data is to calculate the parameter sensitivity.

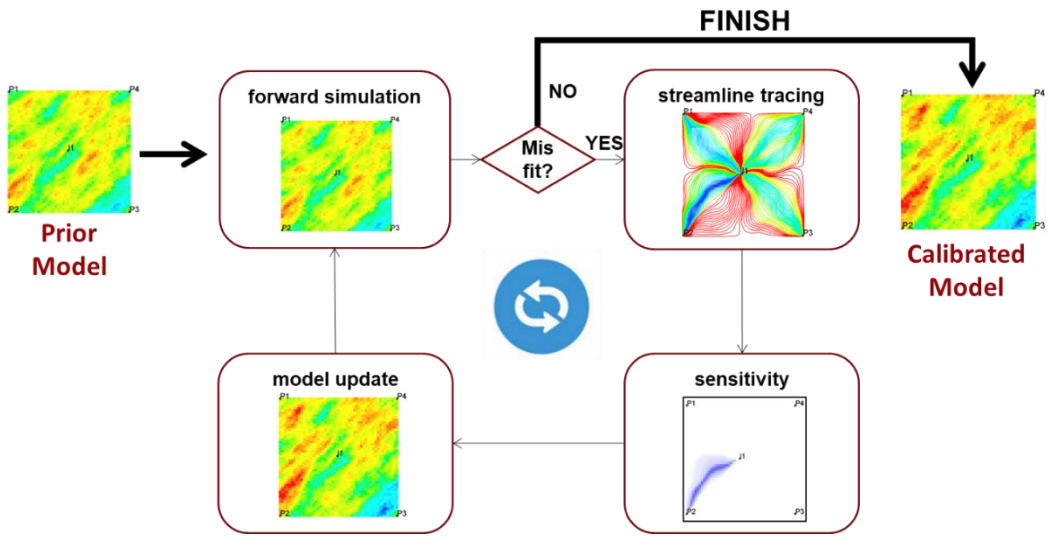

Figure 3.1: Workflow of streamline-based inverse modeling

3.2.2 Inverse Problem Formulation

Integration of dynamic data typically requires the solving an inverse problem to minimize the data misfit between the computed and observed response. The mathematical formulation behind such streamline-based inverse problems has been discussed in detail elsewhere (He et al. 2002; Vasco et al. 1999). We start with a prior static model that has already incorporated geology, well logs, and seismic data, and then minimize a penalized misfit function.

$$\|\delta d - S\delta R\| + \beta_1\|\delta R\| + \beta_2\|L\delta R\| \tag{3.2}$$

In Eq. 3.2, δd is the vector of the data residuals, S is the sensitivity matrix with respect to grid parameters, and δR corresponds to the change in reservoir properties, which are grid block permeabilities in this work. The second term, called the norm constraint, penalizes deviations from the prior model. This helps preserve geologic realism. The third term, roughness penalty, defines the model roughness, and L is a

second-spatial difference operator. The minimum of Eq. 3.2 can be obtained by an iterative least-squares solution to the augmented linear system as follows:

$$\begin{pmatrix} S \\ \beta_1 I \\ \beta_2 L \end{pmatrix} \delta R = \begin{pmatrix} \delta d \\ 0 \\ 0 \end{pmatrix} \tag{3.3}$$

The weight β_1 and β_2 determine the relative strengths of the norm constraint and the roughness penalty. The selection of these weights can be somewhat subjective. An iterative least squares solution approach via the LSQR algorithm (Paige and Saunders, 1982) is used to solve Eq. 3.3 to obtain grid block permeability changes, which is needed to minimize the overall data misfit.

3.3 Amended Travel Time Sensitivity

Travel time means the time that takes a particle from a certain position in a reservoir to travel to a producer. A decrease or increase of its value will cause an advance or delay of the well response in terms of water production, which means causing a horizontal shift of water cut curve of a producer. The grid properties along streamlines, such as permeability or porosity, have impacts on the value of travel time on the streamlines. The strength of the impacts, which are often called travel time sensitivities, can be analytically formulized by streamline methods.

3.3.1 Mathematical Formulation

The formula is derived by using a concept called slowness, which is the reciprocal of particle velocity. By Darcy's law, the slowness can be written as

$$s(x) = \frac{\phi(x)}{\lambda_{rt} k(x) |\nabla P|} \tag{3.4}$$

where λ_{rt} is total relative mobility and ∇P is pressure gradient. The first-order differential of slowness is given by Eq. 3.5, and the partial derivatives are given in Eq. 3.6 and Eq. 3.7.

$$\delta s(x) = \frac{\partial s(x)}{\partial k(x)} \delta k(x) + \frac{\partial s(x)}{\partial \phi(x)} \delta \phi(x) \tag{3.5}$$

$$\frac{\partial s(x)}{\partial k(x)} \approx \frac{-\phi(x)}{\lambda_{rt} \big(k(x)\big)^2 |\nabla P|} = -\frac{s(x)}{k(x)} \tag{3.6}$$

$$\frac{\partial s(x)}{\partial \phi(x)} \approx \frac{1}{\lambda_{rt} k(x) |\nabla P|} = \frac{s(x)}{\phi(x)} \tag{3.7}$$

The approximation for Eq. 3.6 and Eq. 3.7 is that the local perturbations in permeability and porosity generate negligible pressure changes. The implication of this assumption is that streamlines do not have significant shift because of these small perturbations.

The travel time $\delta\tau$ is the integration of slowness along certain streamline trajectory:

$$\delta\tau = \int_{\psi} \delta s(x) dr = \int_{\psi} \left[\frac{\partial s(x)}{\partial k(x)} \delta k(x) + \frac{\partial s(x)}{\partial \phi(x)} \delta\phi(x) \right] dr \tag{3.8}$$

The travel-time sensitivity along a single streamline with respect to the permeability or porosity of a particular grid block at location *x* is given in Eq. 3.9 or Eq. 3.10,

$$\frac{\delta\tau(\psi)}{\delta k(x)} = \int \left[-\frac{s(x)}{k(x)} \right] dr = -\frac{\mathrm{s(x)}}{k(x)} \Delta r(\mathrm{x}) = -\frac{\Delta\tau(\mathrm{x})}{k(x)} \tag{3.9}$$

$$\frac{\delta\tau(\psi)}{\delta\phi(\boldsymbol{x})} = \int \left[\frac{s(\boldsymbol{x})}{\phi(\boldsymbol{x})} \right] dr = \frac{\mathrm{s(x)}}{\phi(\boldsymbol{x})} \Delta r(\mathrm{x}) = \frac{\Delta\tau(\mathrm{x})}{\phi(x)} \tag{3.10}$$

where $\Delta r(\mathrm{x})$ is the arc length of the streamline segment within the grid block x, and $\Delta\tau(\mathrm{x})$ is the time needed for a particle to travel along this streamline segment.

In addition to the travel time, the saturation velocity along a streamline also has significant impact on the horizontal shift of a water cut curve in terms of time.

Consider two-phase incompressible flow of oil and water described by the Buckley-Leverett equation using the streamline TOF as the spatial coordinate (Datta-Gupta and King, 2007).

$$\frac{\partial S_w}{\partial t} + \frac{\partial f_w}{\partial \tau} = 0 \tag{3.11}$$

S_w is water saturation and f_w is fractional flow of water. The velocity of a given saturation S_w along a streamline is given by Eq. 3.12

$$\left(\frac{\partial \tau}{\partial t}\right)_{S_w} = \left(\frac{df_w}{dS_w}\right)_{S_w} \tag{3.12}$$

We can now integrate the previous derivations and get the sensitivity of the water saturation arrival time to the grid block property.

$$\frac{\delta t(S_w, \psi)}{\delta k(\boldsymbol{x})} = -\frac{\Delta \tau(\mathrm{x})}{k(x)} \Big/ \frac{df_w}{dS_w} \tag{3.13}$$

$$\frac{\delta t(S_w, \psi)}{\delta \phi(\boldsymbol{x})} = \frac{\Delta \tau(\mathrm{x})}{\phi(x)} \Big/ \frac{df_w}{dS_w} \tag{3.14}$$

Eq. 3.13 is more often used than Eq. 3.14 in a streamline-based history matching application, since the porosity will also affect the reserves and the average energy level of a field, which is probably has been evaluated before local grid calibration. Thus the following derivation is continued just in terms of permeability. In practice, the given saturation is usually specified with the water front saturation, and the sensitivity will be associated to a certain producer where the streamline ends (Fig. 3.2).

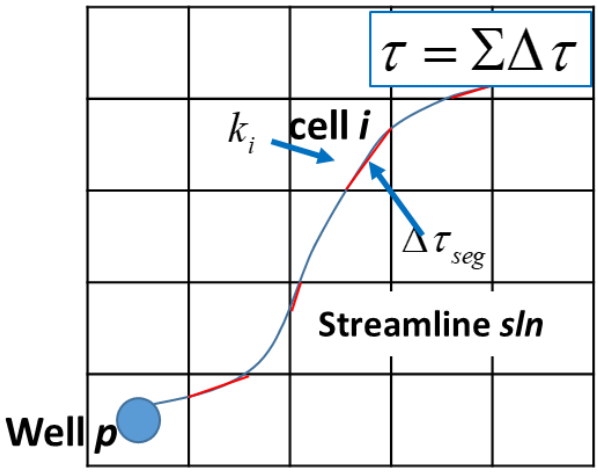

Figure 3.2: Grid block property association with saturation travel time to a producer

Let's denote the sensitivity of a grid block with a variable $sens$, superscripted by the associated producer p and streamline sln, and subscribed by the grid block id i as in Eq. 3.15.

$$sens_i^{p,sln} = \frac{\delta t_p}{\delta k_i}\Big|_{\text{sln}} = -\frac{\Delta\tau_{seg}^{p,sln}}{k_i} \Big/ \frac{df_w}{dS_w}\Big|_{S_{wf}} \tag{3.15}$$

So far, the sensitivity formula for a single grid block along a single streamline has been established. A grid block may be penetrated by multiple streamlines. And the final sensitivity for a single grid block should integrate calculations for all the corresponding streamline segments as in Eq. 3.16.

$$sens_i^{p} = \frac{\delta t_p}{\delta k_i} = \frac{\sum_{sln}\left(sens_i^{p,sln}\right)}{n\_sln} \tag{3.16}$$

where n_sln is the number of streamlines that ended in producer p.

When such sensitivity is applied, the calculated permeability change might be a negative value whose absolute value is even bigger than the prior value of the grid block

permeability, thus cause invalid permeability update. To avoid this, the sensitivity is formulated in terms of logarithm of permeability instead of permeability itself. So Eq. 3.15 and Eq. 3.16 are rewrite as below:

$$sens_i^{p,sln} = \frac{\delta t_p}{\delta \ln(k_i)}\Big|_{\text{sln}} = -\frac{\Delta\tau_{seg}^{p,sln}}{\frac{df_w}{dS_w}\Big|_{S_{wf}}} \tag{3.17}$$

$$sens_i^{p} = \frac{\delta t_p}{\delta \ln(k_i)} = \frac{\sum_{sln}\left(sens_i^{p,sln}\right)}{n\_sln} \tag{3.18}$$

The sensitivity by Eq. 3.18 will lead to permeability calibration in terms of $\Delta\ln(k_i)$, and it will make sure the calibration is valid regardless whether its value is negative or not, because permeability will finally be changed by a multiplier as in Eq. 3.19.

$$k_i^{updated} = k_i \cdot e^{\Delta\ln(k_i)} \tag{3.19}$$

So far, the formulation of legacy sensitivity is finished. As Eq. 3.18 shows, the final average value put equal weights to all the streamlines that ended in the same producer. However, the time of water break through is mainly determined by fast water dominated streamlines instead of all of them. The sensitivity along streamline which conveys small amount of water or has big time of flight will cause unnecessary permeability change and thus has negative impact on history matching. To avoid this, the travel time sensitivity is amended by streamline water fraction and streamline total time of flight.

The streamline water fraction is generated by Eq. 3.20.

$$f_w^{p,sln} = \frac{\sum_{seg}\left(f_{w,seg}^{p,sln}\right)}{n\_seg} \tag{3.20}$$

where $f_{i,seg}^{p,sln}$ is the water flow fraction at a single segment of the streamline. Its value can be fetched from the finite difference simulation result of the underlying grid block. The water fraction for a single streamline is the value averaged from water fractions of all segments.

The streamline total time of flight is generated by Eq. 3.21.

$$TOF_{total}^{p,sln} = \sum_{seg}\left(\Delta\tau_{seg}^{p,sln}\right) \tag{3.21}$$

where $\Delta\tau_{seg}^{p,sln}$ is the time of flight for a single segment of the streamline. The total time of flight for a single line is the value sumed from the time of flight for all segments.

The sensitivity for a single line segment is amended by weighting factor of water fraction and weighting factor of total time of flight, as given in Eq. 3.22-3.24

$$sens_i^{p,sln} = -\frac{\Delta\tau_{seg}^{p,sln}}{\left.\frac{df_w}{dS_w}\right|_{S_{wf}}} \cdot w_{f_w} \cdot w_{TOF} \tag{3.22}$$

$$w_{f_w} = \frac{f_w^{p,sln}}{max\left\{f_w^{p,sln}\right\}_p} \tag{3.23}$$

$$w_{TOF} = \frac{min\left\{TOF_{total}^{p,sln}\right\}_p}{TOF_{total}^{p,sln}} \tag{3.24}$$

where $max\{f_w^{p,sln}\}_p$ is the maximum streamline water fraction among all streamlines ended in producer p, and $min\{TOF_{total}^{p,sln}\}_p$ is the minimum streamline total time of flight among all streamlines ended in producer p.

The segments of streamline of high water fraction will be weighted close to one in terms of the first weighting factor, while the segments of streamline of low water fraction will be weighted close to zero.

The segments of streamline of small total time of flight will be weighted close to one in terms of the second weighting factor, while the segments of streamline of big total time of flight will be weighted close to zero.

3.3.2 Sensitivity Verification

The model we use for verification is a 50 by 50, 5-spot 2D heterogeneous model (Fig. 3.3). The model parameters are given in Tab. 3.1, and the relative permeability is shown in Fig. 3.4. The prior model is similar to the reference model in terms of permeability distribution but less heterogeneous. The difference between prior and reference model shows the model calibration expected in the water cut history matching. And water cut curves (Fig. 3.5) shows the data misfit between prior model and reference model.

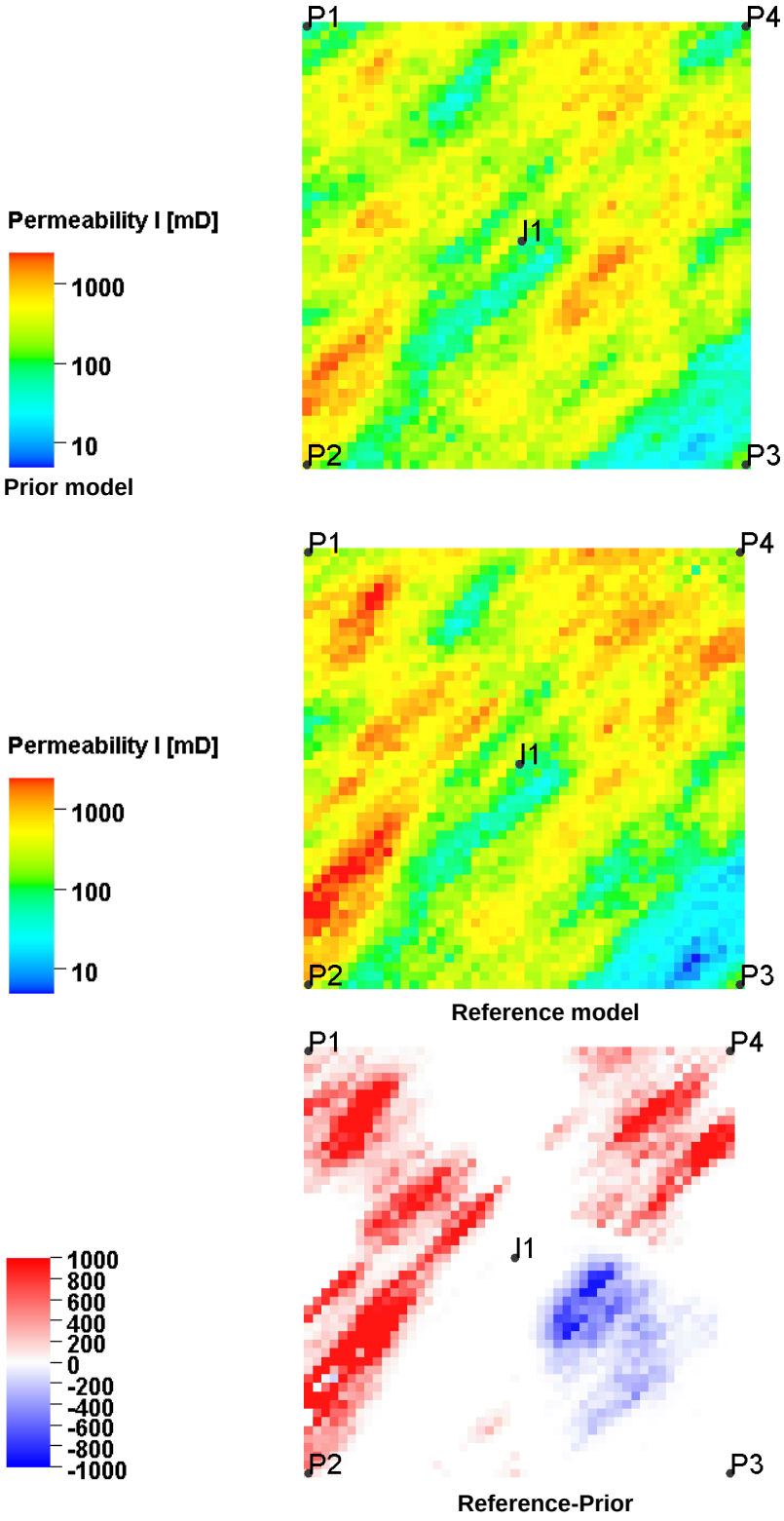

Figure 3.3: Permeability distributions for sensitivity verification

Table 3.1: Reservoir, fluid and rock properties for 2D five spot model

Parameter	Symbol	Unit	Value
Grid dimension	*ni, nj, nk*	-	50, 50, 1
Cell size	*DX, DY, DZ*	*ft*	32.8, 32.8, 32.8
Oil density	ρ_o	lb/ft^3	52
Oil viscosity	μ_o	*cp*	0.29
Oil compressibility	Co	psi^{-1}	3.4E-5
Water density	ρ_w	lb/ft^3	63
Water viscosity	μ_w	*cp*	0.31
Water compressibility	Cw	psi^{-1}	3.3E-6
Rock compressibility	Cr	psi^{-1}	8.1E-6

*PVT values for oil are at the reference pressure of 2897.1 psi
*Values for water and rock are at the reference pressure of 5863.8 psi
*Density is surface condition (14.7 psi)

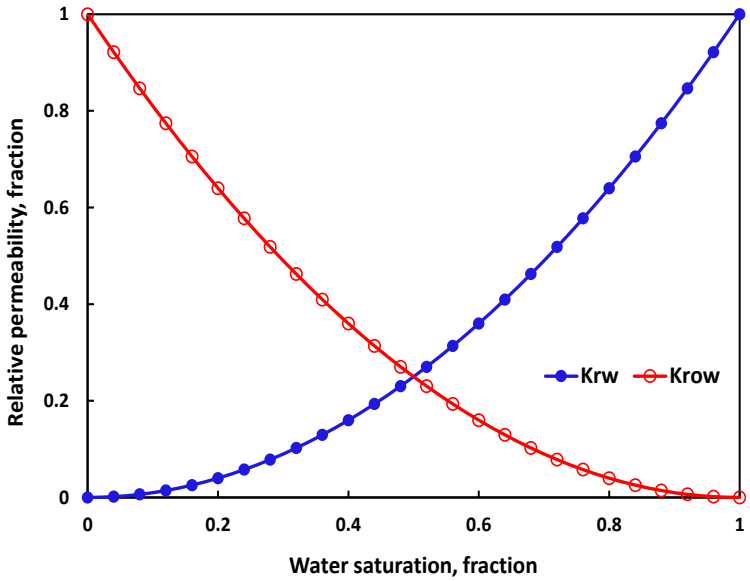

Figure 3.4: Oil-water relative permeability data for 2D five spot synthetic model

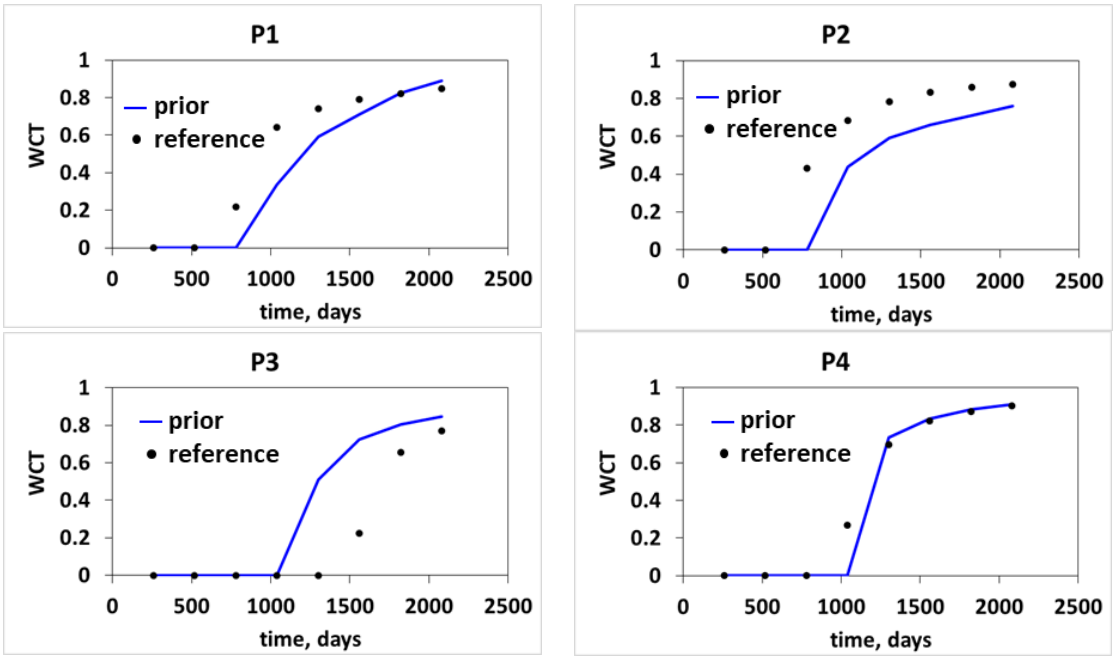

Figure 3.5: Water cut curves for producers in prior and reference model

The history matching is conducted in 2 scenarios. For the first scenario, geological model is calibrated by amended travel time sensitivity. For the second scenario, geological model is calibrated by the legacy travel time sensitivity. The sensitivities generated in this two scenarios are compared with pertubation sensitivity (Fig. 3.6). And the amended sensitivity shows higher similarity to the pertubation sensitivity than the legacy sensitivity.

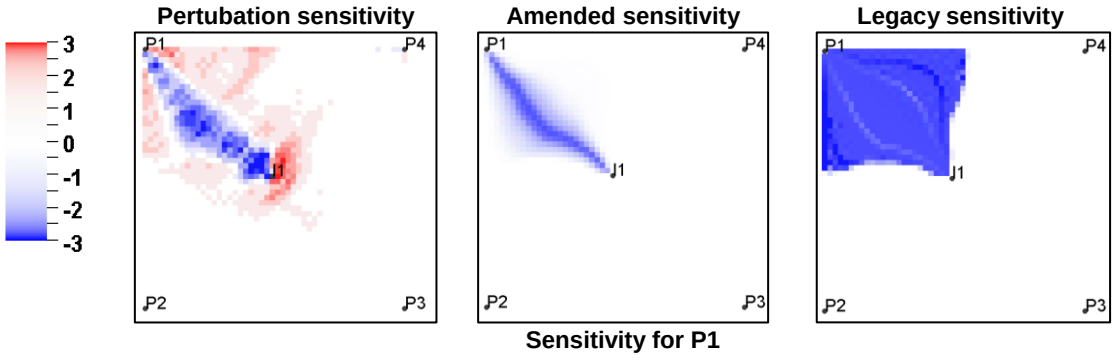

Figure 3.6: Travel time sensitivity compared with the pertubation method

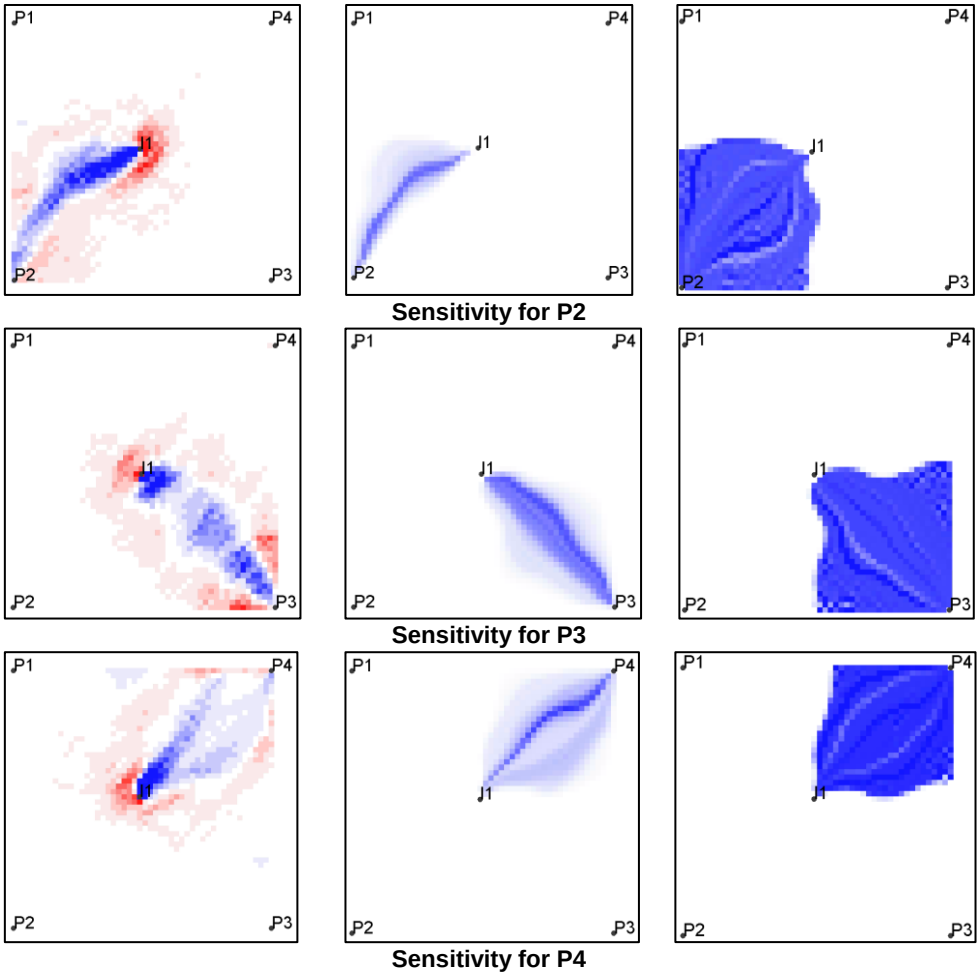

Figure 3.6 Continued.

The geological model is calibrated by ten iterations totally, the calibration by amended sensitivity shows faster datamisfit drop than the legacy sensitivity (Fig. 3.7), and the overall calibration by amended sensitivity is closer to the required calibration by reference model (Fig. 3.8).

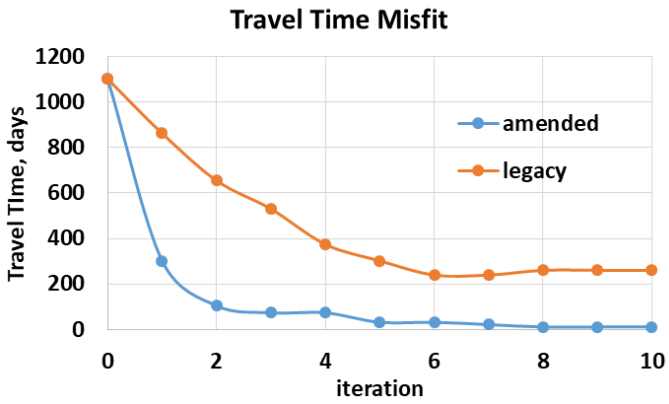

Figure 3.7: Travel time misift comparison

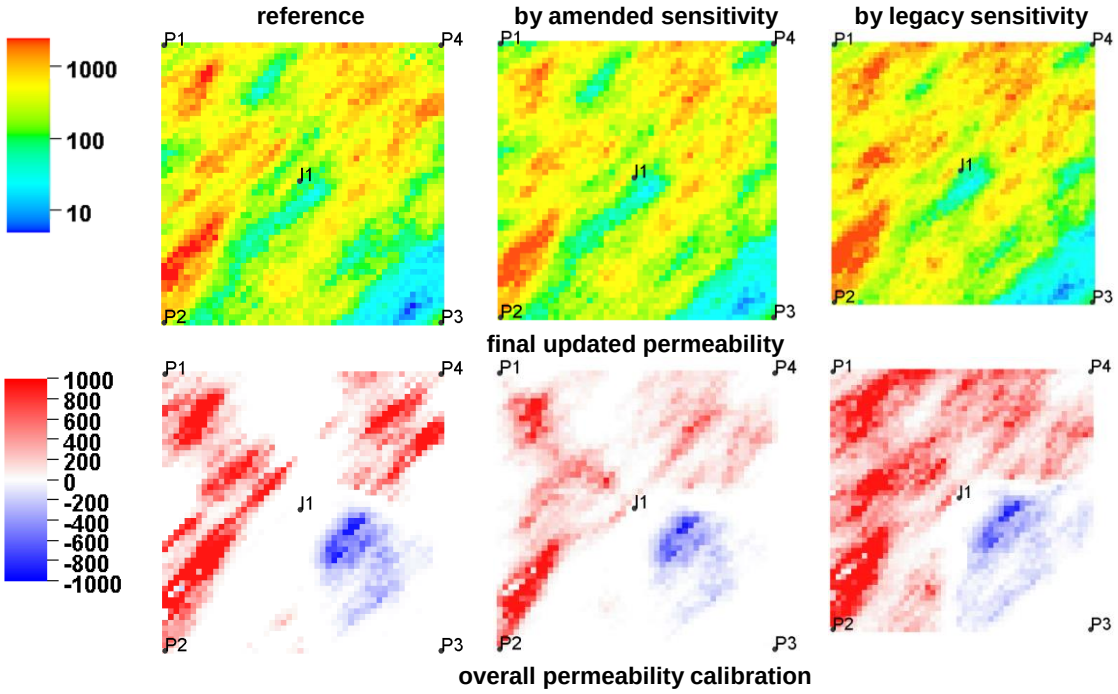

Figure 3.8: Comparison of final updated model and overall calibration

In terms of water cut curves, the amended sensitivity also has more favourable data match (Fig. 3.9).

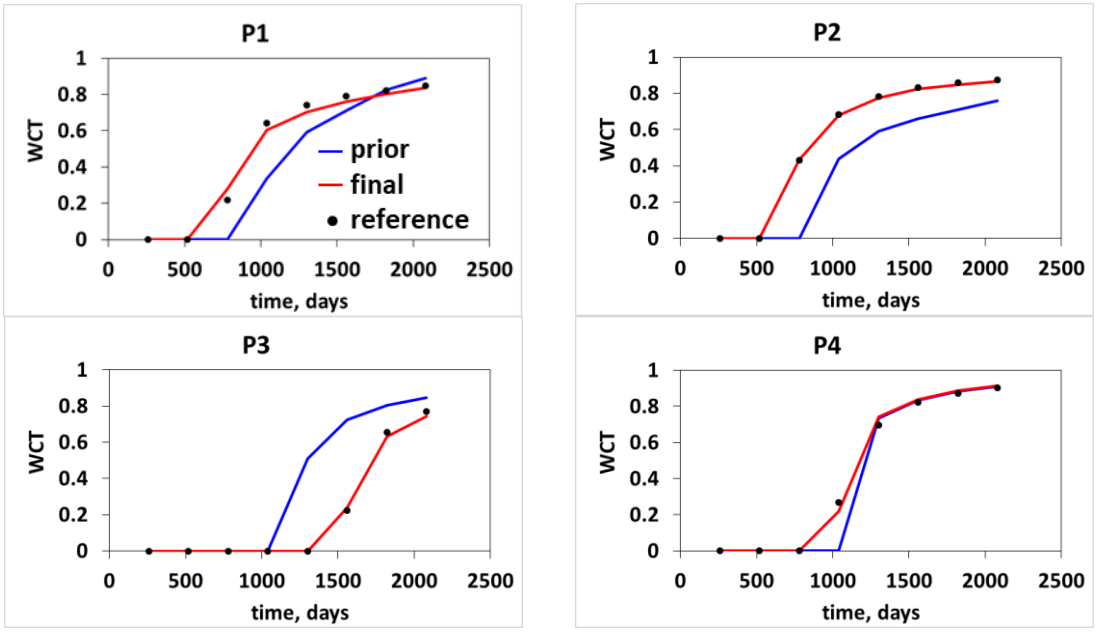

by amended sensitivity

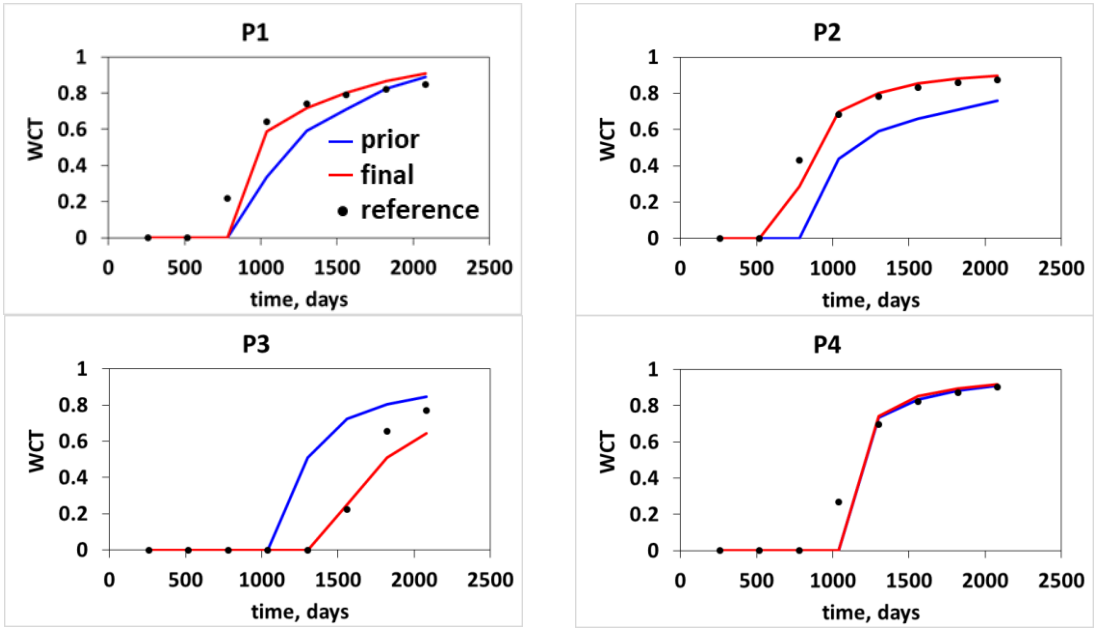

by legacy sensitivity

Figure 3.9: Water cut curves of prior model and final updated models by amended sensitivity and legacy sensitivity

From all the above comparisons between history matching by amended sensitivity and legacy sensitivity, we can see that the weighting factors of streamline water fraction

and streamline total time of flight can improve the accuracy of estimation of sensitivity values, and thus generate more favorable history matching results.

3.4 Novel Implementation of Bottom Hole Pressure Sensitivity

The grid property along a streamline also have an impact on the value of bottom hole pressure of the producer where the streamline ends, and the strength of the impact, which is often called bottom hole pressure sensitivity, can be formulated as an analytical solution (Tanarka 2014). However, the previous study and application is restricted to waterflood of oil field. When it comes to a gas reservoir, usually developed by depletion only, the legacy method doesn't apply.

The challenges lie in two aspects. First, the flux along a streamline in a gas reservoir is highly variable and the legacy formula for pressure drop sensitivity and weighting method doesn't apply in this situation. Second, the streamline itself is also highly variable in the history of gas reservoir depletion. The producers are often put into production at different times, thus making the streamlines distribution quite different from time to time.

In this section, we first derive the bottom hole pressure sensitivity along streamlines, which is valid for gas reservoirs developed by depletion where a streamline starts from a stagnation point and ends in a producer. Then a new grid flux based weighting method is proposed to average streamline segment sensitivities into grid blocks. Finally, the sensitivity for different time steps are weighted by their elapsed times to generate the final sensitivity. The novel sensitivity's accuracy is verified by the perturbation sensitivity.

3.4.1 Mathematical Formulation

The bottom hole pressure of a producer p is evaluated by the pressure drop along streamline from a stagnation point, or far field in the reservoir, to the well bore (Fig. 3.10).

The streamline segments are joined by nodes (m=1,2,…,n) on the intersection of grid blocks, and the first node sits at the well bore. The total pressure drop is the summation of pressure drop along segments.

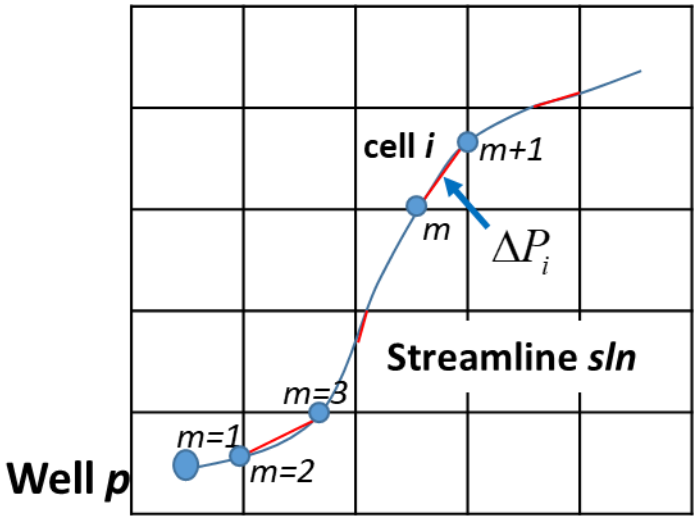

Figure 3.10: Pressure drop along streamline from deep reservoir to well bore

The pressure of far field in the reservoir is approximated by field pressure $\bar{P}$, which is only slightly influenced by local geological model calibration and can be treated as not sensitive to local permeability change.

$$BHP_p = \bar{P} - (\Delta P_1 + \Delta P_2 + \cdots + \Delta P_i + \cdots + \Delta P_n) \tag{3.25}$$

By Darcy's law, the pressure drop within a streamline segment in grid block i can be written as

$$\Delta P_i^{sln} = -\frac{q_i^{sln}}{\lambda_{rt,i} k_i} \frac{L_i}{A_i} + \bar{\rho}_i g \Delta D_i \tag{3.26}$$

where λ_{rt} is total relative mobility and q_i^{sln} is the fluid rate carried by this streamline segment in grid block i. The partial derivatives of pressure drop with respect to the permeability is given in Eq. 3.27 or Eq. 3.28

$$\frac{\partial \Delta P_i^{sln}}{\partial k_i} = \frac{q_i^{sln}}{\lambda_{rt,i}} \frac{L_i}{A_i} \frac{1}{k_i^2} \tag{3.27}$$

$$\frac{\partial \Delta P_i^{sln}}{\partial k_i} = -\frac{\Delta P_i^{sln} - \bar{\rho}_i g \Delta D_i}{k_i} \tag{3.28}$$

In a case of waterflood, the oil is mainly produced by fluid displacement, and the flux carried by a streamline is slightly changed along streamline, thus Eq. 3.27 is usually used to calculate the pressure drop sensitivity. However, in a highly compressible gas reservoir, the actual fluid rate carried by streamline is significantly variable and can't be estimated accurately in each streamline segment. In such case, Eq. 3.28 is used as a more general formula for pressure drop sensitivity calculation, and the main task becomes the implementation of method to estimate pressure drop within a streamline segment. The novel implementation will be presented in the next session.

By combing Eq. 3.25 and Eq. 3.28, the bottom hole pressure sensitivity estimated by a single streamline segment within grid block *i* is given in Eq. 3.29.

$$sens_i^{p,sln} = \left.\frac{\partial BHP_p}{\partial k_i}\right|_{\text{sln}} = -\frac{\partial \Delta P_i^{sln}}{\partial k_i} = \frac{\Delta P_i^{sln} - \bar{\rho}_i g \Delta D_i}{k_i} \tag{3.29}$$

When such sensitivity is applied, the calculated permeability change might be a negative value whose absolute value is even bigger than the prior value of the grid block permeability, thus cause invalid permeability update. To avoid this, the sensitivity is formulated in terms of logarithm of permeability instead of permeability itself. So Eq. 3.29 is rewritten as below:

$$sens_i^{p,sln} = \left.\frac{\delta BHP_p}{\delta \ln(k_i)}\right|_{\text{sln}} = \Delta P_i^{sln} - \bar{\rho}_i g \Delta D_i \tag{3.30}$$

The gravity potential change along streamline is easily made as the calculation of average density and depth change are clear. The next session give the details about how to estimate the pressure change along streamline by directly using the simulation result.

3.4.2 Implementation of Pressure Drop Estimation in Streamline Segments

The pressure drop along a streamline segment is estimated by the pressure difference between the streamline entrance point and exit point on cell faces. And the pressure at different position in the grid is interpolated by grid pressure at grid block center. The involved grid bocks are called the neighborhood for interpolation. In this section, we first present the interpolation in 2D case, then extended the formula to 3D case. For a grid with non-neighbor connections, a simple method about how to create the interpolation neighborhood is also demonstrated, thus the novel implementation will also be valid for faulted and fractured reservoir models.

2D Pressure Interpolation

The selection of grid blocks which will be used to interpolate pressure value depends on the position of the request point on cell face (Fig. 3.11). Node *m* is located where is surrounded by cell centers of cell (i-1, j-1), (i, j-1), (i-1, j), and (i, j). So these four cells are selected as the interpolation environment for P_m. During streamline tracing, the coordinates of point *m* in the unit space of cell (*i, j*) is recorded, and it is used to calculate the coordinates of relative position in the interpolation environment. Finally, the pressure

at position *m* is interpolated by the give cell center pressures and the relative position coordinates.

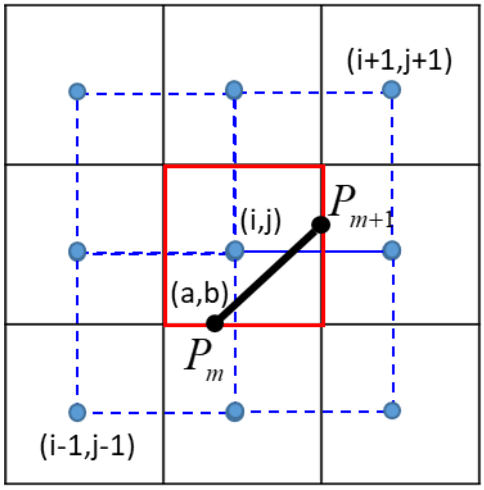

Figure 3.11: Pressure interpolation environment in 2D case

The above presented procedures can be formalized as below.

1. Select neighborhood $N(I, J)$ according to unit coordinates (a, b) within cell (i, j). For a 2D case, the interpolation neighborhood includes four cells, and I equals to the smallest i coordinate among the four cells, while J equals to the smallest j coordinate among the four cells. Thus, cell (I, J), $(I+1, J)$, $(I, J+1)$, and $(I+1, J+1)$ construct the neighborhood of the given point. And value of I and J is determined by the relative position of given point in cell (i, j), as is given in Eq. 3.33 and Eq. 3.34.

$$I = \begin{cases} i-1 & a \in [0, 0.5] \\ i & a \in (0.5, 1] \end{cases} \tag{3.33}$$

$$J = \begin{cases} j-1 & b \in [0, 0.5] \\ j & b \in (0.5, 1] \end{cases} \tag{3.34}$$

2. Generate unit coordinates (α, β) which describes the relative position of given point within neighborhood $N(I, J)$. The value of α or β is also a function of a and b.

$$\alpha = \begin{cases} 0.5 + a & a \in [0, 0.5] \\ a - 0.5 & a \in (0.5, 1] \end{cases} \tag{3.35}$$

$$\beta = \begin{cases} 0.5 + b & b \in [0, 0.5] \\ b - 0.5 & b \in (0.5, 1] \end{cases} \tag{3.36}$$

3. Interpolate node pressure by grid pressure. The pressure at selected node is interpolated by the cell center pressure of the four cells within the neighborhood.

$$\begin{aligned} P_{node} = {} & P_{I,J}(1-\alpha)(1-\beta) + \\ & P_{I,J+1}(1-\alpha)\beta + \\ & P_{I,J+1}\alpha(1-\beta) + \\ & P_{I+1,J+1}\alpha\beta \end{aligned} \tag{3.37}$$

In some circumstances, some of the four neighborhood pressures might refer to invalid grid block. For example, when the streamline node sits at the bottom face of cell (1, 2) with (a, b)=(0.1, 0), then $P_{I,J}$ and $P_{I,J+1}$ refers to pressure of cell (0, 1) and cell (0, 2), which are non-existed cells. And sometimes the referred cells exist but is inactive. If any of these happens, just replace the invalid cell pressure with $P_{i,j}$, the pressure of the cell the streamline segment belongs to.

3D Pressure Interpolation

The 2D linear interpolation is easily extended to 3D cases. In 3D model, the interpolation environment consists of eight cells instead of four. And the similar steps and formulas are given as below.

1. Select neighborhood $N(I, J, K)$ according to unit coordinates (a, b, c) within cell (i, j, k). The formulas for I and J are the same and can be referred in Eq. 3.33 and Eq. 3.34. The formulas for K is given in Eq. 3.38.

$$K = \begin{cases} k-1 & c \in [0, 0.5] \\ k & c \in (0.5, 1] \end{cases} \tag{3.38}$$

2. Generate unit coordinates (α, β, γ) which describes the relative position of given point within neighborhood $N(I, J, K)$. The value of α or β is available in Eq. 3.35 and Eq. 3.36. The value of γ is given in Eq. 3.39

$$\gamma = \begin{cases} 0.5 + c & c \in [0, 0.5] \\ c - 0.5 & c \in (0.5, 1] \end{cases} \tag{3.39}$$

3. Interpolate node pressure by grid pressure. The pressure at selected node is interpolated by the cell center pressure of the eight cells within the neighborhood.

$$\begin{aligned} P_{node} = {} & P_{I,J,K}(1-\alpha)(1-\beta)(1-\gamma) + P_{I,J,K+1}(1-\alpha)(1-\beta)\gamma \\ & P_{I,J+1,K}(1-\alpha)\beta(1-\gamma) + P_{I,J+1,K+1}(1-\alpha)\beta\gamma \\ & P_{I,J+1,K}\alpha(1-\beta)(1-\gamma) + P_{I,J+1,K+1}\alpha(1-\beta)\gamma \\ & P_{I+1,J+1,K}\alpha\beta(1-\gamma) + P_{I+1,J+1,K+1}\alpha\beta\gamma \end{aligned} \tag{3.40}$$

Just as it is discussed in 2D linear interpolation, if any of the neighborhood pressures refers to invalid grid block, just replace the invalid cell pressure with $P_{i,j}$, the pressure of which cell the streamline segment belongs to.

Pressure Interpolation in NNC

If the grid cells are connected by non-neighbor connections, boundary layer is constructed for streamline tracing (Fig. 3.12). In such case, boundary layer is treated as the extension of cell (i, j, k) and all its cells share the same pressure of $P_{i,j,k}$. And pressure of streamline node m+1 on boundary layer is interpolated within the neighborhood created by boundary layer and its connected cells.

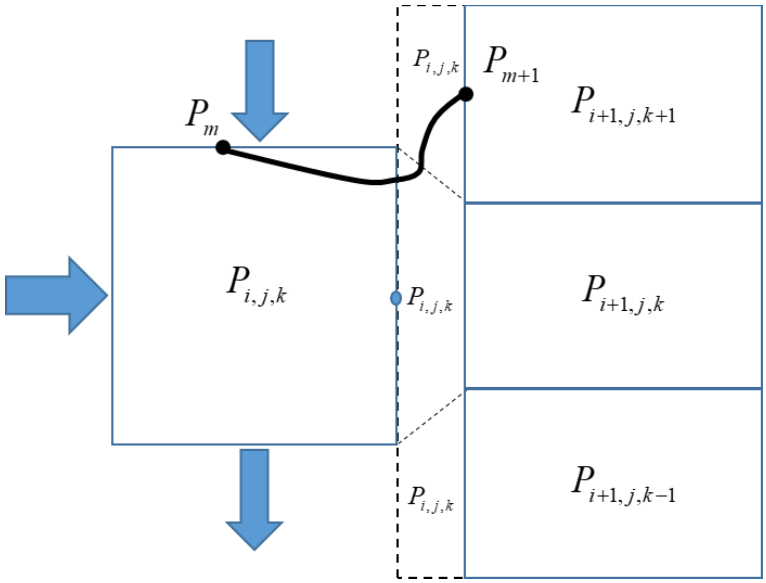

Figure 3.12: Interpolation environment creation for non-neighbor connection

3.4.3 Average Sensitivity by Grid Flux and Elapsed Time

Now the bottom hole pressure sensitivity on each streamline segment is developed. A grid block usually contains multiple streamline segments and have different streamline

segments at different time. The sensitivity for a grid block is an average value of all the streamline segment sensitivity values at different times. The averaging is done by using the weighting factors based on grid flux, and elapsed time.

The sensitivity of a grid block for a single time step is usually weighted by the total flux carried by the streamlines (Fig. 3.13), and the total bypass flux is normally represented by the number of streamlines which have equal rate for incompressible flow. For a gas reservoir, the flux cannot be easily estimated by streamline numbers, instead we use grid flux represented by the summation of absolute values of flux on each cell face.

$$sens_i^{p,t} = \frac{\partial BHP_p}{\partial k_i} = \frac{\sum_{seg}\left(sens_i^{p,seg}\right)}{n\_sln} \cdot \frac{cell\_flux_i}{cell\_flux_{well\_cell}} \tag{3.31}$$

$$cell\_flux_i = \sum_{face} abs\left(flux_{face}\right) \tag{3.32}$$

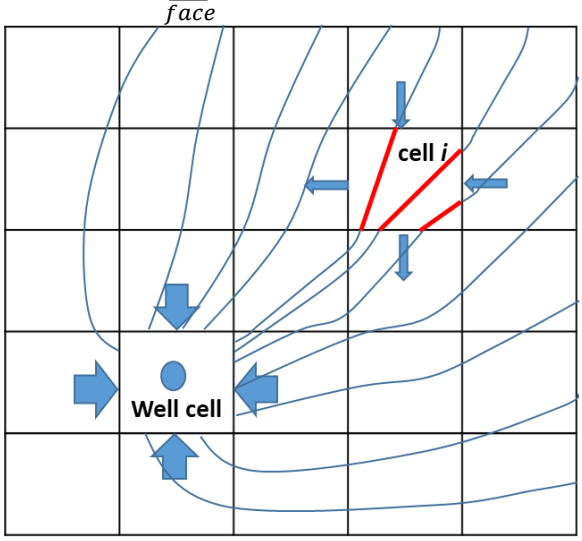

Figure 3.13: Average BHP sensitivity by grid flux

And the sensitivity for each time step is weighted by the elapsed time of the step to generate the final sensitivity for use in the model calibration (Fig. 3.14), and the formula is given as below.

$$sens_i^p = \frac{\partial BHP_p}{\partial k_i} = \frac{\sum_m \left(sens_i^{p,t_m} \Delta t_m\right)}{\sum_m (\Delta t_m)} \tag{3.33}$$

Where $\Delta t_m$is the elapsed time of step m.

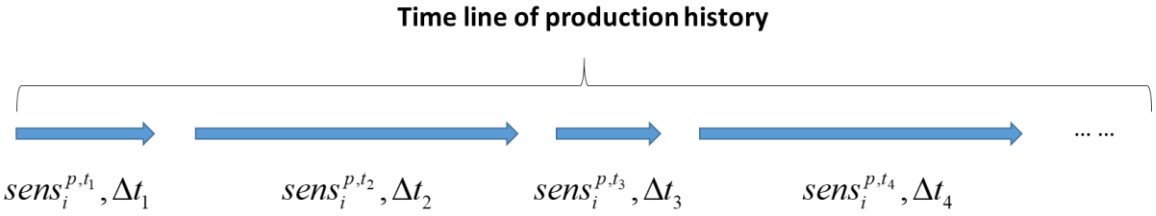

Figure 3.14: Average BHP sensitivity by elapsed time of each step

3.4.4 Validation by Perturbation Method

The proposed bottom hole pressure sensitivity is validated by the numerical sensitivity by perturbation method. The validation synthetic case is a gas reservoir with 2 producers (Fig. 3.15). The first producer is put to work at the beginning at the rate of 1000 Mscf/day, the second producer is put to work since the second month at the rate of 1000 Mscf/day. The streamlines of the two months are quite different (Fig. 3.16).

Table 3.2: Model parameters of BHP sensitivity validation case

Parameter	Symbol	Unit	Value
Grid dimension	*ni, nj, nk*	-	50, 50, 1
Cell size	*DX, DY, DZ*	*ft*	32.8, 32.8, 32.8
Porosity	ϕ	-	0.3
Gas density	ρ_g	lb/ft^3	52
Rock compressibility	C_r	psi^{-1}	8.1E-6

Table 3.3: Gas property of BHP sensitivity validation case

Pressure, psi	Volume factor, rb/Mscf	Viscosity, cp
14.65	178.1076	0.01429
400	9.0906	0.01461
600	6.0076	0.01487
800	4.4705	0.01519
1000	3.5532	0.01541
1500	2.3403	0.01611
2000	1.7467	0.01707
2500	1.4010	0.01804
3000	1.1784	0.01905
3500	1.0254	0.02020
4000	0.9148	0.02136
5000	0.7676	0.02376

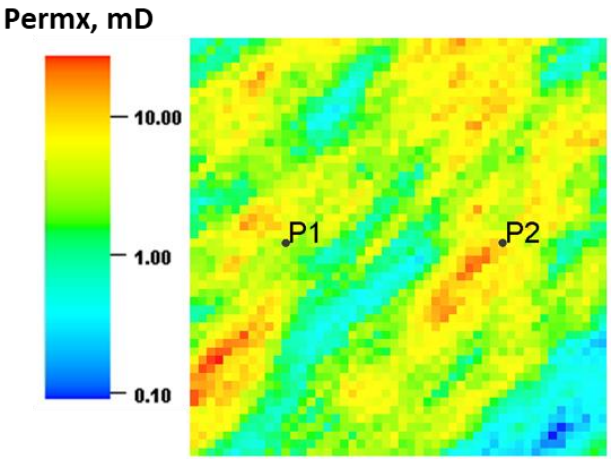

Figure 3.15: Permeability of BHP sensitivity validation case

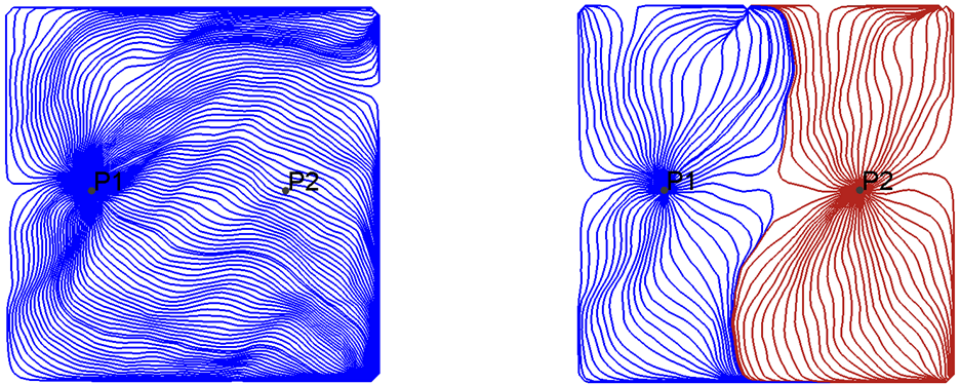

1st month **2nd month**

Figure 3.16: Streamline distribution of BHP sensitivity validation case

The sensitivity by the proposed novel implementation is compared with the numerical sensitivity by perturbation method (Fig. 3.17). And the sensitivity here is calculated by perturbation of permeability instead of logarithm of permeability for the convenience of perturbation method. The results from both methods show good agreement.

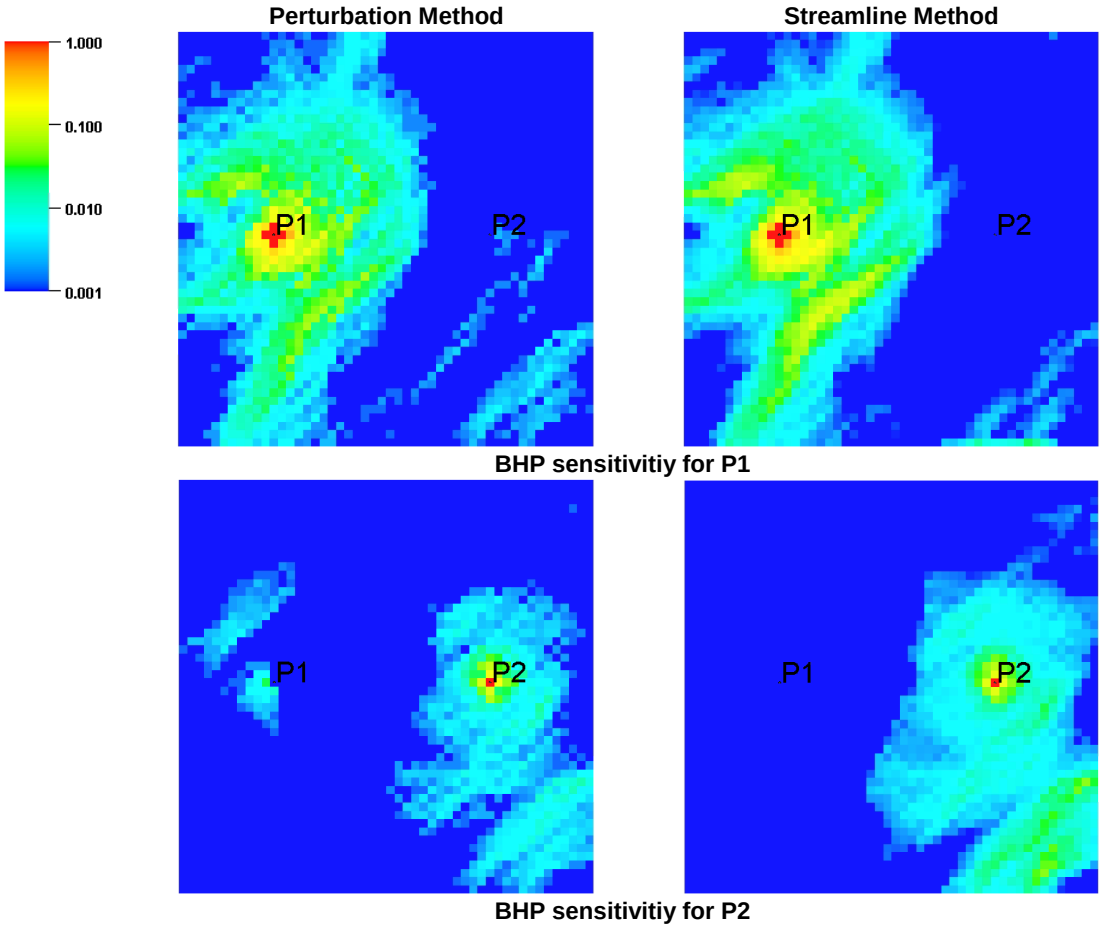

Figure 3.17: Producer bottom hole pressure sensitivity by perturbation method (left) and proposed method (right)

3.5 Field Application of Gas Reservoir

The feasibility of the newly developed sensitivity is tested by a field application to history match the bottom hole pressure of a high pressure high temperature tight gas reservoir in the Tarim basin, China. The wells are located at an average depth of 7500 meters and the pressure is in excess of 18,000 psi. The novelty of our approach lies in the application of streamlines derived from dual porosity finite-difference simulation to facilitate history matching and well placement optimization in a gas reservoir.

A hierarchical multi-scale approach is used for history matching high resolution reservoir models using a sequence of coarse-scale and fine-scale models. The proposed multi-scale history matching approach consists of two-stages: global and local. For the global stage, we calibrate large scale static and dynamic parameters using an evolutionary algorithm. The global calibration uses coarse-scale simulations and applies regional multipliers to match well rates and field average pressure. For the local stage, we calibrate fracture cell properties using the newly implemented sensitivity to match the well bottom-hole pressures. The local-scale updating, which is typically the most time-consuming element, is carried out efficiently using analytic sensitivities computed from streamlines derived from dual porosity finite difference simulation. To our knowledge, this is the first time streamlines have been used to facilitate history matching of gas reservoirs. Based on the streamlines, we can visualize the evolution of the drainage volume for each well. The well drainage volume in conjunction with static reservoir properties is used to define a ‘depletion capacity map’ which is used for optimal infill well placement.

3.5.1 Methodology of Multiscale Approach

We propose a hierarchical multiscale calibration using global and local updates in both coarsened and fine grid (as shown in Fig. 3.18). The inclusion of multiscale approach is critical to history matching high resolution reservoir models because the initial integration process in the coarsened grid allows for significant reduction of simulation time, resulting in improved computational efficiency.

The fine scale model is first upscaled to coarsened scale, where a quality check process is necessary to ensure the model is upscaled properly. With large uncertainty in the static and dynamic parameters, sensitivity analysis is then carried out to identify the heavy-hitters. The global parameters calibration is aimed at matching and balancing the field level energy, while the local update is designed to match well by well production history. After the global update, the calibrated parameters and multipliers are transferred to the fine scale model. Then, local update is performed using the streamline technique. The streamline based sensitivity allows calibrating the permeability on each cell basis. It generally requires less than ten iterations for the local update if a good match is obtained at the global energy level.

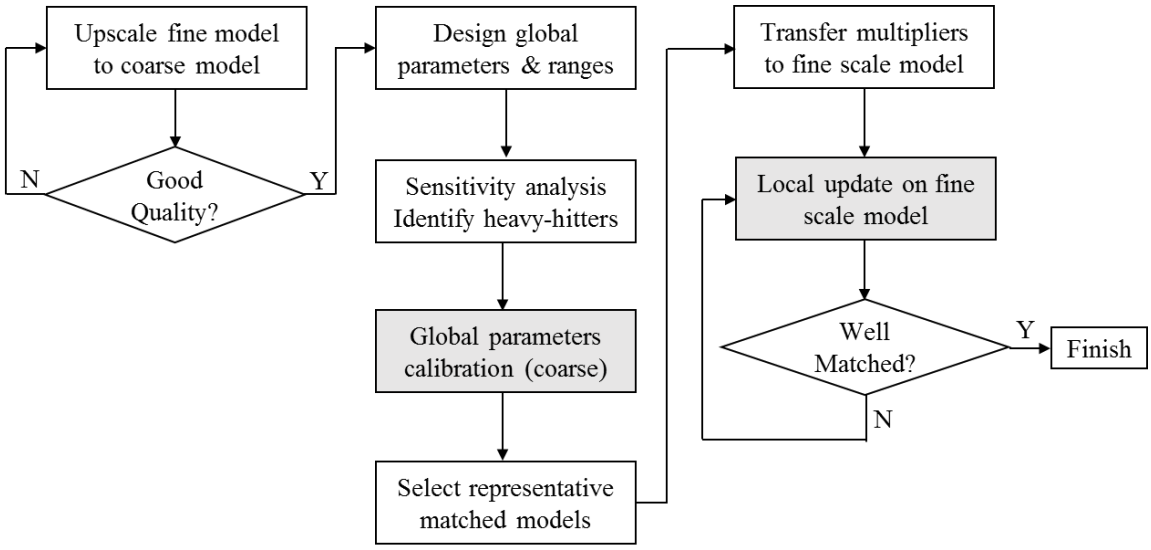

Figure 3.18: Overview of workflow for hierarchical and multiscale inversion

We have used the Genetic Algorithm (GA), one of the evolutionary algorithms, for calibration of global parameters. The genetic algorithm imitates biological principals of evolution – survival of the fittest. It has been extensively applied to the history matching problem (Bittencourt and Horne 1997; Floris et al. 2001; Romero and Carter 2001; Schulze-Riegert et al. 2002; Williams et al. 2004). Usually, solutions are represented as binary strings of 0's and 1's. The full binary string containing all variables is called a genome or chromosome. The evolution starts from a population of randomly generated individuals. In each generation, the fitness of every individual in the population is evaluated. Multiple individuals are stochastically selected from the current population (based on their fitness), and modified (recombined and possibly randomly mutated) to form a new population. The new population is then used in the next iteration of the algorithm. Commonly, the algorithm terminates when either a maximum number of

generations has been produced, or a satisfactory fitness level has been reached for the population.

To evaluate the objective function and thus the fitness of a newly generated genome, we first check the proxy value for that genome. If it has a value smaller than a predefined threshold then a flow simulation will be carried out. Otherwise it is assigned a large objective score with zero fitness and will be discarded in the next GA generation. A flowchart of all the steps is shown in Fig. 3.19.

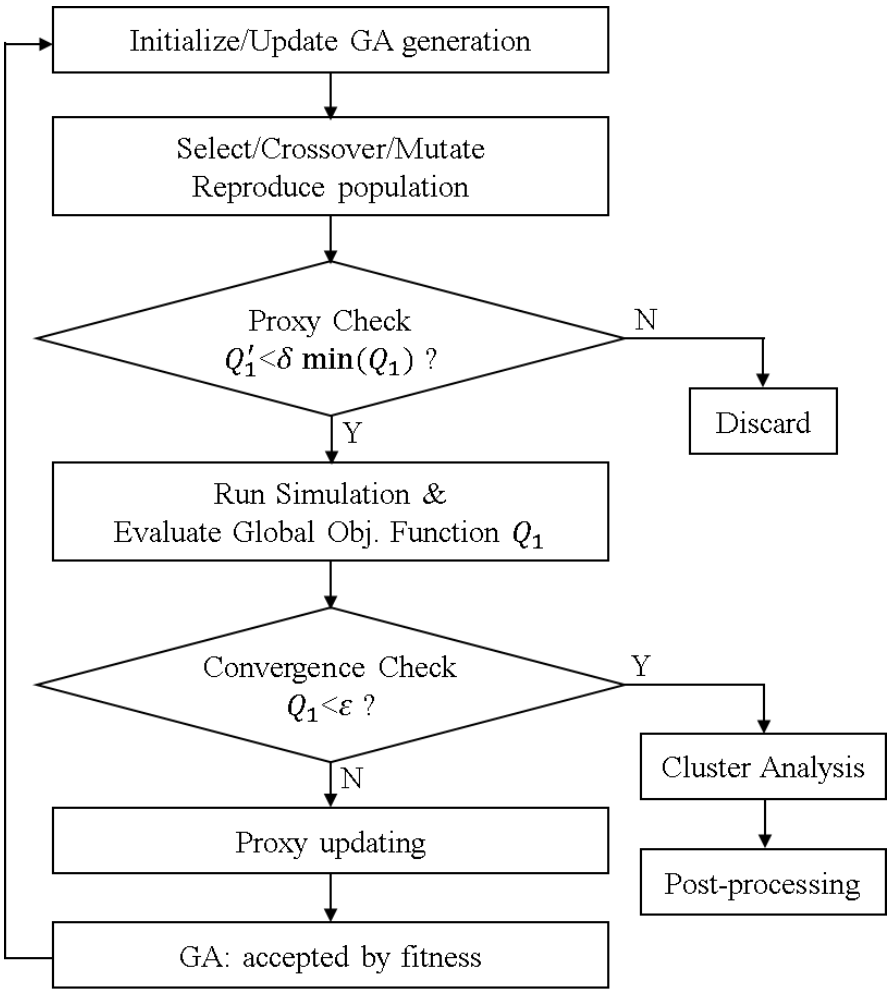

Figure 3.19: Flowchart of GA with proxy

Inversion process using streamline based sensitivity is demonstrated in Fig. 3.1. With the flux information from conventional simulator, the streamline is traced starting from wells and sensitivity is calculated. After sensitivity computation, we calibrate the local permeability to match the bottom hole pressure response for each well.

3.5.2 Tarim Field Tight Gas Reservoir

This hierarchical multiscale history matching workflow is applied to Keshen8 reservoir block (Tab. 3.4), which is a tight gas reservoir at depth range of 5200m – 7700m. With such big depth underground, the tight gas reservoir has pressure of 18000 psi and temperature of 340 F^o.

Table 3.4: Reservoir parameters for HPHT tight gas reservoir

Parameter	Symbol	Unit	Value
Depth	h	m	5200-7700
Pressure	P	psi	18000
Temperature	T	F^o	340
Gas viscosity	μ_g	cp	0.04
Gas compressibility	c_g	psi^{-1}	2.0E-5
Matrix porosity	ϕ_m	-	0.035
Fracture porosity	ϕ_f	-	5.00E-06
Matrix permeability	k_m	mD	0.001-0.6
Fracture permeability	k_f	mD	0.01-1000

The formation is divided into 7 geological zones using the seismic surfaces and well top information. It has two major sealing faults one at north side and the other at south side, and there are 24 minor faults. The variogram of facies is calculated for each zone based on facies well logs and then populated to each grid with geostatistical technique. The facies distribution and faults are shown in Fig. 3.20. Five rock types (RT1,

RT2, RT3, RT4, and RT5) are identified based on the porosity logs and water saturation along with capillary pressure curves. RT1 is non-reservoir rock. It is found that the reservoir is in the region where the capillary pressure curve is vertical, therefore, constant water saturation is assigned for each rock type, which are 1.0, 0.85, 0.399, 0.352, and 0.287 respectively. The gas reservoir is located at top of incline formation and is supported by side aquifers. It is developed by 16 gas producers.

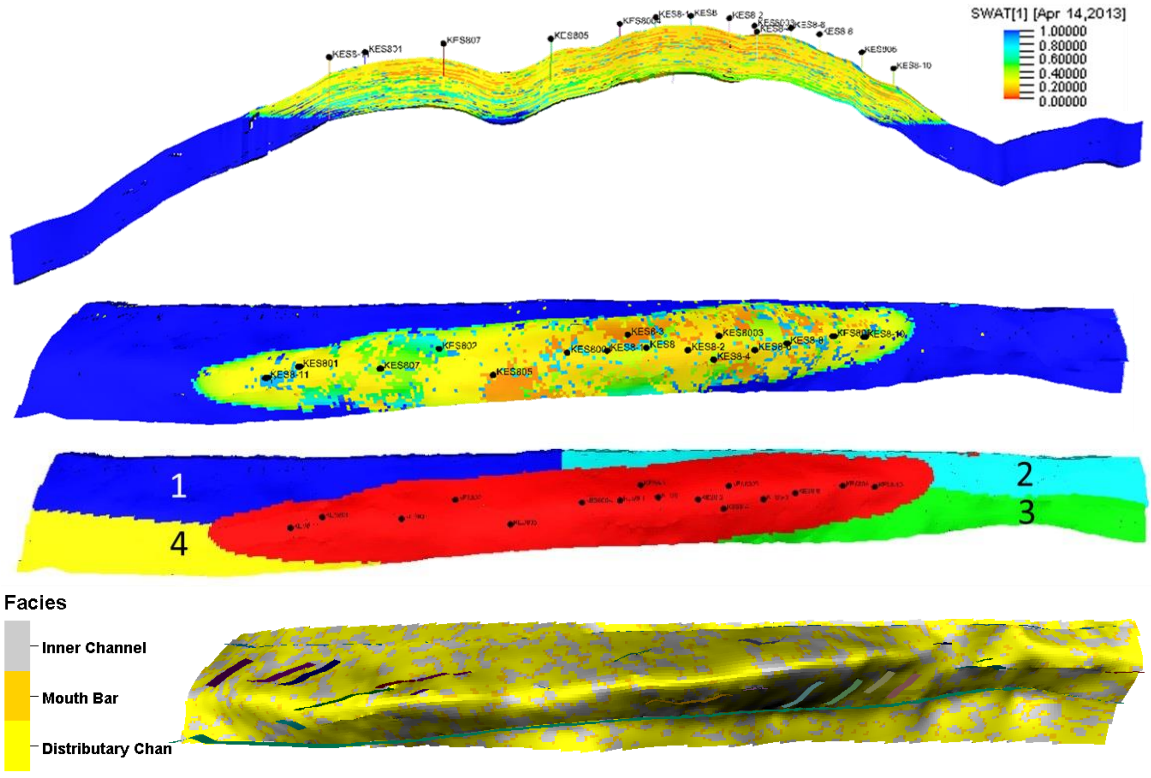

Figure 3.20: Aquifers and faults for HPHT tight gas field

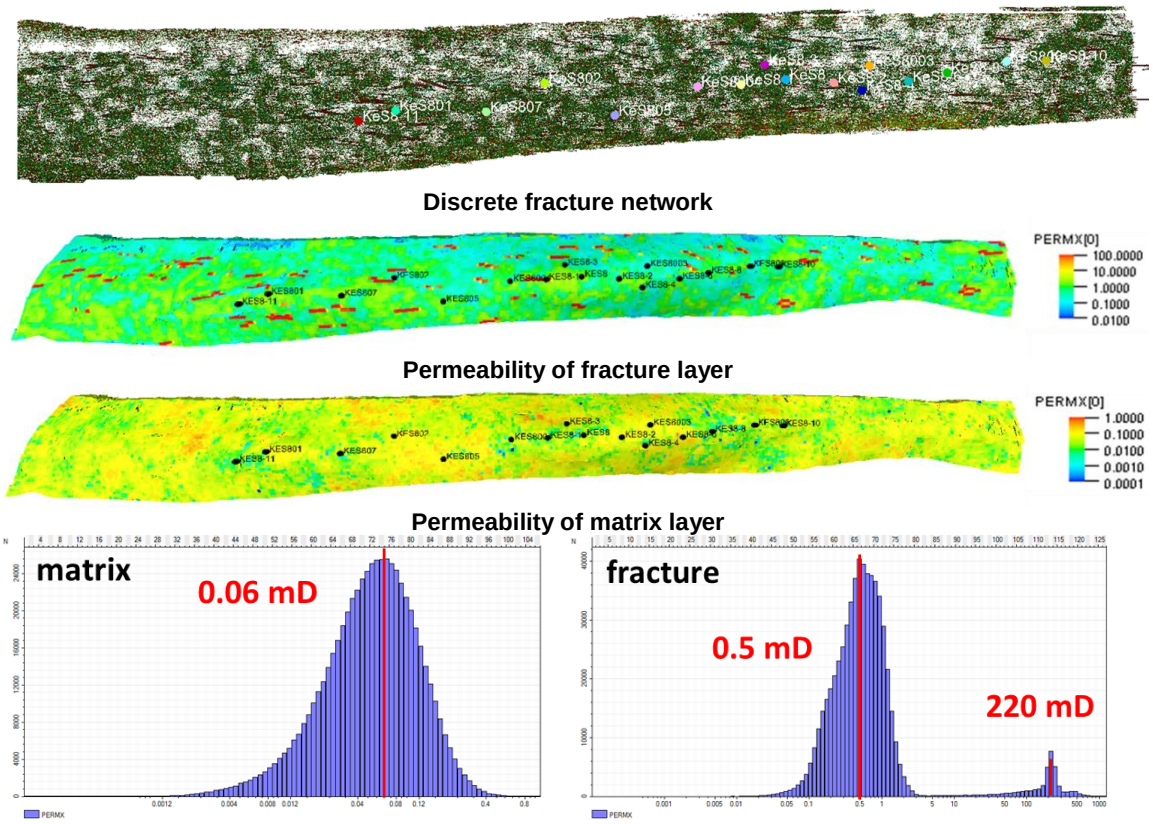

Figure 3.21: The DFN and dual porosity model for HPHT tight gas field

Dual porosity model is utilized to account for the effect of dense natural fractures. Discrete fracture network (DFN) is generated and then upscaled for each zone to get fracture permeability in X, Y, Z directions, fracture porosity and matrix-fracture transfer function. Fig. 3.21 shows the DFN for the first zone. The areal grid cell size of the simulation model is 100m×100m, resulting in about 1.5million cells (378×78×50). The reservoir is simulated under gas production rate constraint and the bottom-hole pressure is to be history matched.

The history data given for history matching consists of RFT data among 5 wells and flowing bottom-hole pressure data for each well. Genetic Algorithm is applied to

match the RFT data and streamline method is applied to match flowing bottom-hole pressure data.

Table 3.5: Time line of producers whose RFT data is measured

	RFT Measured	Well Starts
KES8	2012.11	2013.04.15
KES801	2013.12	2015.08.12
KES802	2013.11	2014.10.03
KES806	2014.02	2014.10.09
KES8003	2013.11	2014.10.20

Each RFT data was measured before the measured well began to produce. KES8 is the first well to produce, its RFT data is used for model initialization, and the following measured RFT values for other wells are used to calibrate the whole reservoir's energy level during simulation.

3.5.3 History Matching Result

Global Calibration using Genetic Algorithm

Our global matching approach closely follows the method outlined by Cheng et al. (2008) and Yin et al. (2010). Design of Experiments (DOE), Genetic Algorithm (GA) and Response Surface Methodology (RSM) are used for calibrating reservoir geological features at the global and regional scales. The global objective (misfit) function is defined as:

$$f(\mathbf{m}) = f(m_1, m_2, \dots, m_N) = ln|\Delta P_{RFT}| + ln|\Delta P_{BHP}| \qquad (3.34)$$

where multiple objectives are handled by using the logarithm of the absolute misfit in Eq. 3.34 rather than weighing the data based on their measurement errors, which are typically

not readily available. It is critical to select the correct uncertainty variables and their ranges.

For this dry gas reservoir, the 13 uncertainty parameters and the associated uncertainties are listed in Tab. 3.6. We assume a uniform distribution for each of the parameters. To evaluate the impact of various parameters, a sensitivity analysis is performed and the result is plotted using a tornado plot (shown in Fig. 3.22). The line in the middle shows the objective function value of the base model. We vary one parameter at a time and rerun the simulation to obtain the response.

From Fig. 3.22, based on the sensitivity results, the top 8 uncertainty parameters to be estimated via history matching are the permeability multiplier for seven zones, and water gas contact.

Table 3.6: Uncertain parameters and designed uncertainty ranges

Uncertainty Variables	Base	Low	High
Perm multiplier zone 1 (KMULT1)	1	0.1	50
Perm multiplier zone 2 (KMULT2)	1	0.1	50
Perm multiplier zone 3 (KMULT3)	1	0.1	50
Perm multiplier zone 4 (KMULT4)	1	0.1	50
Perm multiplier zone 5 (KMULT5)	1	0.1	50
Perm multiplier zone 6 (KMULT6)	1	0.1	50
Perm multiplier zone 7 (KMULT7)	1	0.1	50
Rock compressibility (RCOMP), 1/bar	2.0E-4	3.0E-5	3.0E-4
Water gas contact (WGC), m	5830	5800	5860
Aquifer PV multiplier region 1 (MULTPV1)	1	0.6	1.4
Aquifer PV multiplier region 2 (MULTPV2)	1	0.6	1.4
Aquifer PV multiplier region 3 (MULTPV3)	1	0.6	1.4
Aquifer PV multiplier region 4 (MULTPV4)	1	0.6	1.4

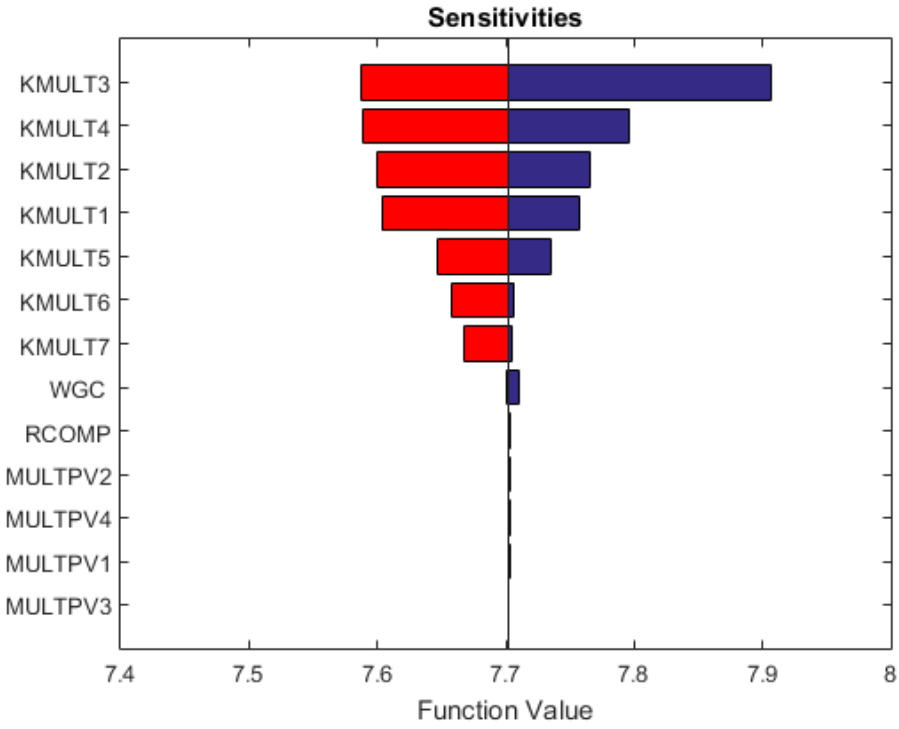

Figure 3.22: Sensitivity analysis of uncertain parameters

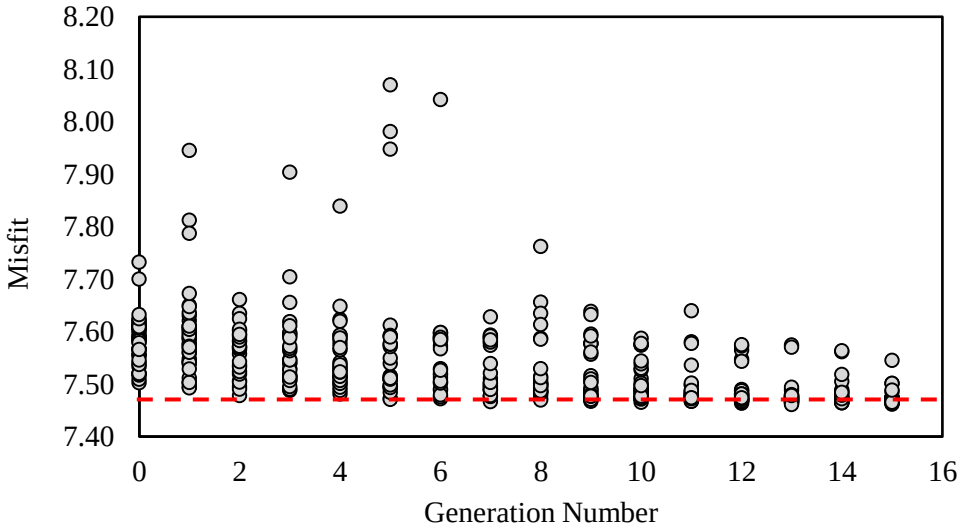

Figure 3.23: The misfit function versus generation number

The first stage global parameter calibration starts with initializing the proxy model, where 40 realizations are generated using Latin Hypercube Sampling (LHS) method and then evaluated. The genetic algorithm is carried out for 15 generations and each generation

has 40 realizations. The realizations of first generation are just randomly generated. Fig. 3.23 shows the misfit function, which is defined as Eq. 3.34, versus generation number. After all the simulations, we select the best model for second stage history matching. From Fig. 3.24, it can be seen that the energy of the reservoir is generally well matched for these selected models.

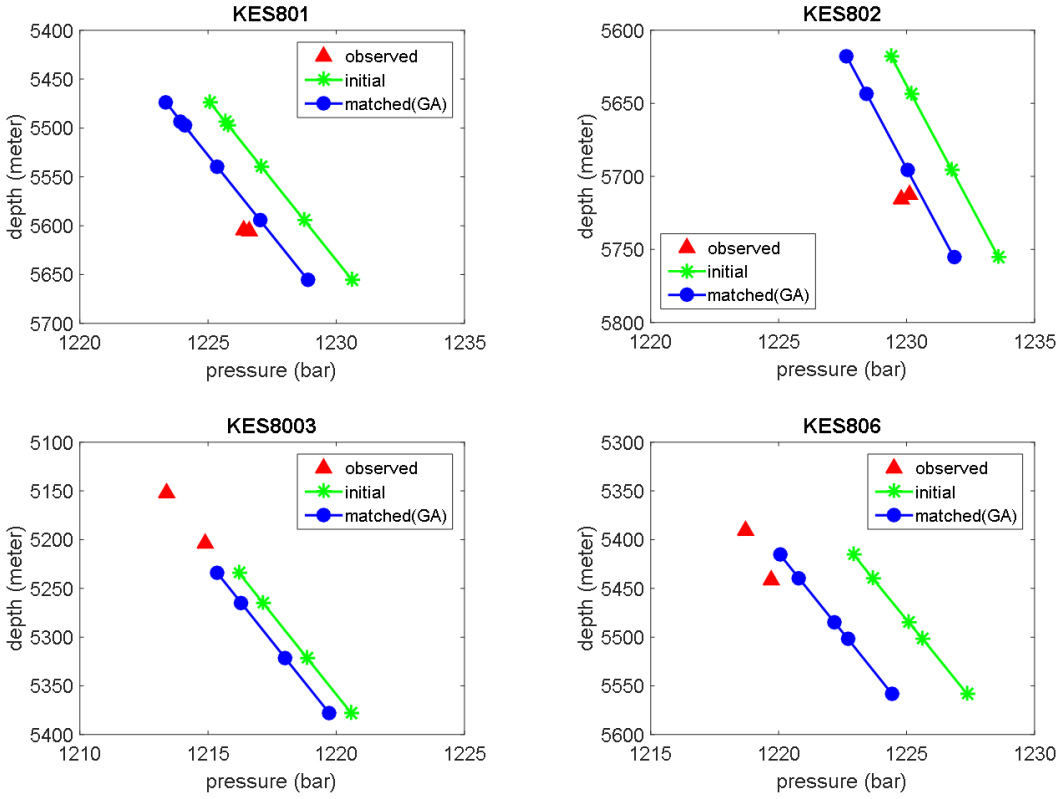

Figure 3.24: RFT data matching results

Fig. 3.25 is a bubble map shows the data misfit between simulation value and observed data (BHP) for each well. The x, y coordinates shows the wells' positions underground and the size of bubble shows the amount of BHP misfit. The hollow bubble shows the BHP misfit before global match and the green bubble shows the BHP misfit after global match.

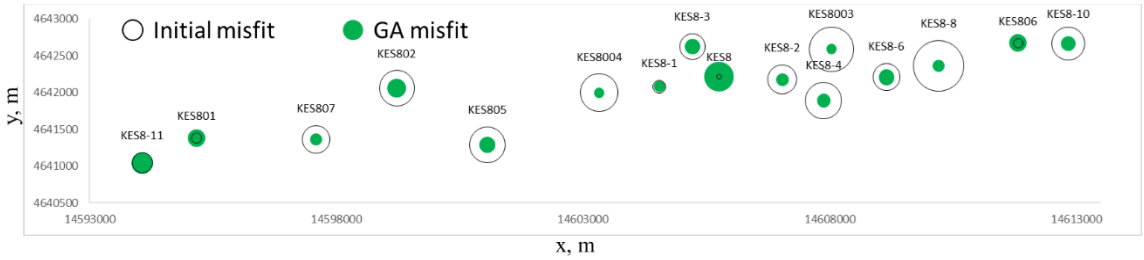

Figure 3.25: BHP data misfit bubble map for each well

Fig. 3.26 shows the misfit between simulation value and observed data (BHP) for each well at each time step. The black dot is the observed data, the blue line is the simulation value before global match and the green line is the simulation value after global match. Most of the wells have a bottom hole pressure data misfit drop, the local data misfit for wells of KES8, KES8-6, KES801, and KES8-11 are hardly decreased.

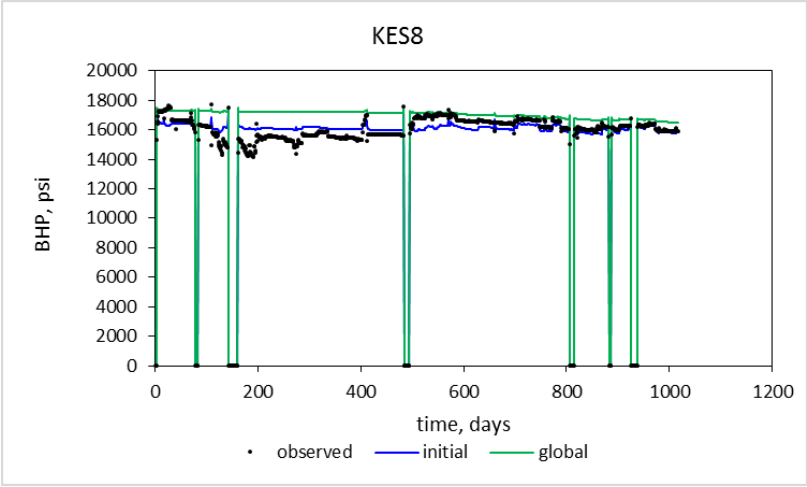

Figure 3.26: Pressure response of wells before and after global match

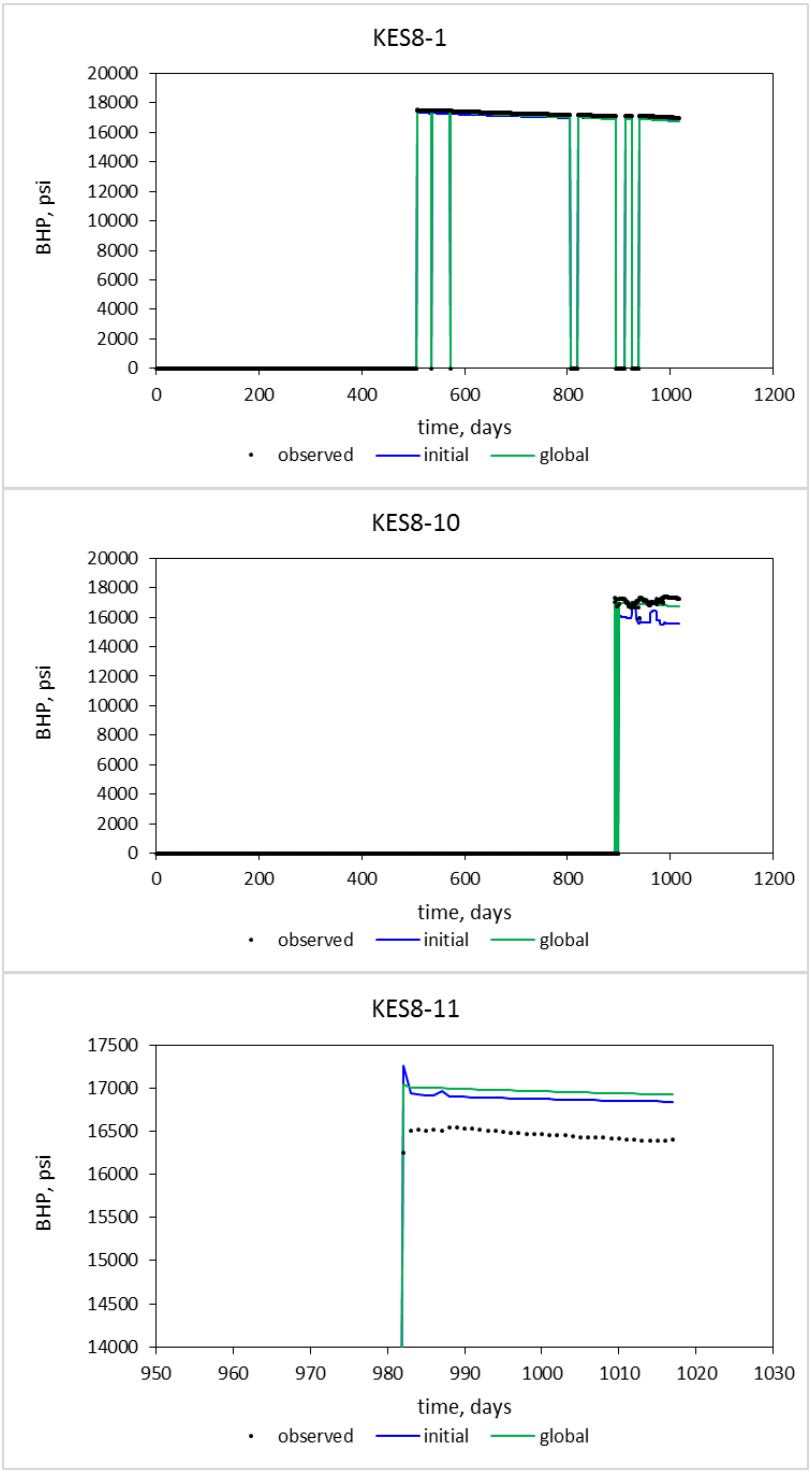

Figure 3.26 Continued.

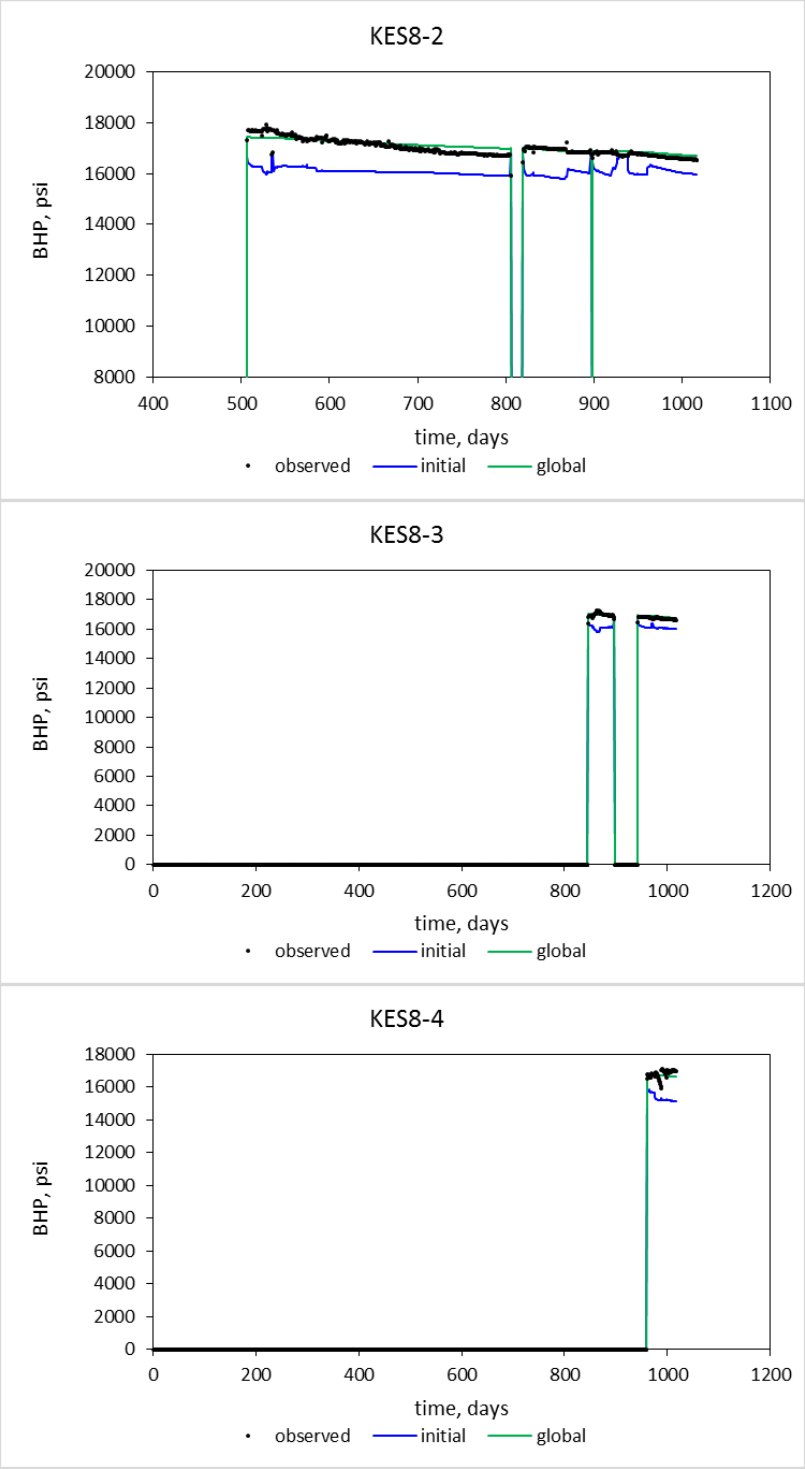

Figure 3.26 Continued.

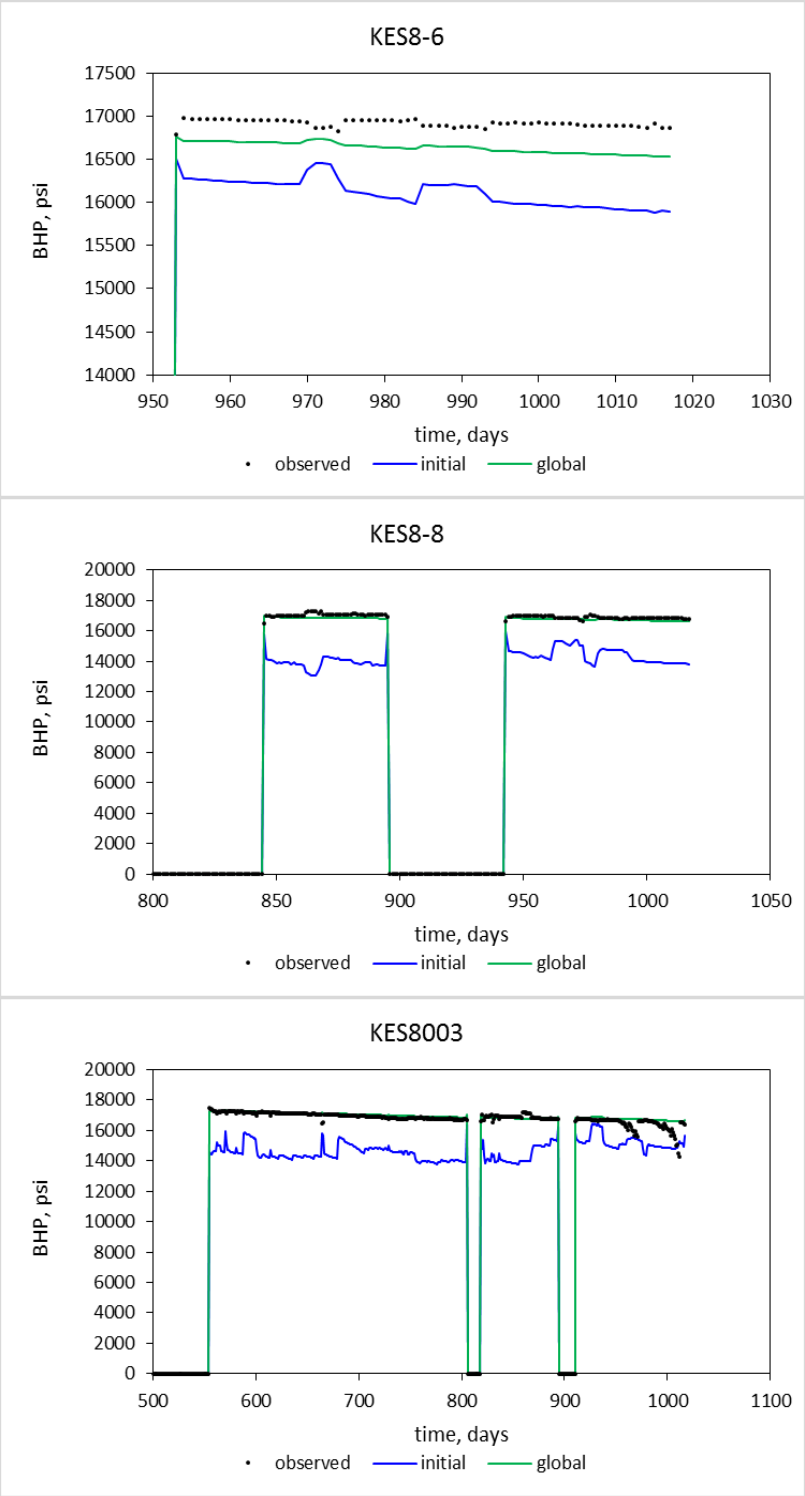

Figure 3.26 Continued.

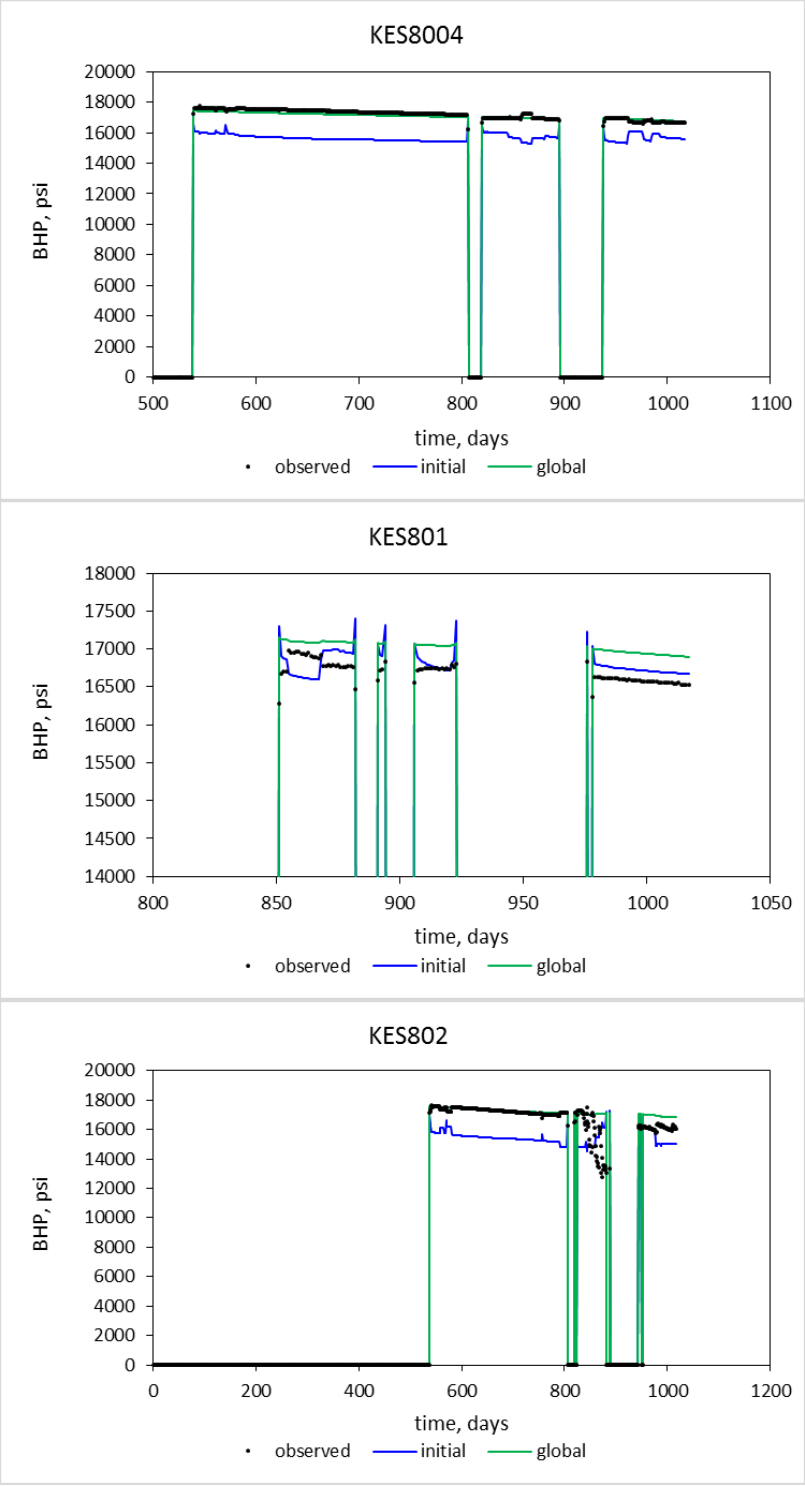

Figure 3.26 Continued.

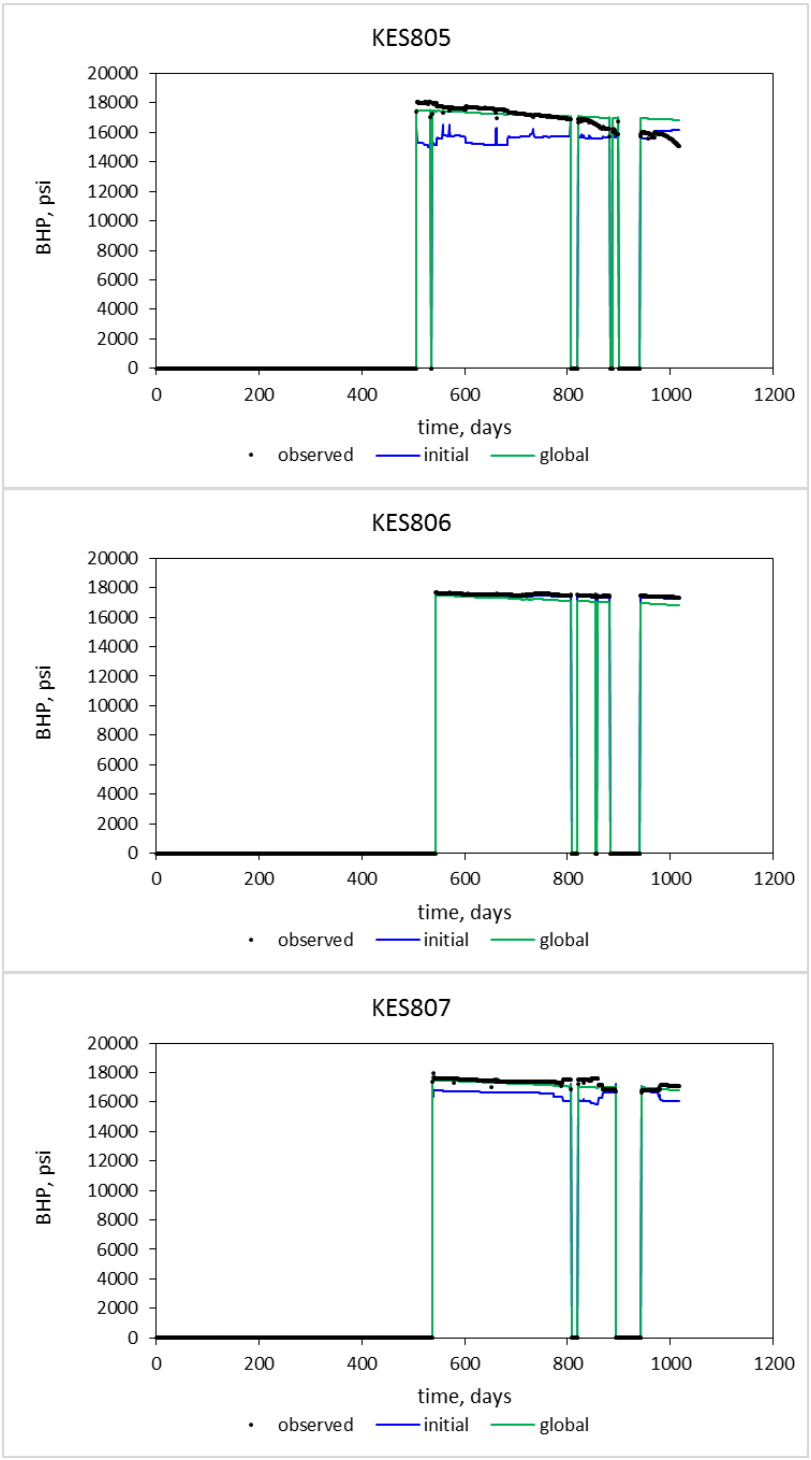

Figure 3.26 Continued.

Local Calibration based on Streamline-derived Sensitivity

With the selected models from genetic algorithm, we then perform the local calibration with streamline based sensitivity. Since other global parameters, such as the zone permeability and gas-water-contact, have been well calibrated by the first stage, here only the local fracture permeability is calibrated cell by cell to match bottom hole pressure data well by well.

As we discussed, the sensitivity of the BHP at each well with respect to the grid permeability is calculated based on streamline method. For this dual porosity case, we trace streamline from each producer inside fracture grid. And calculate sensitivity along streamlines from each well (Fig. 3.27). Then for each inversion iteration, we calculate the permeability adjustment. Within iterations, the BHP data misfit drops and becomes stable (Fig. 3.29).

The BHP misfit bubble map (Fig. 3.30) shows the data misfit decreased significantly for most of wells. Compared to BHP misfit bubble map before local update (Fig. 3.25), streamline derived BHP sensitivity shows its significant advantage and power in history matching flowing well response.

The fracture permeability and its difference maps (Fig. 3.31) show the whole calibration of permeability during local update. The initial permeability is the permeability after global calibration but before local calibration using genetic algorithm; final permeability is after local calibration by streamline sensitivity. From the permeability changes and permeability histograms, it can be seen the permeability change is constrained on the high permeability fractures which are the main flow paths for producing gas.

The well responses (Fig. 3.27) show the improvement of history data matching for the global stage unmatched wells of KES8, KES8-6, KES801, and KES8-11.

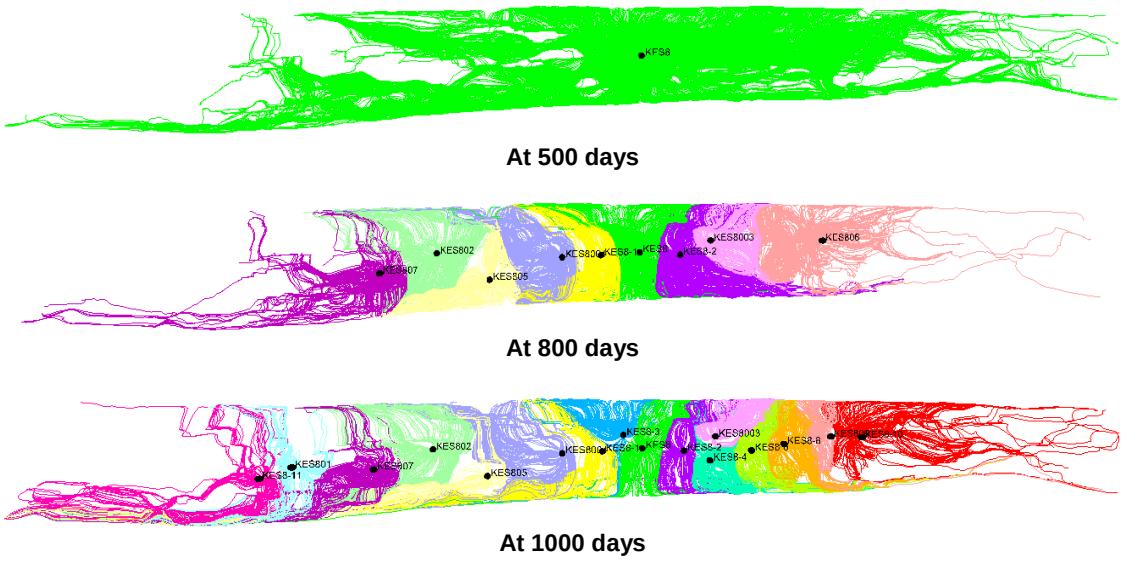

Figure 3.27: Streamlines of HPHT gas reservoir at different time

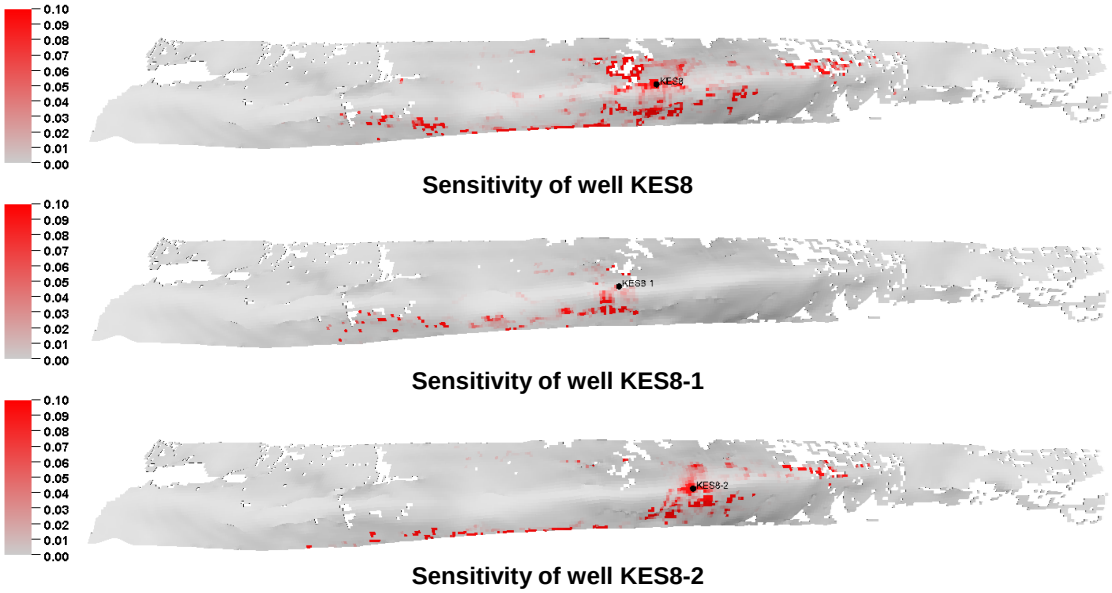

Figure 3.28: BHP sensitivity on layer 10

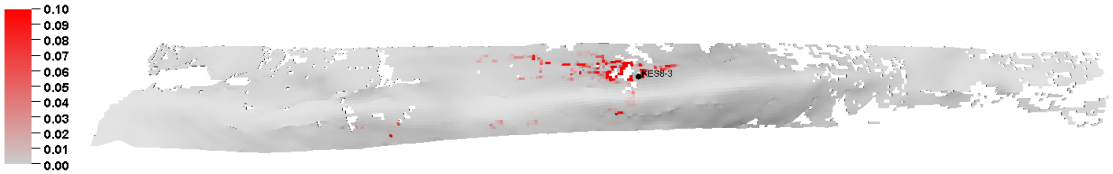

Sensitivity of well KES8-3

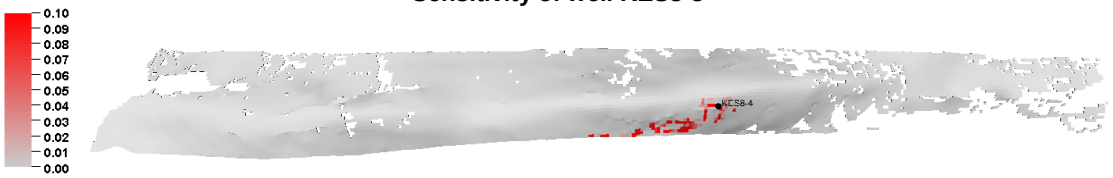

Sensitivity of well KES8-4

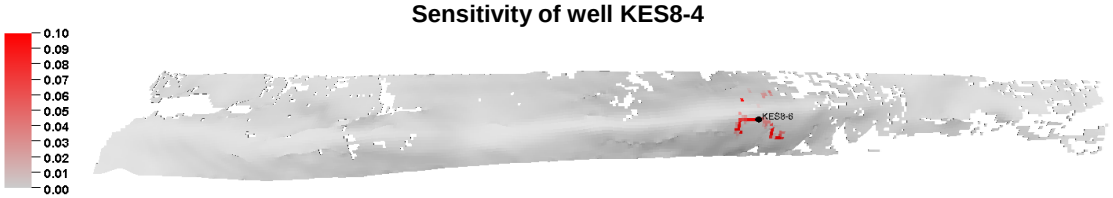

Sensitivity of well KES8-6

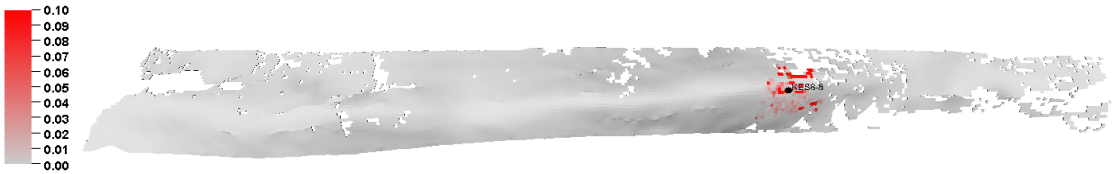

Sensitivity of well KES8-8

Sensitivity of well KES8-10

Sensitivity of well KES8-11

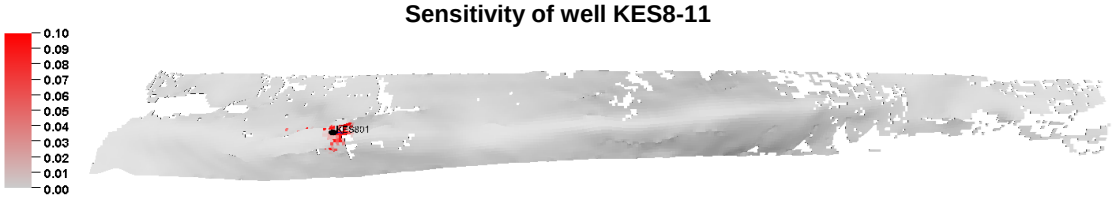

Sensitivity of well KES801

Figure 3.28 Continued.

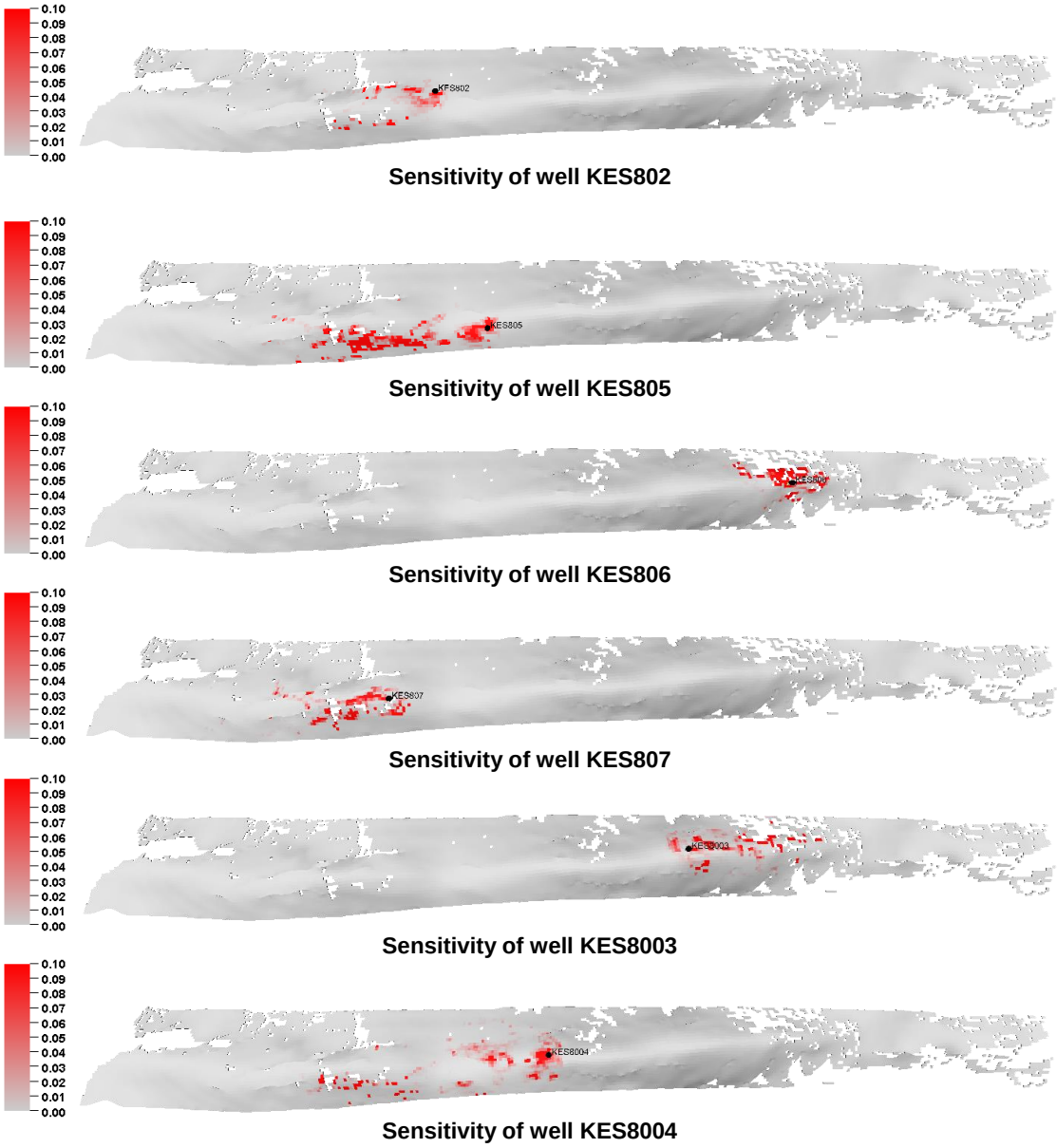

Figure 3.28 Continued.

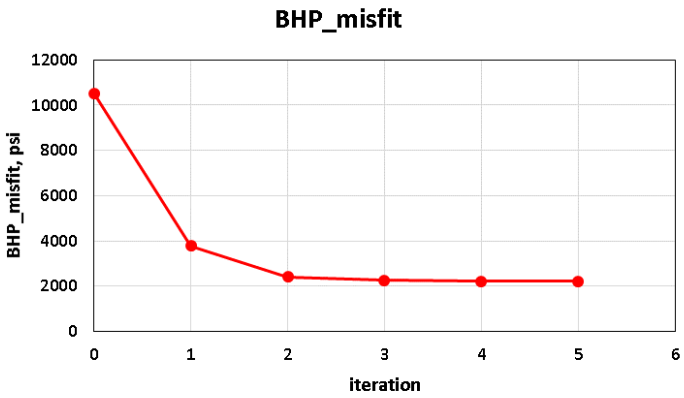

Figure 3.29: BHP misfit after local history matching

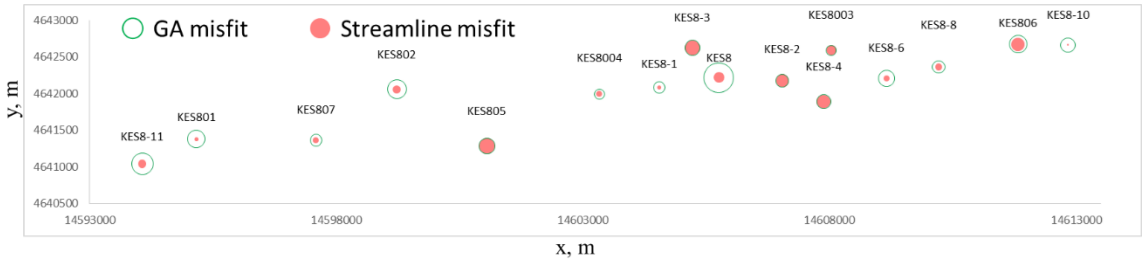

Figure 3.30: BHP misfit bubble map before and after model calibration by streamline sensitivity

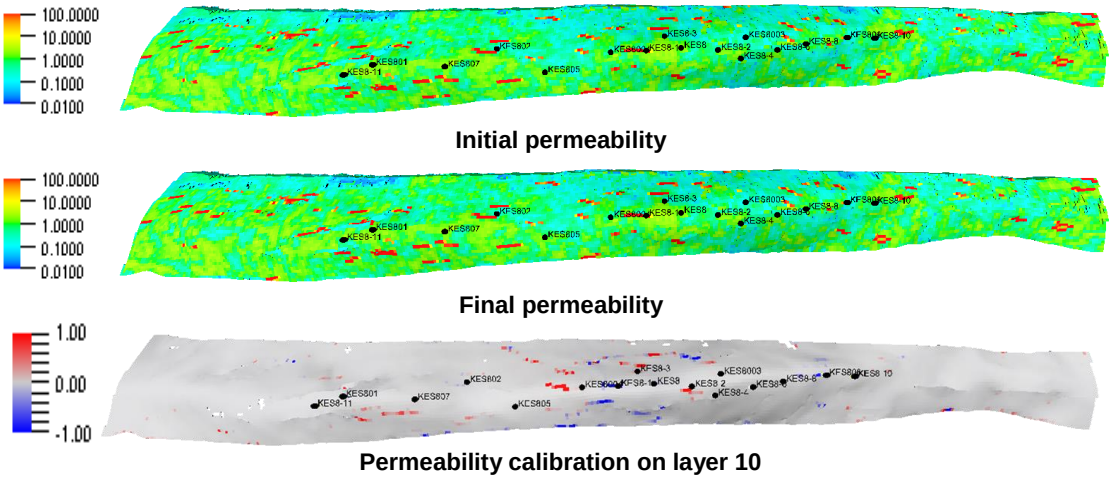

Figure 3.31: Permeability calibration by streamline method

All cells with filter (ΔPerm>1 mD or ΔPerm<-1 mD)

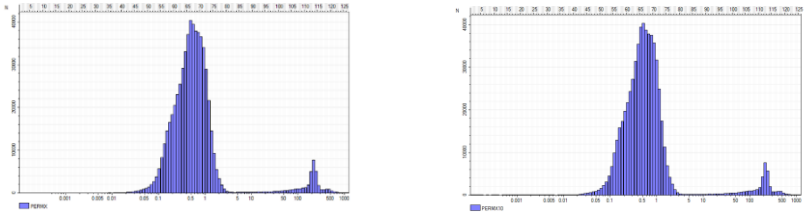

before local matching | after local matching

Fracture permeability histogram

Figure 3.31 Continued.

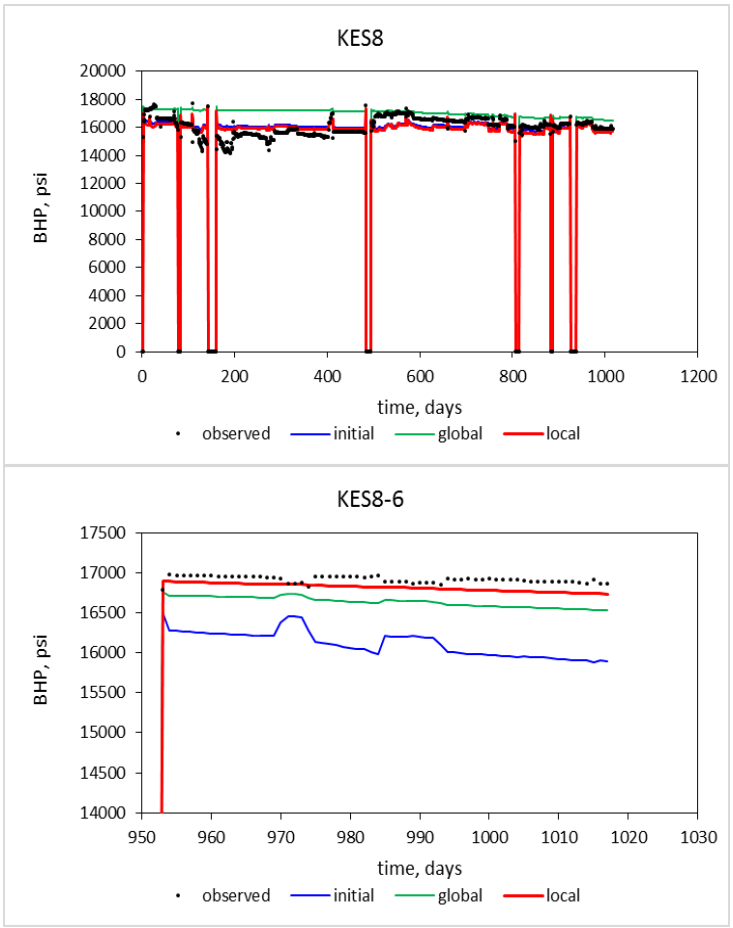

Figure 3.32: Well response update for global stage unmatched wells

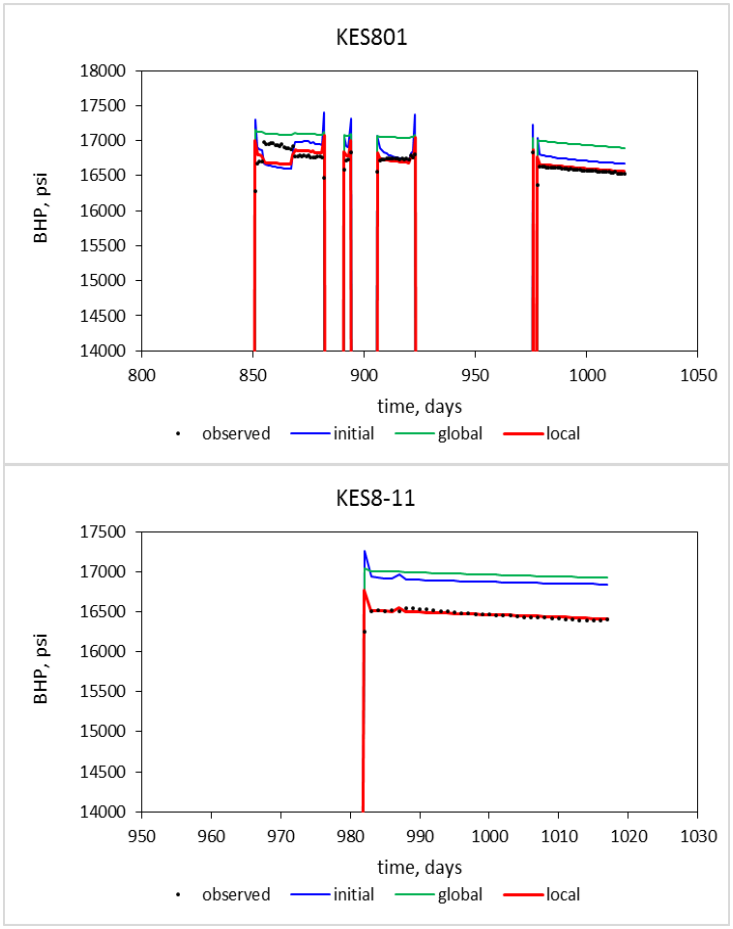

Figure 3.32 Continued.

With the history matched model, we then calculate the time of flight based on streamline and diffusive time of flight to help understand how much reservoir volume is drained at particular time (Fig. 3.33, Fig. 3.34). Additionally the partitioning can help illustrate which section is governed by particular well. According to drainage volume in fracture (Fig. 3.33), within 180 days, pressure drop reached full contact of the reservoir, which is consistent with the fact that pressure interference were observed on gas field when measuring the RFT data 220 days after KES8 began to produce.

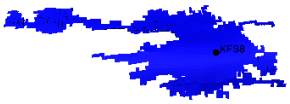

drainage volume at 10 days

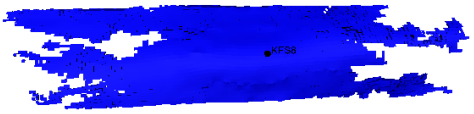

drainage volume at 30 days

drainage volume at 180 days

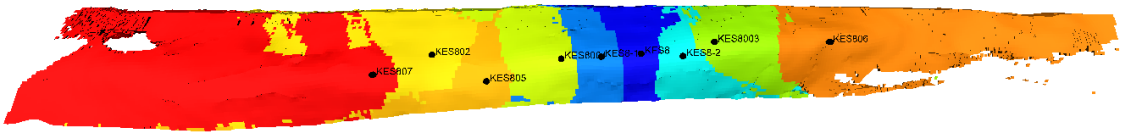

drainage volume at 800 days

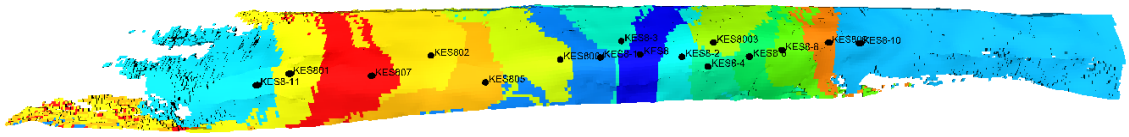

drainage volume at 1000 days

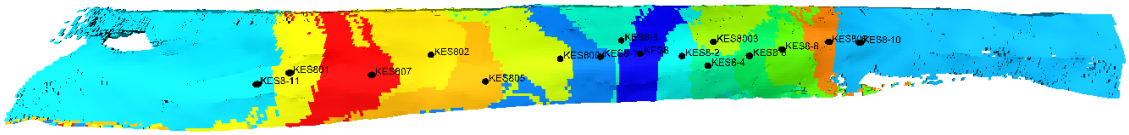

drainage volume at 1060 days

Figure 3.33: Drainage volume in fracture

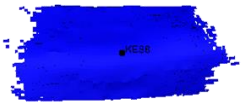

drainage volume at 500 days

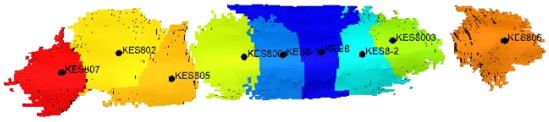

drainage volume at 800 days

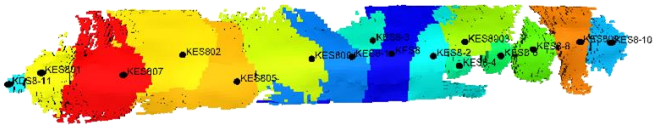

drainage volume at 1000 days

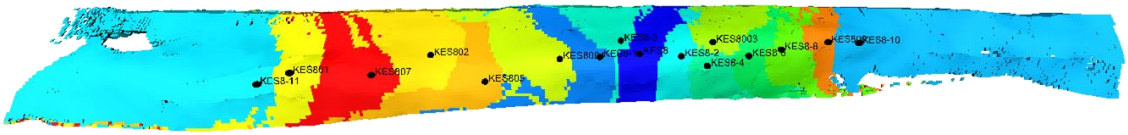

drainage volume at 5000 days

Figure 3.34: Drainage volume in matrix

The drainage volume in matrix (Fig. 3.34) is useful for picking the infill well position. Here, a gas depletion capacity is derived with the normalized values of matrix diffusive time of fight, pore volume, gas permeability and reservoir pressure change (Eq. 3.35).

$$depletion\_capacity = \sum_{k=1}^{nz} \left\{ \widehat{Porv} \cdot \widehat{Kg} \cdot (P - \widehat{P_{init}}) \cdot \widehat{DTOF} \right\} \tag{3.35}$$

Where the maximum value of each normalized variable is one.

A gas depletion capacity map (Fig. 3.35) is generated the history matched model and the bigger values of depletion capacity indicate favorable spots for well infill.

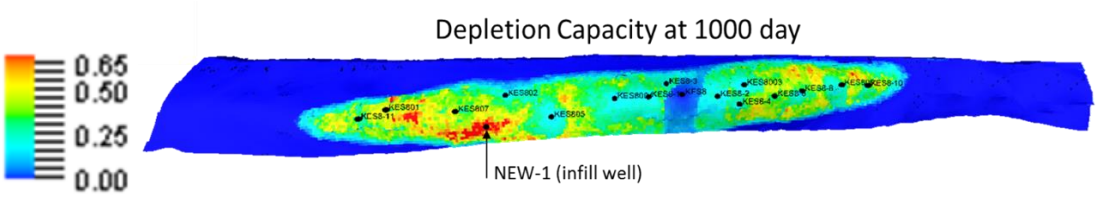

Figure 3.35: Depletion capacity and newly picked infill well position

3.6 Chapter Conclusions

We have presented an amended travel time sensitivity and a novel implementation of bottom hole pressure sensitivity based on streamlines. The travel time sensitivity is amended by streamline water flow fraction and total time of flight, and validated with a 5 spot synthetic case of waterflood. The novel implementation of bottom hole pressure sensitivity is to estimate pressure on streamline node based on grid block center pressure, and the effectiveness of the bottom hole pressure sensitivity is tested in a field history matching application to a high pressure high temperature tight gas reservoir. The major findings from this chapter are summarized below.

1. Using sensitivities generated by perturbation method as reference, the amended travel time sensitivity is more accurate than legacy travel time sensitivity. And amended travel time sensitivity outperforms legacy travel time sensitivity in terms of data misfit drop and geological model calibration.
2. Novel implementation of bottom hole pressure sensitivity is applicable for both incompressible and highly compressible fluid, and is also valid for grid with non-neighbor connections.
3. We apply the bottom-hole pressure sensitivity to a high pressure high temperature tight gas field history matching. It is the first time streamline application has been extended to gas reservoir depletion. The history matching is conducted by a multiscale approach. After the global stage calibration, the RFT data is matched while the bottom hole pressure for some gas producers are still far from matched. The local stage calibration by newly implemented bottom hole pressure sensitivity

significantly decreases the data misfit for the unmatched wells. The streamline method is proved to be also effective in gas reservoir developed by depletion.

CHAPTER IV

RATE ALLOCATION OPTIMIZATION IN FRACTURED RESERVOIRS BASED ON FAST ESTIMATION OF OIL RECOVERY[*]

4.1 Chapter Summary

Streamline-based methods have been proven to be effective for reservoir management by providing injector-producer connection pairs and allocation factors for wells. The information obtained from streamlines is useful in understanding the fluid allocation patterns and can be utilized for a variety of applications. In this chapter, we introduce applications of our approach to rate allocation optimizations.

The new optimization algorithm is developed based on a fast oil recovery estimation by streamlines. The novel method is firstly applied to a synthetic case of fractured reservoir via EDFM, and it is compared with another two streamline based optimization methods, equalizing injection efficiency, and equalizing time of flight. It is shown that for such highly contrasted permeability reservoir, our new method outperforms

[*] Part of data reported in this chapter is reprinted with permission from "Streamline Tracing and Applications in Naturally Fractured Reservoirs Using Embedded Discrete Fracture Models" by Chen, H., Onishi, T., Olalotiti-Lawal, Feyisayo, and Datta-Gupta, A. 2018, Paper SPE-191475-MS Presented at the SPE Annual Technical Conference and Exhibition 2018, 24-26 September, Dallas, Texas, U.S.A. Copyright 2018 Society of petroleum Engineers

[*] Part of data reported in this chapter is reprinted with permission from "A Generalized Derivative-free Rate Allocation Optimization for Water and Gas Flooding Using Streamline-based Method" by S. Tanaka, D. Kam, J. Xie, X. Wen, K. Dehghani, P. Fjerstad, H. Chen, A. Datta-Gupta. 2017, Paper SPE-187298-MS Presented at the SPE Annual Technical Conference and Exhibition 2017, 9-11 October, San Aantonio, Texas, U.S.A. Copyright 2017 Society of petroleum Engineers

the other two methods. Finally, we verify the new method by testing a field-scale fractured reservoir for waterflood rate allocation optimization.

4.2 Introduction

The well injection and production rate control is a key decision parameter through the asset development process. The optimization of flow rate control is typically challenging due to large dimensionality in control variables, nonlinearity in a system with multiple constraints as well as geological uncertainties. There are several techniques available to solve this problem, and they are mainly categorized as gradient based methods (Hiriart-Urruty and Lemarechal 1996, Suwartadi 2012, Wang 2003) or non-gradient based methods (Spall 2005).

The gradient based methods calculate parameter sensitivity first by taking perturbation, adjoint method, or ensemble-based method with multiple realization (Chen, Oliver, and Zhang 2010). The solutions of the gradient optimization methods often converge at local minima when the model complexity increases, and thus additional treatments will be required such as combining with non-gradient (derivative-free) approaches (Cetin, Burdick, and Barhen 1993)

The non-gradient based methods are often applied to solve general optimization problems including rate allocation optimizations (Spall 2005). Because this algorithm is to evaluate objective function by samples updated iteratively by random process, it is able to find global optima. However, the number of simulation increases exponentially as number of control variable increases (Harding, Radcliffe, and King 1996). It is difficult to apply to a rate allocation optimization problem without special treatment for model

dimensions. Typically, the upscaling of geological model and speed-up techniques are often applied in reservoir management applications (Yeten, Durlofsky, and Aziz 2003) to reduce the computational load.

The use of streamline information for rate allocation optimization problems has proven to be effective (Alhuthali, Oyerinde, and Datta-Gupta 2007; Thiele and Batycky 2003). Streamlines provide flow diagnostic results that are useful for reservoir management (Shahvali et al., 2012; Møyner et al., 2015). Because streamlines capture the convective flow between wells with spatiotemporal information from line trajectories and time-of-flight, streamlines are able to evaluate injector-producer patterns and rank the well performance. Several literatures can be found for the application of the rate allocation problems by streamline-derived information. Of these available methods, two main approaches established the concept of streamline-based rate allocation methods. The first approach is to find optimal injection rate by equalizing the injection efficiencies of all the injectors (Thiele and Batycky 2003). The second approach is to equalize the average travel time to the producers, (Alhuthali, Oyerinde, and Datta-Gupta 2007). Both approaches use the streamline information to increase the oil production total by reallocating injector or producer flow rate.

The premise of these techniques lies on flow diagnostics generated by the parameters along streamlines. Once streamlines are traced between wells, the time-of-flight is calculated based on velocity or flux field. In addition to the time-of-flight, dynamic reservoir properties, such as phase saturation and mobility, can also be mapped to streamlines. These information provides quantitative values of the reservoir features

such as heterogeneity or sweep efficiency between wells. They are quite useful for the reservoir management, but cannot be provided by conventional finite difference simulator. Once the flow diagnostic information is derived using streamlines, well performance is then evaluated for rate reallocation. Although many literatures and field applications about improving recovery efficiency by diagnostic information can be found, the underlying concepts are quite similar and the common objective is to improve the oil rate by optimizing streamline-derived properties, for instance, equalizing injection efficiency (Thiele and Batycky 2003), equalizing travel time (Alhuthali, Oyerinde, and Datta-Gupta 2007), or reducing the variance of the travel time (Park and Datta-Gupta 2011) etc.

The streamline-based optimization remains challenging for complex reservoir models of fractured reservoirs. The optimization based on arrival times may not work if injectors are located below oil-water contact, and is not applicable after water breakthrough. In contrast, the optimization based on the injection efficiency works well after water breakthrough, while difficult to apply if wells do not have clear breakthrough observations. In addition, in a fractured reservoir of highly contrasted permeability field, the well connections become much more complicated than a conventional reservoir due to the fracture network, and the oil recovery by the end of the optimization time window may not be maximized even when the injection efficiency of injectors or the average time of flight to producers is equalized.

4.3 Methodology of Rate Allocation Optimization

Streamline-based rate allocation optimization relies on analysis of fluid flow and transport, which is conducted by using static and dynamic parameters along streamlines. Once streamlines are traced from injectors to producers or vice-versa, the time-of-flight is calculated based on the total fluid velocity or total flux field. In addition to the time-of-flight, reservoir properties along streamlines such as porosity and phase saturation are also available along streamlines. These information provides quantitative values to characterize the impact of heterogeneity of a reservoir on sweep efficiency between wells. Once flow diagnostic information are derived using streamlines, performance of each injector-producer pair is then evaluated for optimal rate reallocation. The difference between our study and previous ones is the way to rank injector-producer pairs. Instead of using the average time of flight to producers (Alhuthali et al., 2007, Park and Datta-Gupta, 2011) or injection efficiency of injectors (Thiele and Batycky, 2003), we will evaluate the expected oil recovery within an optimization time window for each injector-producer pair by incorporating pore volume and phase saturation along streamtubes.

In this chapter, we will formulate the oil recovery evaluation functions and illustrate the full workflow to conduct rate allocation optimization. The objective is to maximize oil recovery within certain time interval. The allowable constraints include field injection rate, field production rate, maximum well injecting pressure, minimum well producing pressure, and maximum allowable well rate change between two adjacent optimization steps.

The implemented optimization framework will be linked to commercial simulators such as ECLIPSE and CMG. And the effectiveness and advantage of the novel method will be demonstrated with challenging complex fractured reservoirs via embedded discrete fracture models.

The difference between the novel approach and equalizing injection efficiency method is that the way to calculate well pair efficiencies. Injection efficiency is based on instant oil rates at producers, and the novel well pair efficiency is based on the potential mobile oil volumes produced by producers within the optimization period. The novel method accounts for oil and water distributions while previous study did not. The previous injection efficiency study is based on streamline simulation, while the newly developed optimization workflow is based on streamlines derived from some finite difference simulator, such as ECLIPSE and CMG. The novel optimization workflow is able to apply to general simulation cases.

4.3.1 Objective Function

Our objective is to maximize the oil recovery within the drainage volume of a given optimization period Δt, which is from current time to the end of field life (Fig. 4.1). The drainage volume is estimated along streamlines with a time of flight cutoff that equals to the optimization period.

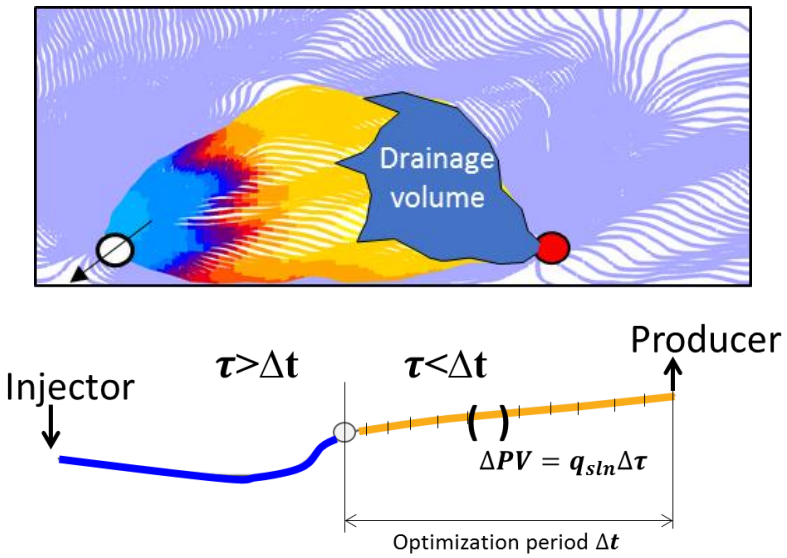

Figure 4.1: Oil recovery estimation along streamline within drainage volume

The oil recovery along a single streamtube is given in Eq. 4.1.

$$Oil_{sln} = \sum_{seg}\{q_{sln}\Delta\tau(S_o - S_{or})/B_o\}, (\tau < \Delta t) \quad (4.1)$$

Where q_{sln} is the flow rate carried by current streamline, S_o is the oil saturation, S_{or} is the residual oil saturation, B_o is the oil volume factor, Δt is the time of flight cutoff. When a streamtube segment whose travel time to the producer is less than Δt, it is considered to be within the drainage volume and the local mobile oil within the streamtube segment will be recovered no later than the end moment of optimization period.

Then, the oil recovery by a well pair of injector *i* and producer *p* is calculated by summation of oil recovery along all streamlines from injector *i* to producer *p*, as shown in Eq. 4.2.

$$OR_{i,p} = \sum_{sln}\{Oil_{sln}\} \quad (4.2)$$

The oil recovery of the whole field is the summation of oil recovery by all well pairs, and the objective is to maximize the field oil recovery in Eq. 4.3.

$$obj = maximize\{\sum_p \sum_i (OR_{i,p})\} \quad (4.3)$$

4.3.2 Optimization Workflow

The proposed optimization method is a streamline-based gradient free method. The objective is to maximize total oil production by the end of field life. The allowable constraints include field injection rate, field production rate, maximum well injecting pressure, minimum well producing pressure, maximum and minimum production rates, maximum and minimum injection rates, and maximum well rate change ratio between two adjacent optimization steps. The optimization is done over pre-defined optimization intervals (Fig. 4.2). For each interval, the objective is to maximize the oil recovery within its optimization period, which is varying from interval to interval as shown in the full optimization workflow.

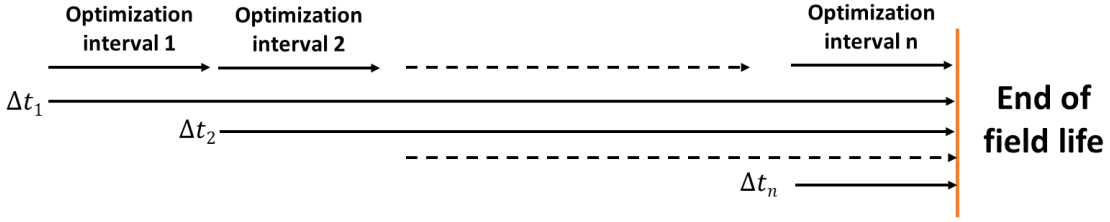

Figure 4.2: Full optimization workflow

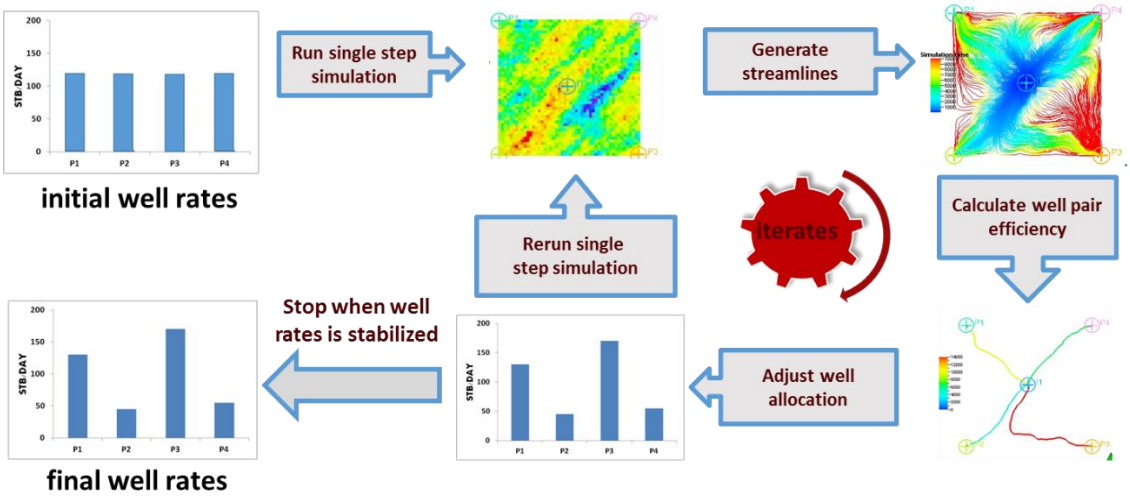

Figure 4.3: Single interval optimization

For a single optimization interval, the details of well rate optimization is shown schematically in Fig. 4.3. It starts with an initial well rates schedule and includes the following steps:

I. *Conducting flow Simulation and streamline tracing*. The first step is to perform a waterflood simulation for a single time interval and compute the streamlines and time-of-flight from producers to injectors. We trace streamlines using the fluid fluxes derived from the finite-difference flow simulation via the method proposed in this paper.

II. *Computing well pair efficiency*. This step involves selecting an injector-producer well pair and computing the well pair efficiency defined as the STB of oil produced per STB of fluid injected (Eq. 4.2). The efficiency is calculated for all the well pairs in the simulation model.

$$e_{ip} = \frac{OR_{ip}}{q_{ip}\Delta t} = \frac{oil\ volume\ recovered}{water\ \text{volume}\ injected} \tag{4.4}$$

where q_{ip} is the water injection rate allocated from injector *i* to producer *p*.

III. *Updating the well rates*. This step involves updating the injection and production rates based on the well pair efficiencies. It includes the following steps:

Compute field efficiency in the similar way as the well pair efficiency.

$$e_f = \frac{\sum OR_{ip}}{\sum q_{ip}\Delta t} = \frac{field\ oil\ volume\ recovered}{field\ water\ volume\ injected} \tag{4.5}$$

Compute well pair rate multipliers by comparing well pair efficiencies and field efficiency.

$$\lambda_{ip} = \frac{e_{ip}}{e_f} \tag{4.6}$$

Update well injection rates and well production rates.

$$\hat{q}_i = \sum_p \lambda_{ip} q_{ip} \tag{4.7}$$

$$\hat{q}_p = \sum_i \lambda_{ip} q_{pi} \tag{4.8}$$

Rescale the updated well rates to follow the field rate constraints.

$$q_i^{updated} = \frac{\sum q_i}{\sum \hat{q}_i} \hat{q}_i \tag{4.9}$$

$$q_p^{updated} = \frac{\sum q_p}{\sum \hat{q}_p} \hat{q}_p \tag{4.10}$$

IV. *Accounting for changing streamlines by repeating from step-I to step-III until the updated well rates are stabilized*. Use the updated rates to regenerate the streamlines and repeat steps I to III. Continue the process until rates are stabilized or a pre-specified number of iterations is exceeded.

V. *Moving to next optimization interval*. Repeat step I to IV for all subsequent optimization intervals.

The proposed optimization method is heuristic, the well rates will be stabilized when the well pair efficiency is equalized for an optimization interval. However, equalized well pair efficiencies will not necessarily lead to equalized injection efficiencies. Because the well pair efficiencies are based on the potential mobile oil volumes to be produced within the optimization period, while the injection efficiencies are based on instant oil production rate. The novel method will reduce to equal time of flight for specific cases. At the beginning of waterflood, if oil saturation is homogeneous in the formation, the mobile oil saturation is also identical everywhere, and then the potential mobile oil volumes are proportional to drainage volumes. A drainage volume divided by its well pair flux allocation is the average time of flight from the injector to the producer. So the well pair efficiency is proportional to the well pair average time of flight in this case, and thus equal well pair efficiencies lead to equal average time of flight among all well pairs.

4.3.3 Synthetic Case Validation

A synthetic fractured reservoir via EDFM is used to test the effectiveness of the novel optimization algorithm. The basic parameters are given in Tab. 4.1. The discrete fractures are intersected with each other, and its permeability is highly contrasted compared to matrix permeability (Fig. 4.5).

Table 4.1: Reservoir, fluid and rock properties for 2D EDFM model

Parameter	Symbol	Unit	Value
Grid dimension	*ni, nj, nk*	-	50, 50, 1
Cell size	*DX, DY, DZ*	*ft*	32.8, 32.8, 32.8
Oil density	ρ_o	lb/ft^3	52
Oil viscosity	μ_o	*cp*	0.29
Oil compressibility	C_o	psi^{-1}	3.4E-5
Water density	ρ_w	lb/ft^3	63
Water viscosity	μ_w	*cp*	0.31
Water compressibility	C_w	psi^{-1}	3.3E-6
Rock compressibility	C_r	psi^{-1}	8.1E-6
Matrix porosity	ϕ_m	-	0.035
Fracture porosity	ϕ_f	-	5.00E-06
Matrix permeability	k_m	*mD*	0.01-500
Fracture permeability	k_f	*mD*	1,000,000

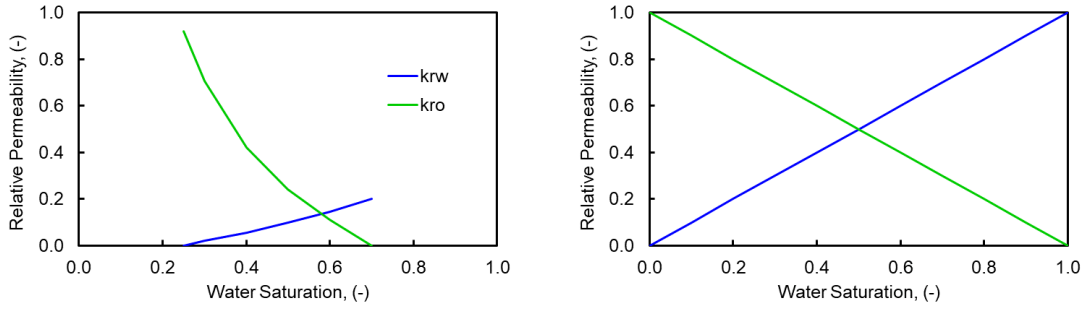

(a) Reservoir domain **(b) Fracture domain**

Figure 4.4: Relative permeability curves for synthetic EDFM

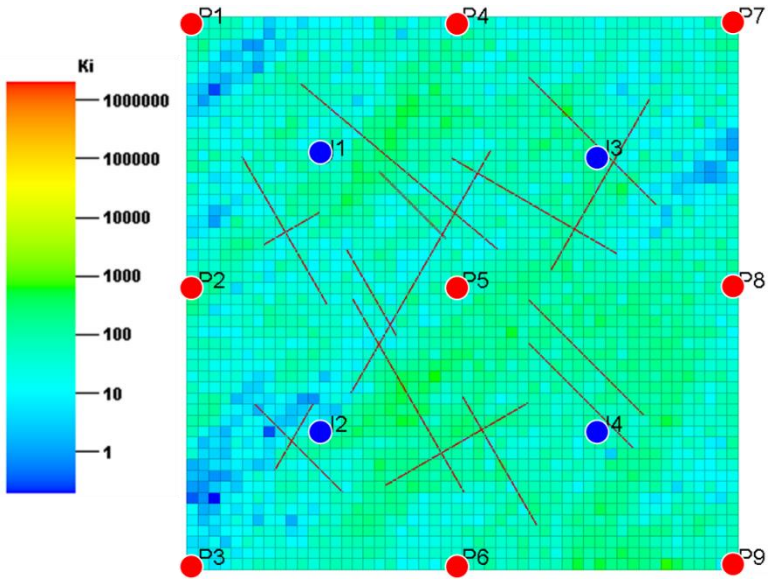

Figure 4.5: Synthetic EDFM

There are four injectors and nine producers in the model, forming four five-spot groups for waterflood. The field water injection rate and liquid production rate are both set to 1000 STB/day. To start with, each injector is allocated with 250 STB/day water injection rate. The producer at center (P5) is allocated with 250 STB/day liquid production rate, each producer on side (P2, P4, P6, P8) is allocated with 125 STB/day liquid production rate, and each producer on corner (P1, P3, P7, P9) is allocated with 62.5 STB/day liquid production rate. Such well schemes continued for 2 years as an initial waterflood history, so that many of the producers have water break through. And the remaining oil by the end of the second year is shown in Fig. 4.6.

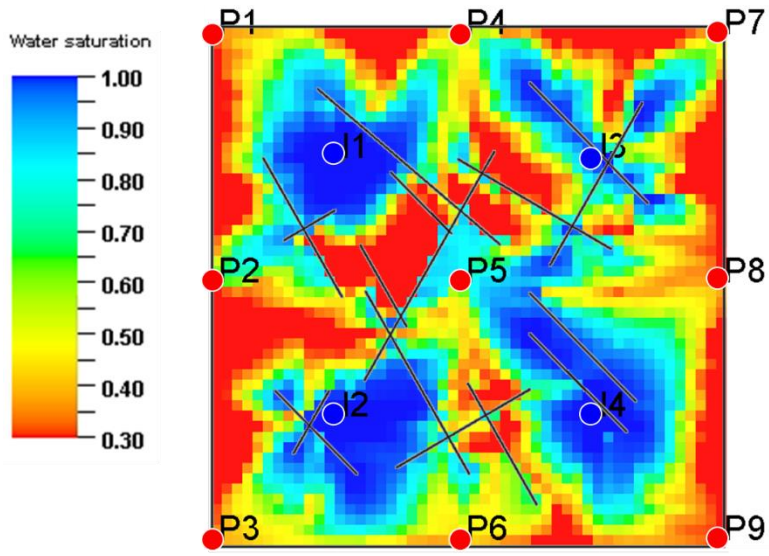

Figure 4.6: Remaining oil after 2 years waterflood (synthetic EDFM)

The rate allocation optimization is set to begin after two years waterflood and last for four years. The production and injection well rate allocations are adjusted every half year. The field injection rate and production rate are both constrained to 1000 STB/day. Each producer is limited to a minimum bottom hole pressure of 1000 psi, and each injector is limited to a maximum bottom hole pressure of 8000 psi.

The waterflood for the next four years are conducted in four scenarios. The first scenario (ConstRate) is to maintain the initial well schemes, the second scenario (OR_OPT) is to optimize well schemes by our method, the third scenario (IE_OPT) is to optimize well schemes by equalizing injection efficiencies (Thiele and Batycky 2003), and the last scenario (TOF_OPT) is to optimize well schemes by equalizing average time of flight to producers (Alhuthali, Oyerinde, and Datta-Gupta 2007). The well rate schemes are given in Fig. 4.7.

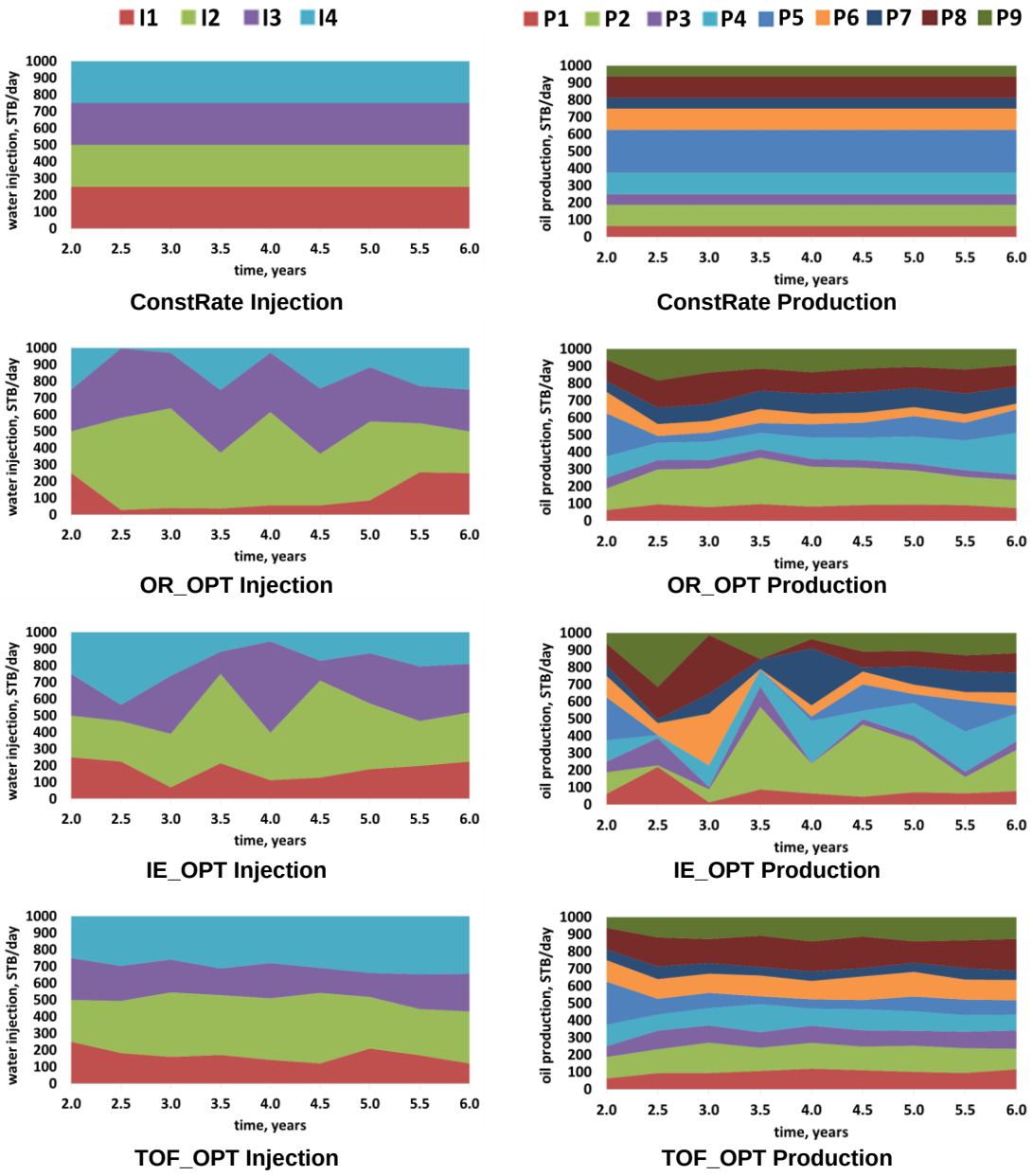

Figure 4.7: Well schemes for different scenarios

The four scenarios are also compared in terms of injection efficiency (Fig. 4.8), time of flight distribution (Fig. 4.8), and total oil and water production (Fig. 4.9).

Injection efficiency plot is a cross plot of injected fluid flux and offset oil production for each injector-producer pair. The objective of equalizing injection efficiency

method is to align the data point to a straight line starting from the coordinate origin. It is shown in Fig. 4.8 that the injection efficiencies are best optimized in IE_OPT scenario than the other scenarios.

Average time of flight to producers are not easily equalized in a fractured reservoir. The well connections are complicated and the time of flight is also highly variable because any producer can connect to any injector through the fracture network. The TOF_OPT scenario tries to equalize the time of flight of the most important well pairs which conduct high pair fluxes. The TOF distribution figures (Fig. 4.8) plot time of flight of well pairs in an order that the well pair fluxes ranked from big value to small value. It is shown that the time of flight of major well pairs are better equalized in TOF_OPT scenario than the other scenarios.

All the optimization scenarios result in improved oil production and reduced water production compared to the non-optimized scenario, ConstRate (Fig. 4.9). The oil production relative changes demonstrate that the total oil production improvements of the optimization scenarios (OR_OPT, IE_OPT, TOF_OPT) compared to the non-optimized scenario (ConstRate). The water production relative changes demonstrate that the total water production reductions of the optimization scenarios. Although OR_OPT is not the best optimized in terms of either injection efficiencies or average time of flight to producers, it outperforms the other scenarios in terms of total oil production within the optimization period.

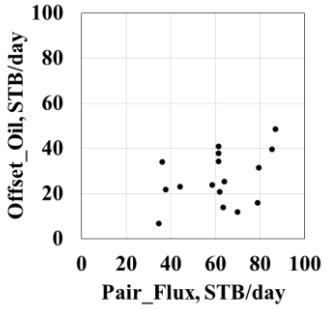

ConstRate Injection Efficiencies

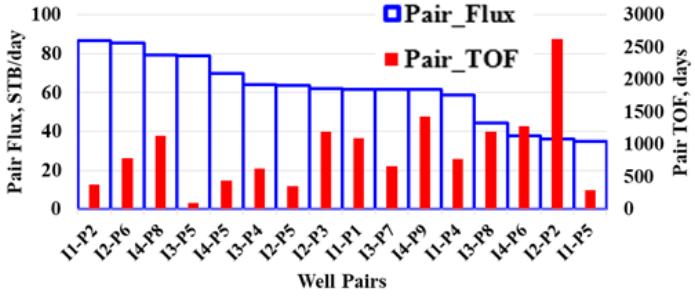

ConstRate TOF Distribution

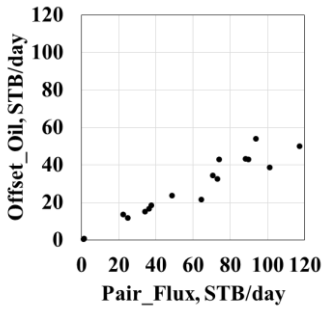

OR_OPT Injection Efficiencies

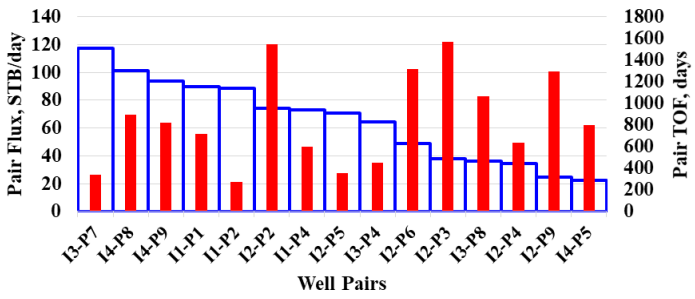

OR_OPT TOF Distribution

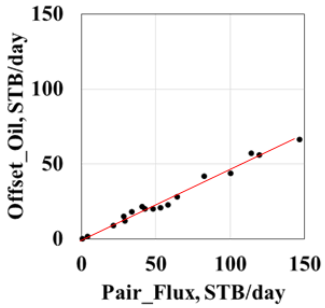

IE_OPT Injection Efficiencies

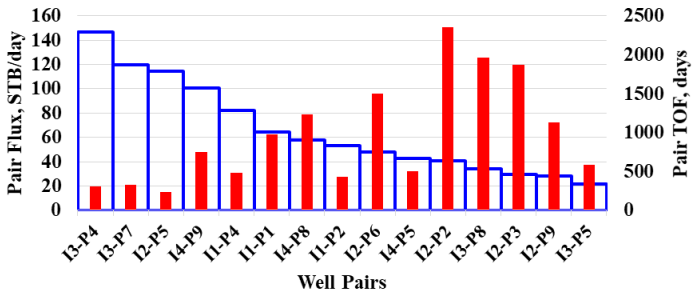

IE_OPT TOF Distribution

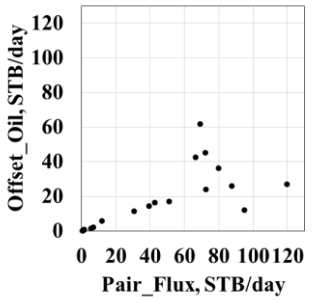

TOF_OPT Injection Efficiencies

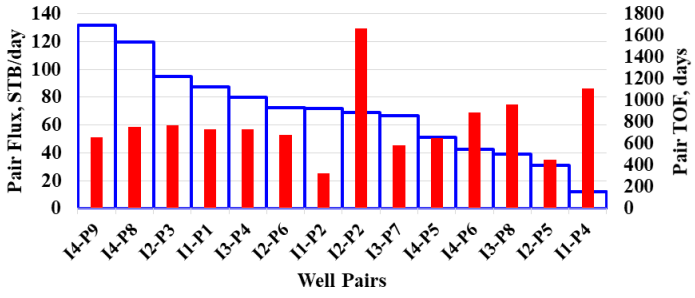

TOF_OPT TOF Distribution

Figure 4.8: Injection efficiencies and time of flight distribution for different scenarios

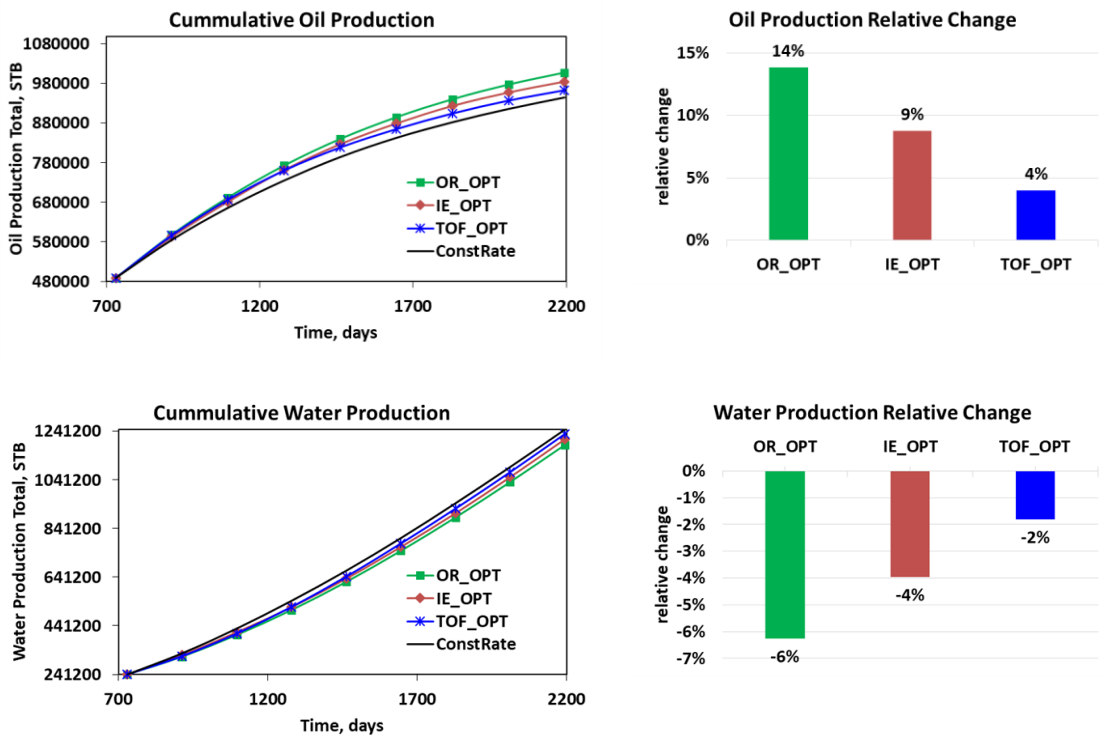

Figure 4.9: Oil and water production for different scenarios

The reason why OR_OPT outperforms the other scenarios can be explained by comparing the remaining oil maps and streamline maps (Fig. 4.10). It is shown that most remaining oil is aggregated around highly fractured areas. Optimization by injection efficiencies focuses on the oil recovery around producers, it tries to maximize the oil production within a short term rather than a long term which is from current time to the end of field life. Optimization by time of flight tries to balance the swept volume between well pairs. However, the time of flight for all streamlines of the same well pair is also highly heterogeneous in a fractured reservoir, so the oil that can be recovered by the well pair under a given injection volume has big uncertainty. Treating each well pair equally and balancing the water injection among well pairs may not generate a quite favorable result in such situation. The optimization by streamline-based oil recovery estimation will

evaluate the oil and water production in a long term and balance the water injection according to potential oil recovery by each well pair. By comparing the streamline distributions in Fig. 4.10, OR_OPT makes the streamlines covering the oil rich areas and thus enhances the remaining oil recovery.

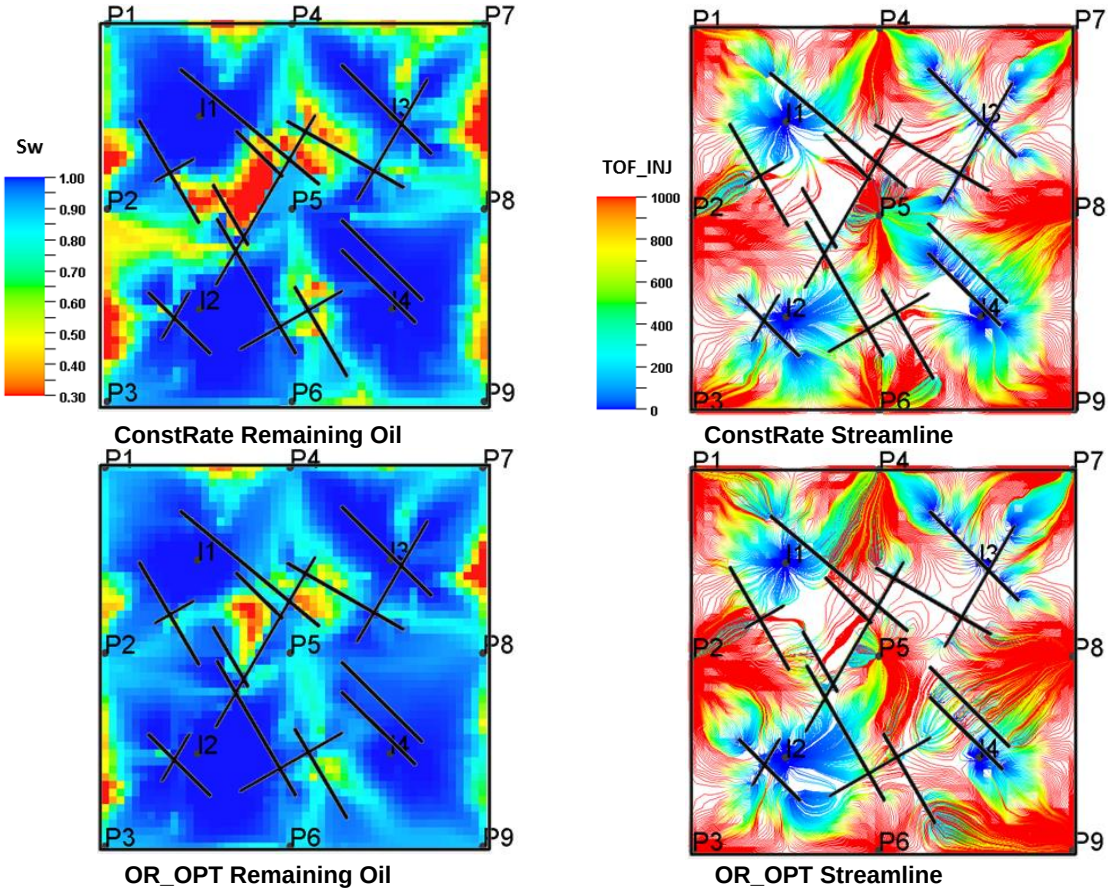

Figure 4.10: Remaining oil and streamline distribution for different scenarios

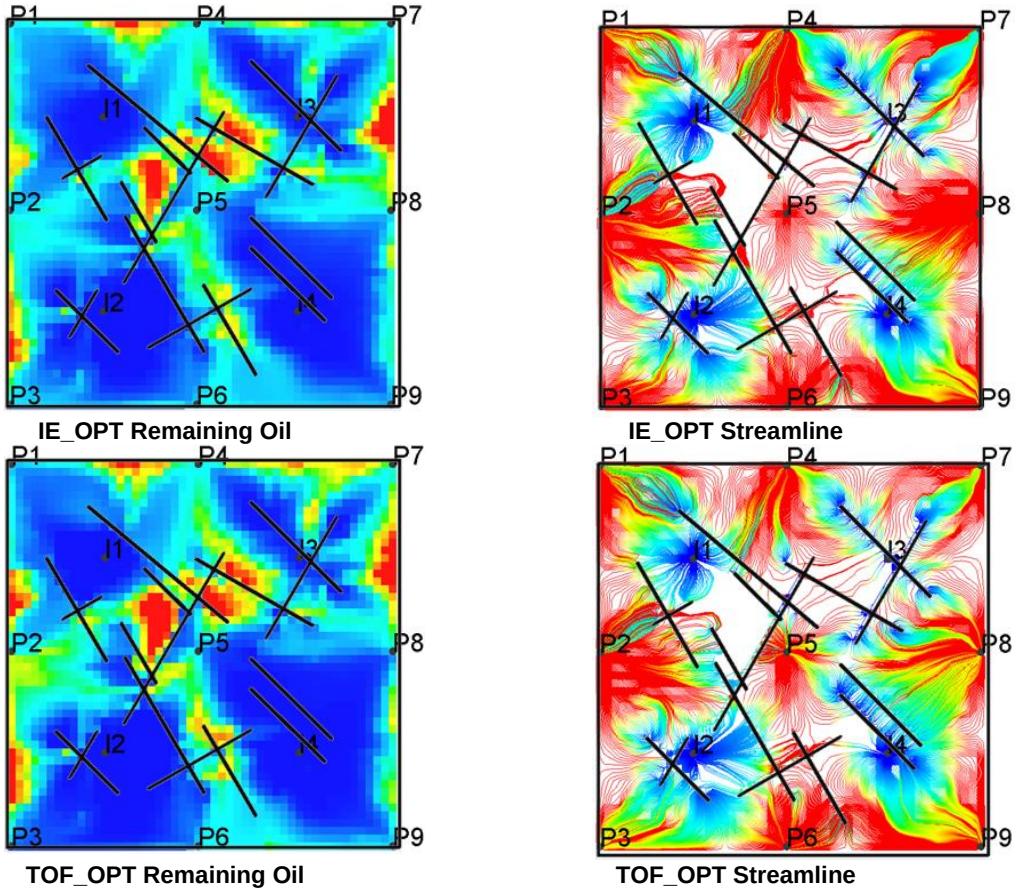

Figure 4.10 Continued.

4.4 Field-scale Application

4.4.1 Optimization Settings

The same reservoir model and settings (SAIGUP) from the previous section 2.5.1 is used in our optimization study. For comparisons, two scenarios are examined, a uniform injection/production scenario and an optimized injection/production scenario. In both scenarios, 3 years of uniform waterflood at a field injection rate of 12,000 STB/day and field production rate of 12,000 STB/day is conducted. The water saturation field after 3 years is shown in Fig. 4.11.

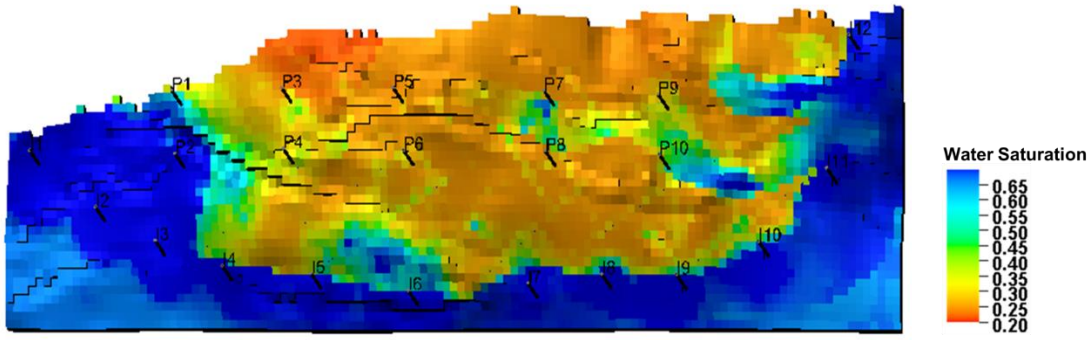

Figure 4.11: Water saturation after 3 years of waterflood (SAIGUP) [4]

Rate allocations will be adjusted in the optimization scenario using the newly proposed gradient free algorithm discussed in the previous section, while the base scenario continues the uniform injection/production after the first 3 year period. The waterflood optimization time window is set as 10 years. The time interval for well rate allocations update is 6 months. The field water injection rate and liquid production rate remains at 12,000 STB/day, the maximum and minimum well production rates are 5000 STB/day and 100 STB/day, the maximum and minimum well injection rates are 4000 STB/day and 100 STB/day, the maximum well injection bottom hole pressure is 5000 psi, the minimum

well production bottom hole pressure is 3000 psi, and the maximum fractional well rate change between two adjacent optimization steps is 0.5.

4.4.2 Optimization Results

The cumulative oil production and cumulative water production comparisons are presented in Fig. 4.12. It is obvious that the results obtained from the optimized well rate schedule outperforms the uniform well rate schedule. The optimized scenario improved the cumulative oil production by 15.9 % and reduced cumulative water production by 4.0 % compared to the uniform allocation scenario. In addition to the field development improvement, Fig. 4.13 shows injection and production allocations over the optimization time. In the optimized scenario, the dominance of I1 and I12 at the edge of the reservoir and P3, P5, P6, and P7 at the center of the oil zone forms a primary control of the oil displacement. Such pattern is adaptive to the remaining oil distribution and effective in recovering the remaining oil.

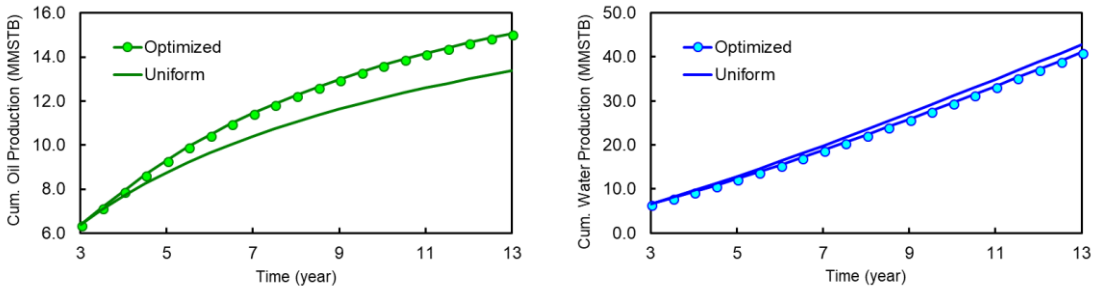

(a) cumulative oil production **(b) cumulative water production**

Figure 4.12: Oil and water production (SAIGUP) [4]

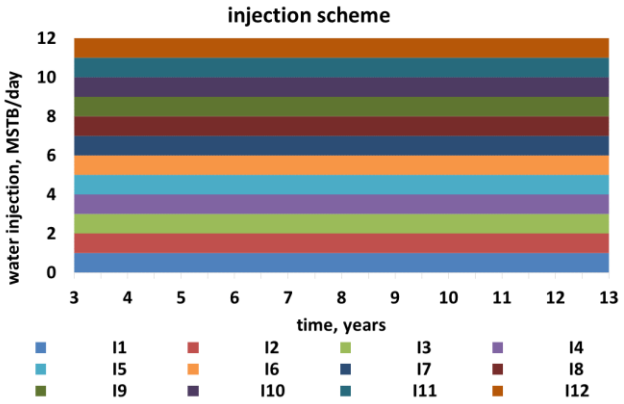

(a) Uniform injection allocation

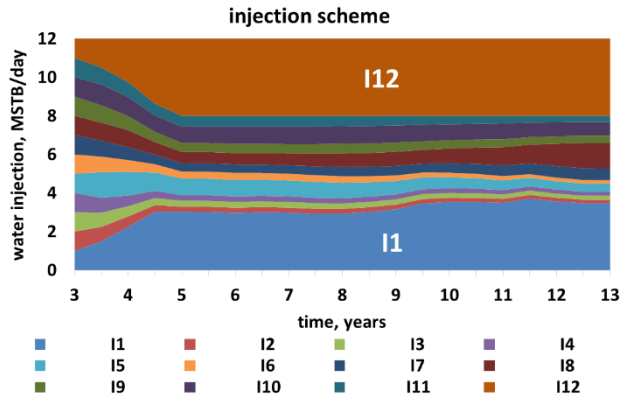

(b) Optimized injection allocation

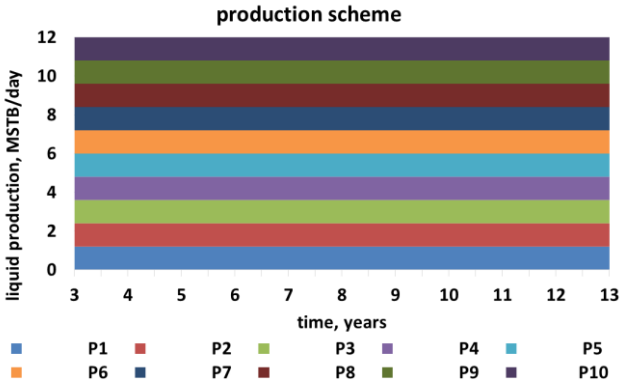

(c) Uniform production allocation

Figure 4.13: Well schemes (SAIGUP) [4]

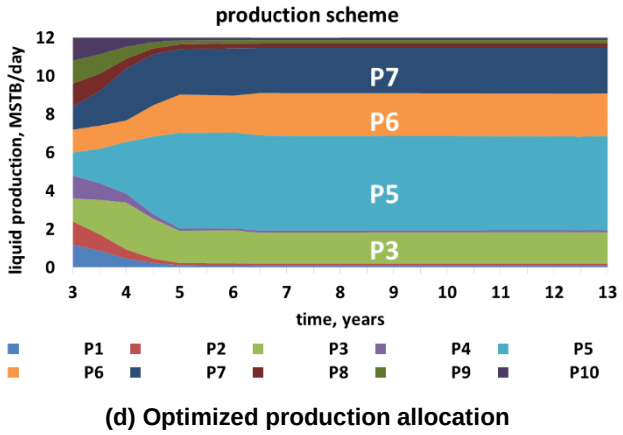

(d) Optimized production allocation

Figure 4.13 Continued.

Remaining oil distribution comparisons at the end of the optimization time are presented in Fig. 4.14. It is easy to notice that an improved sweep efficiency is obtained from the optimized well schedule. What's more, the shape of the remaining oil in uniform allocation scenario is a long channel from west to east around the crest of the reservoir, which indicates that the sweep efficiency is relatively weak in west-east direction and oil recovery needs to be enhanced around reservoir crest. These critical reasons that hinder the oil recovery by waterflood are diagnosed by streamlines and resolved to the maximum extent by the proposed optimization workflow.

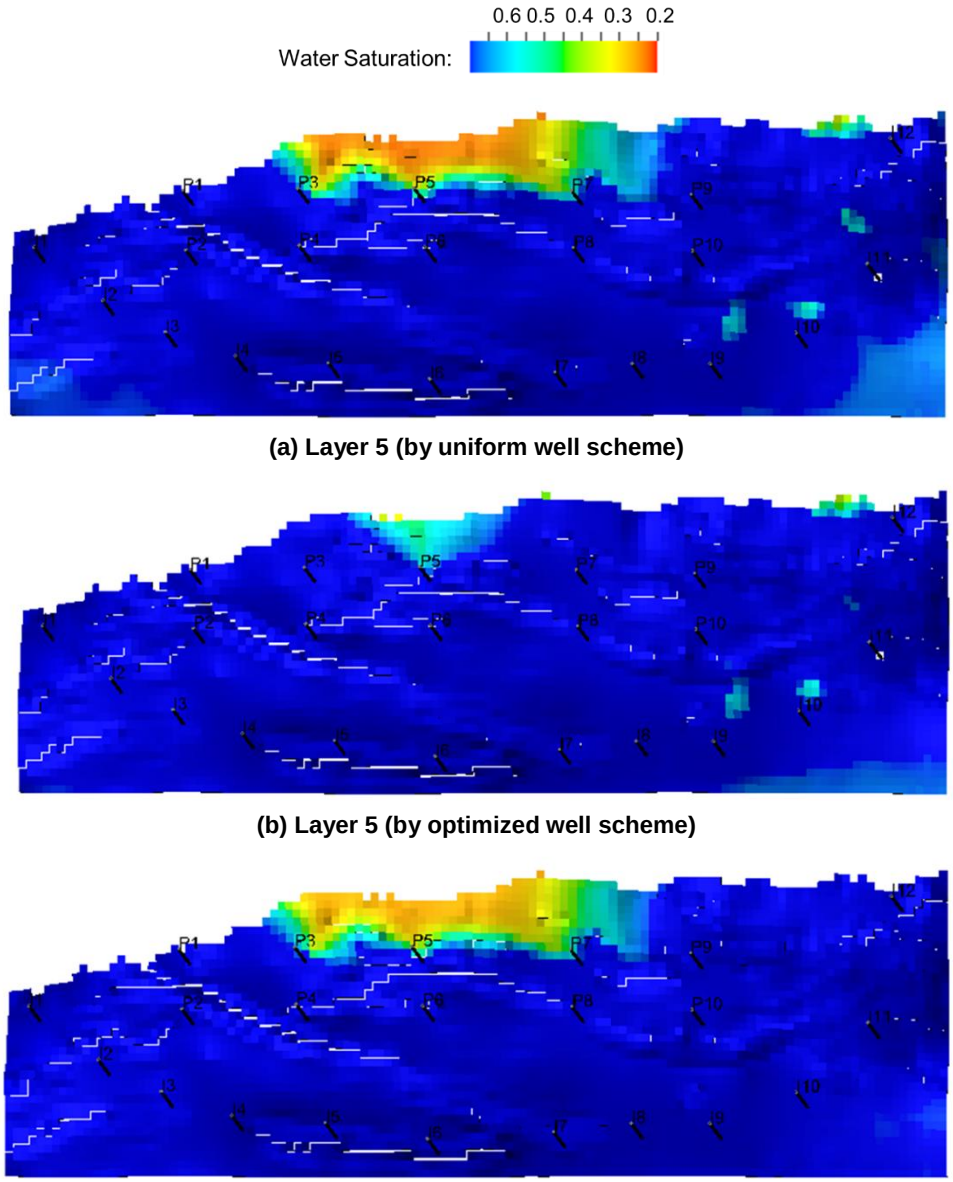

(a) Layer 5 (by uniform well scheme)

(b) Layer 5 (by optimized well scheme)

(c) Layer 10 (by uniform well scheme)

Figure 4.14: Remaining oil on layer samples (SAIGUP) [4]

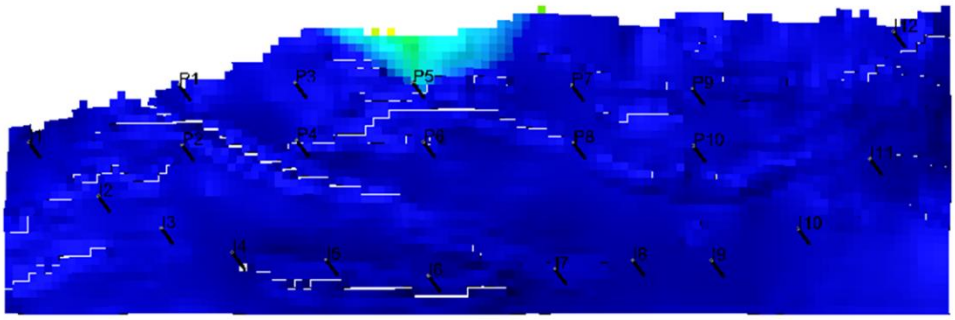

(d) Layer 10 (by optimized well scheme)

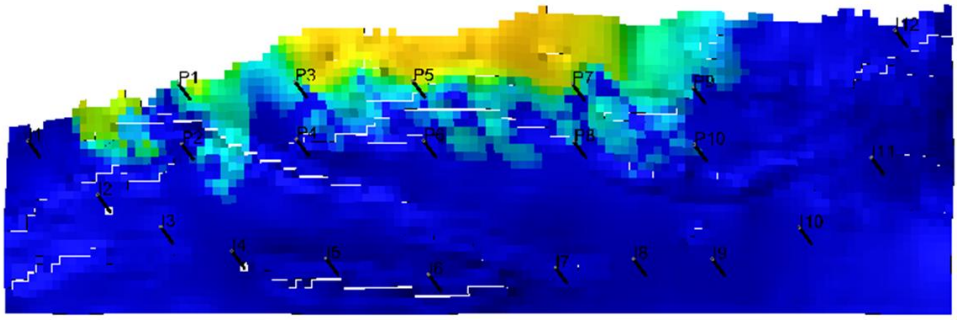

(e) Layer 15 (by uniform well scheme)

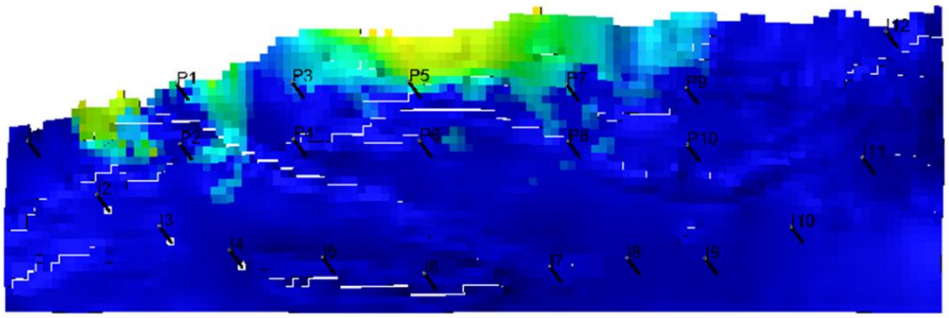

(f) Layer 15 (by optimized well scheme)

Figure 4.14 Continued.

Remaining oil and flow patterns comparisons by streamlines are shown in Fig. 4.15. The dominance of I1, I12 changed the sweep pattern by enhancing injection along west-east direction. On the other hand, the dominance of P3, P5, P6, and P7 changed the drainage pattern by enhancing oil recovery around reservoir peak area. With a view of streamlines, we can clearly see that the results obtained by streamlines can capture detailed

flow patterns in a sub-grid resolution, while it is difficult to recognize fracture effects on grid (Fig. 4.14).

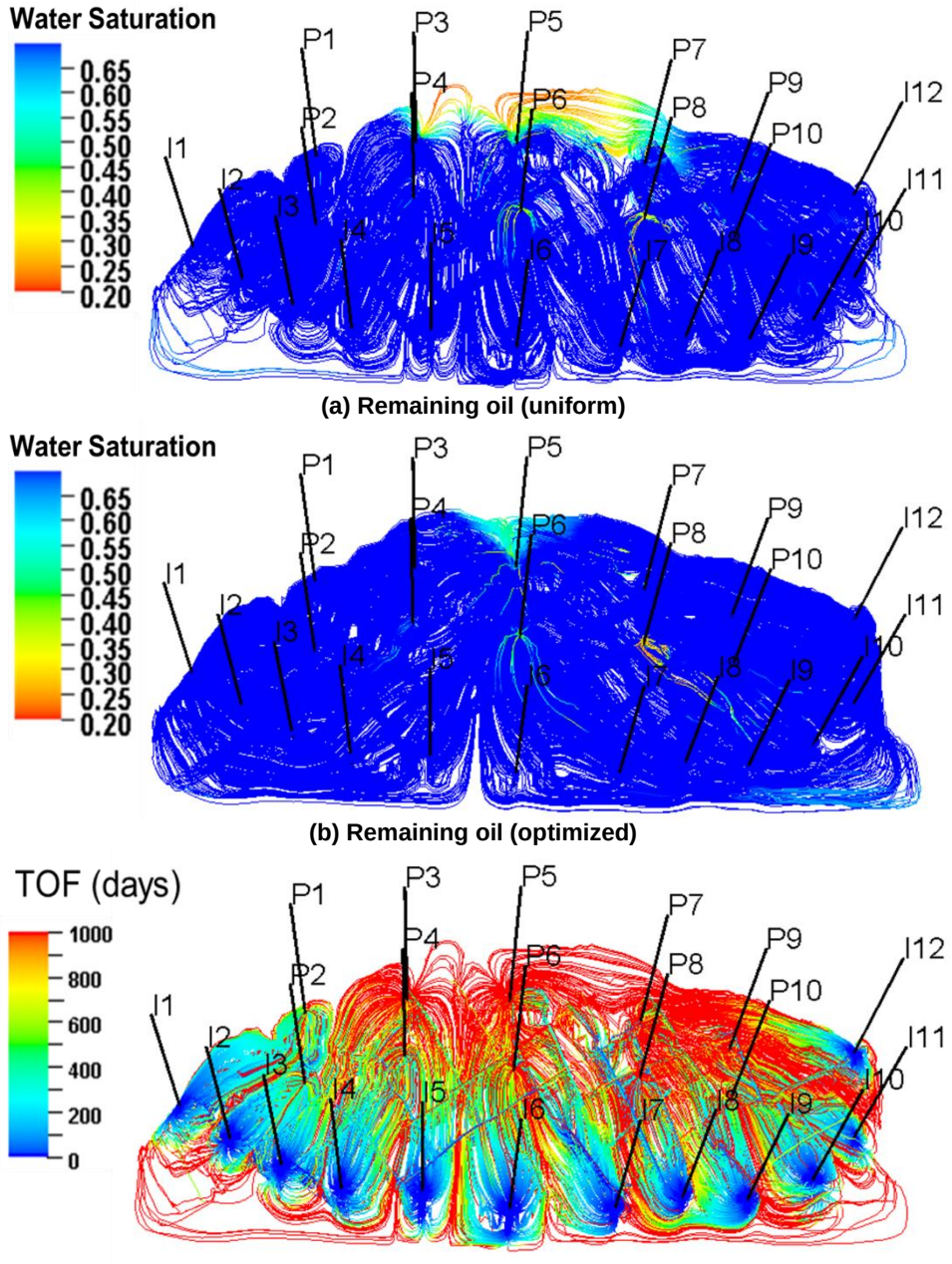

(a) Remaining oil (uniform)

(b) Remaining oil (optimized)

(c) time of flight from injector (uniform)

Figure 4.15: Remaining oil and flow patterns based on streamline (SAIGUP) [4]

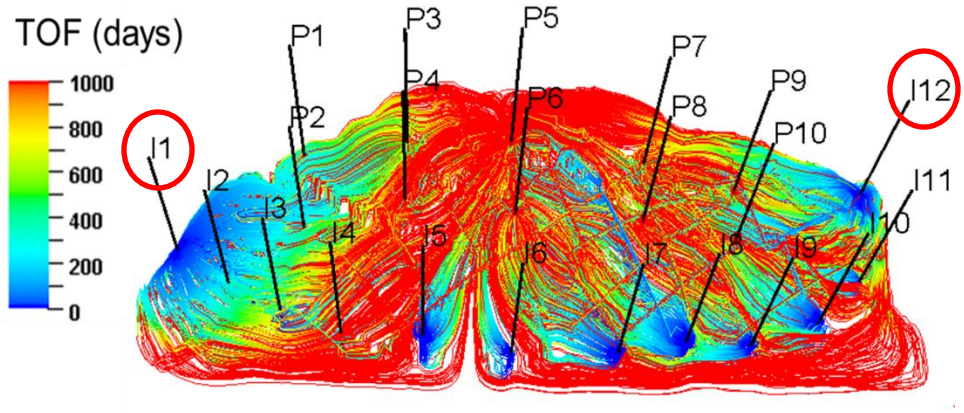

(d) time of flight from injector (optimized)

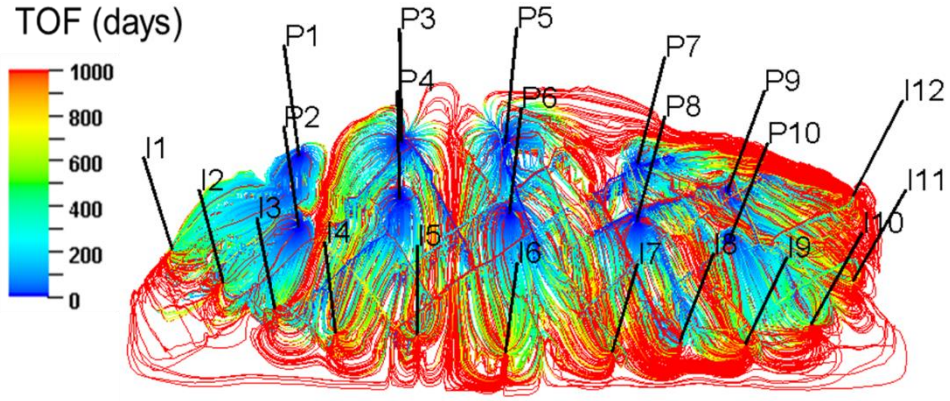

(e) time of flight to producer (uniform)

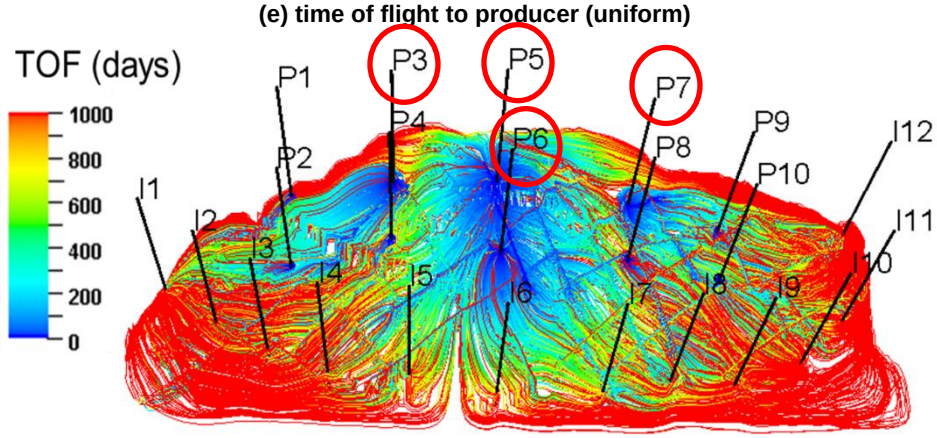

(f) time of flight to producer (optimized)

Figure 4.15 Continued.

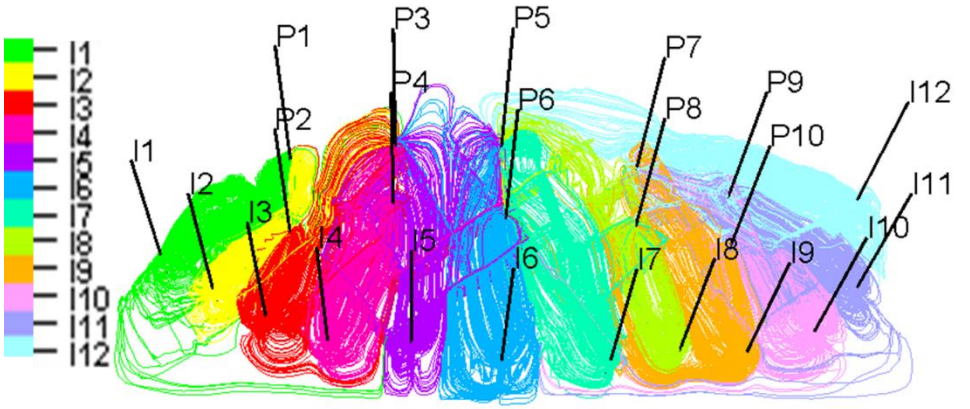

(g) injector partition (uniform)

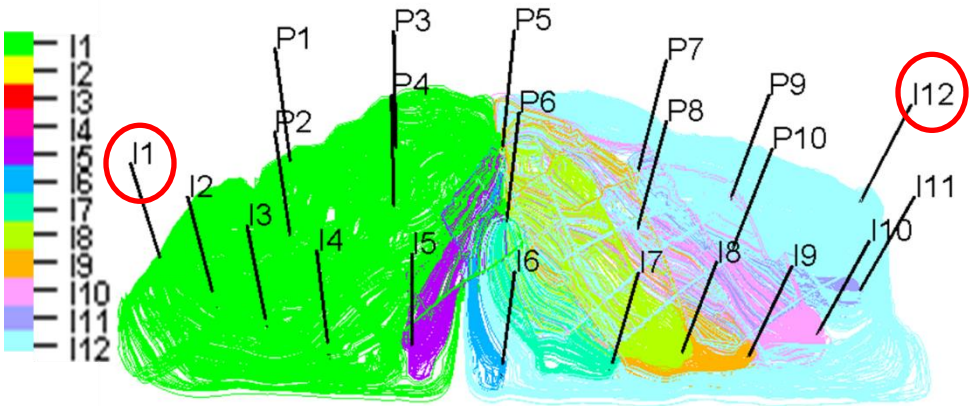

(h) injector partition (optimized)

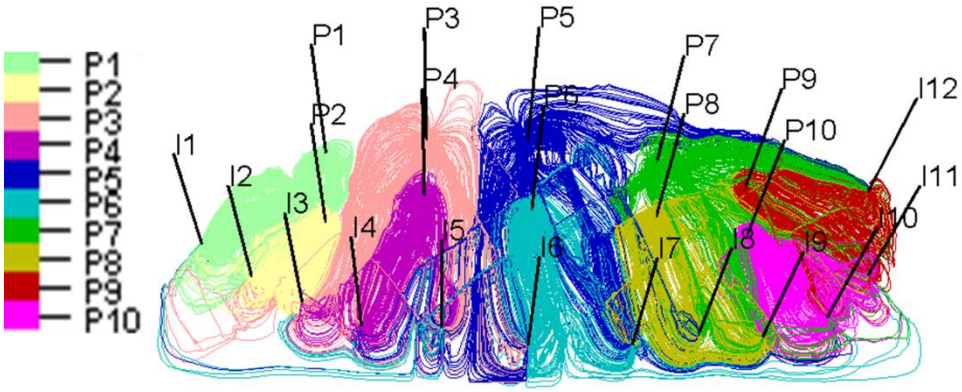

(i) producer partition (uniform)

Figure 4.15 Continued.

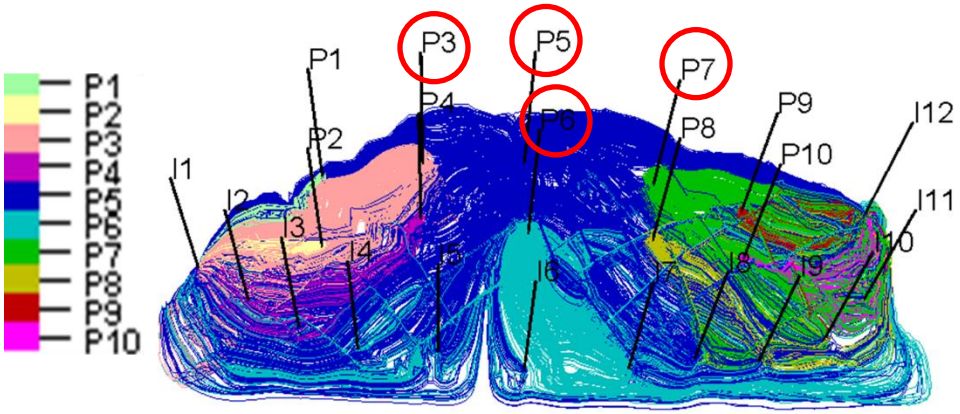

(j) producer partition (optimized)

Figure 4.15 Continued.

4.5 Chapter Conclusions

We have developed a new well rate allocation optimization workflow based on a fast streamline-based oil recovery estimation. The streamline-based oil recovery is estimated using pore volume, oil saturation, and oil formation volume factor along streamlines within a time of flight cutoff. Its advantages against optimization methods of equalizing injection efficiency or equalizing average time of flight to producers is discussed in a synthetic fractured reservoir application. The new method has been successfully applied to a field-scale fractured reservoir, the SAIGUP model. The major findings from this chapter are summarized below.

1. For a fractured reservoir where the permeability field is highly contrasted and well connections are extremely complicated, the novel optimization method outperforms the optimization methods by equalizing injection efficiency or equalizing average time of flight to producers in terms of oil production improvement and water production reduction.
2. The maps of remaining oil and streamline distribution show that the novel optimization method will direct streamlines to cover the oil rich area and thus enhance remaining oil recovery.
3. The field-scale application demonstrates the feasibility of our approach for real rate optimization problems. Regardless of strong heterogeneity created by channelized sedimentary formation, faults, and discrete fractures, the total oil production has been improved by more than 10 percent.

4. The implementation of the rate allocation optimization method is very practical. It interfaces with commercial simulators, Eclipse and CMG, and thus is ready for use for most of the field cases from industry.

CHAPTER V

CONCLUSIONS AND FUTURE WORK

5.1 Conclusions

This study summarized the development and applications of streamline-based flow visualization, history matching, and well rate allocation optimization in fractured reservoirs with complex geometry. In addition to the demonstration of our methods, this study emphasized the applicability of our approaches to the field-scale reservoir models.

First, we have developed the streamline tracing algorithms in fractured reservoirs. The fractured reservoirs were implemented via embedded discrete fracture models. Both faults and fractures in EDFM were realized by non-neighbor connections. Streamlines through non-neighbor connections of faults or discrete fractures were traced by the boundary layer method.

The streamline has been applied to the history matching and the rate allocation optimization problems. The previous studies of streamline-based history matching and well rate allocation optimization have been reviewed and the corresponding limitations are stated. New approaches have been developed and implemented to avoid these limitations, and tested cases showed that the newly proposed approaches and implementations outperform previous methods.

The summary of all the works and findings are listed below.

- The streamline tracing algorithm in EDFM based on the boundary layer method has been successfully implemented. This method can be applied to arbitrary fracture

geometry and fault geometry, and it is generalized for 3D cases. The implementation is validated by comparing the generated streamlines with semi-analytical solutions.

- Comparisons between the semi-analytical method, our tracing method, and the grid-based method with 2D examples suggest that our tracing method outperforms the grid-based method in terms of computational accuracy of time of flight and tracer responses.
- Our method has been applied to the flow diagnostics for a field scale model, SAIGUP reservoir that includes realistic features such as faults, channels, and inactive cells. The results showed how the wells were connected underground in terms of flux allocations from injectors to producers. Streamline maps showed fluid flow through complex geometries of fractures and faults. These diagnostics are also useful to determine when and where to drill additional wells. Through this exercise, we demonstrated the robustness and utility of our streamline-based approach to a field-scale application.
- An amended travel time sensitivity has been proposed for the water cut history matching. A new approach to calculate the streamline-based bottom hole pressure sensitivity in gas reservoirs has also been developed for the bottom hole pressure history matching. The amended travel time sensitivity outperforms the legacy travel time sensitivity in terms of water cut data misfit drop and the sensitivity accuracy, which is judged by taking the perturbation sensitivity as the reference. The novel implementation of bottom hole pressure sensitivity calculation in gas reservoirs was validated by the perturbation sensitivity. The novel sensitivity generated favorable

results in the history matching of bottom hole pressure of a high pressure high temperature tight gas reservoir, which is developed only by primary depletion.

- A novel well rate allocation optimization workflow has been developed to maximize the oil recovery within a certain optimization time window. The novel method can be applied at any point of time in the project life. Its applications in fractured reservoirs showed that the novel method outperforms previously proposed method based on the equalizing injection efficiency and the equalizing the time of flight. It has also been applied to the field-scale SAIGUP model which has high heterogeneity introduced by intersected fractures. The optimized well schedules resulted in improved oil recovery and reservoir sweep.
- In our applications, we coupled the streamline software with commercial simulators. The framework is practical and capable of streamline applications at the field scale.

5.2 Future Work Recommendations

There are several recommendations that can be drawn from this study.

- Now that we have streamlines in fractured models, a further implementation of streamline simulation in embedded discrete fracture models can be done to represent dual porosity dual permeability behavior.
- The embedded discrete fracture model can be further developed to include inclined discrete fractures, which will improve the ability of describing fractured reservoir models.
- The developed history matching and optimization methods need to be applied for more unconventional field scale models to examine the benefits and limitations.
- The streamline-based history matching has been limited to permeability field calibration. For a fractured reservoir, the angel and length of discrete fractures will significantly affect the well response and should also be treated as potential variables for calibration, the corresponding sensitivities for angels and lengths of discrete fractures need to be developed.
- EDFM Streamlines can also be applied to stochastic history matching of fractured reservoirs. For stochastic methods, multiple model realizations will be generated. The simulation of EDFM is still time consuming, and streamlines can be used as an efficient way to rank the geological models.

NOMENCLATURE

A = area, ft^2

B_α = formation volume factor of phase α, $\alpha = o$ or w, *bbl/STB*

BHP = bottom hole pressure, *psi*

c_α = compressibility of phase α, psi^{-1}

c_r = rock compressibility, psi^{-1}

c_t = total compressibility $c_r+S_oc_o+S_wc_w+S_gc_g$, psi^{-1}

c_α = viscosibility of phase α, psi^{-1}

d = observed or calculated data

D = depth, *ft*

e_{ip} = efficiency between injector i to producer p, day

e_f = efficiency of field, day

f_α = fractional flow of phase α, dimensionless

g = gravity acceleration constant, ft/day^2

G = parameter sensitivity matrix

k = absolute permeability, *mD*

k_{fwf} = fracture permeability, *mD*

k_m = matrix permeability, *mD*

$k_{r\alpha}$ = relative permeability of phase α, dimensionless

L = length, *ft*

m = reservoir static property

n_sln = number of streamlines

n_seg = number of segments of one streamline

n_d = number of data observed or calculated, dimensionless

Oil_{sln} = estimated oil recovery along a single streamline *sln*, *STB*

OR_{ip} = estimated oil recovery by injector *i* and producer *p*, *STB*

q_α = volumetric rate of phase α at surface condition, *STB/day*

S_α = saturation of phase α, dimensionless

t = time, day

T = pseudo time of flight, day

V = volume, ft^3

X_I = cell position vector, from current cell to cell *I*, [*ft*, *ft*, *ft*]

X_{fi} = face position vector, from cell center to its face f_i, [*ft*, *ft*, *ft*]

x, y, z = physical space coordinates, *ft*

α, β, γ = unit space coordinates, dimensionless

ρ_α = molar density of phase α, lb/ft^3

ϕ = porosity, dimensionless

λ_α = relative phase mobility of phase, α , cp^{-1}

μ_α = viscosity of phase, *cp*

τ = time-of-flight, *day*

ξ = streamline trajectory

μ_α = viscosity of phase α, *cp*

REFERENCES

Al-Huthali, Ahmed and Datta-Gupta, Akhil. 2004. Streamline simulation of counter-current imbibition in naturally fractured reservoirs. Journal of Petroleum Science and Engineering 43 (3-4): 271-300.

Allan, Jack and Sun, S Qing. 2003. Controls on recovery factor in fractured reservoirs: lessons learned from 100 fractured fields. Proc., SPE Annual Technical Conference and Exhibition.

Bratvedt, F, Gimse, T, and Tegnander, C. 1996. Streamline computations for porous media flow including gravity. Transport in Porous Media 25 (1): 63-78.

Chen, Hongquan, Onishi ,Tsubasa, Olalotiti-Lawal, Feyi, Datta-Gupta, Akhil. 2018. Streamline Tracing and Applications in Naturally Fractured Reservoirs Using Embedded Discrete Fracture Models. In SPE Annual Technical Conference and Exhibition. Society of Petroleum Engineers.

Cheng, Hao, Osako, Ichiro, Datta-Gupta, Akhil et al. 2006. A rigorous compressible streamline formulation for two and three-phase black-oil simulation. SPE Journal 11 (04): 407-417.

Datta-Gupta, Akhil, Alhuthali, Ahmed HH, Yuen, Bevan et al. 2010. Field applications of waterflood optimization via optimal rate control with smart wells. SPE Reservoir Evaluation & Engineering 13 (03): 406-422.

Datta-Gupta, Akhil and King, Michael Joseph. 2007. Streamline simulation: theory and practice, Vol. 11: Society of Petroleum Engineers Richardson.

Di Donato, Ginevra, Huang, Wenfen, and Blunt, Martin. 2003. Streamline-based dual porosity simulation of fractured reservoirs. Proc., SPE Annual Technical Conference and Exhibition.

Du, S., Liang, B., & Yuanbo, L. (2017, October). Field Study: Embedded Discrete Fracture Modeling with Artificial Intelligence in Permian Basin for Shale Formation. In SPE Annual Technical Conference and Exhibition. Society of Petroleum Engineers.

He, Zhong, Yoon, Seongsik, and Datta-Gupta, Akhil. 2002. Streamline-based production data integration with gravity and changing field conditions. Spe Journal 7 (04): 423-436.

Hetz, Gill, Kim, Hyunmin, Datta-Gupta, Akhil et al. 2017. History Matching of Frequent Seismic Surveys Using Seismic Onset Times at the Peace River Field, Canada. Proc., SPE Annual Technical Conference and Exhibition.

Ibrahima, F., Maqui, A., Negreira, A. S., Liang, C., Olalotiti, F., Khebzegga, O. and Zhai, X. (2017). Reduced-Physics Modeling and Optimization of Mature Waterfloods. In SPE Abu Dhabi International Petroleum Exhibition & Conference. Society of Petroleum Engineers.

Idrobo, Eduardo A, Choudhary, Manoj K, and Datta-Gupta, A. 2000. Swept volume calculations and ranking of geostatistical reservoir models using streamline simulation. Proc., SPE/AAPG Western Regional Meeting.

Iino, Atsushi and Arihara, Norio. 2007. Use of streamline simulation for waterflood management in naturally fractured reservoirs. Proc., International Oil Conference and Exhibition in Mexico.

Jessen, K and Orr Jr, FM. 2002. Compositional streamline simulation. Proc., SPE Annual Technical Conference and Exhibition.

Jimenez, E., Datta-Gupta, A., & King, M. J. (2010). Full-Field Streamline Tracing in Complex Faulted Systems With Non-Neighbor Connections. Society of Petroleum Engineers. doi:10.2118/113425-PA

Kam, Dongjae and Datta-Gupta, Akhil. 2016. Streamline-Based Transport Tomography With Distributed Water Arrival Times. SPE Reservoir Evaluation & Engineering 19 (02): 265-277.

Lantz, R. B. (1971). Quantitative evaluation of numerical diffusion (truncation error). SPE Journal, 11(03), 315-320.

Li, Liyong and Lee, Seong H. 2008. Efficient field-scale simulation of black oil in a naturally fractured reservoir through discrete fracture networks and homogenized media. SPE Reservoir Evaluation & Engineering 11 (04): 750-758.

Moinfar, Ali. 2014. Development of an efficient embedded discrete fracture model for 3D compositional reservoir simulation in fractured reservoirs. SPE Journal.

Møyner, O., Krogstad, S. and Lie K.-A. (2015) The application of flow diagnostics for reservoir management. SPE J., Vol. 20, No. 2, pp. 306-323, 2015. DOI: 10.2118/171557-PA

Nakashima, T., Sato, K., Arihara, N., & Yazawa, N. (2000, January). Effective permeability estimation for simulation of naturally fractured reservoirs. In SPE Asia Pacific Oil and Gas Conference and Exhibition. Society of Petroleum Engineers.

Noorishad J, Mehran M. 1982. An upstream finite element method for solution of transient transport equation in fractured porous media. Water Resources Research.

Olalotiti-Lawal, Feyi, Onishi, Tsubasa, Datta-Gupta, Akhil et al. 2017. Post-Combustion CO2 EOR Development in a Mature Oil Field: Model Calibration Using a Hierarchical Approach. Proc., SPE Annual Technical Conference and Exhibition.

Pollock, D. W. (1988). Semianalytical computation of path lines for finite ‐ difference models. Groundwater, 26(6), 743-750.

Prévost, M., Lepage, F., Durlofsky, L. J., & Mallet, J. L. (2005). Unstructured 3D gridding and upscaling for coarse modelling of geometrically complex reservoirs. Petroleum Geoscience, 11(4), 339-345.

Rasmussen, A. F. (2010, September). Streamline tracing on irregular geometries. In ECMOR XII-12th European Conference on the Mathematics of Oil Recovery.

Sato, K., & Abbaszadeh, M. (1996). Tracer flow and pressure performance of reservoirs containing distributed thin bodies. SPE Formation Evaluation, 11(03), 185-193.

Shahvali, M., Mallison, B., Wei, K. and Gross, H. (2012) An alternative to streamlines for flow diagnostics on structured and unstructured grids. SPE Journal, Vol. 17, No. 3, September 2012, pp. 768-778. Doi: 10.2118/146446-PA

Shook, G. M. and Mitchell, K. M. (2009) A robust measure of heterogeneity for ranking earth models: the F Phi curve and dynamics Lorenz coefficient. Paper SPE 124625. SPE Annual Technical Conference and Exhibition, New Orleans, 4-7 October, 2009. Doi: 10.2118/12465-MS.

Stenerud, V.R. and Lie, K.-A. 2006. A Multiscale Streamline Method for Inversion of Production Data. *Journal of Petroleum Science and Engineering* 54 (1–2): 79-92.

Tanaka, S., Kam, D., Datta-Gupta, A., and King, M. J. 2015. Streamline-based History mathing of Arrival Times and Bottom-hole Pressure Data for Multicompnent Compositional Systems. Paper SPE 174750 presented at the SPE Annual Technical Conference and Exhibition, Houston, Texas, 28-30 September. (accepted)

Tanaka, Shusei, Datta-Gupta, Akhil, and King, Michael J. 2013. A novel approach for incorporation of capillarity and gravity into streamline simulation using orthogonal projection. Proc., SPE Reservoir Simulation Symposium.

Tanaka, Shusei; Kam, Dongjae; Xie, Jiang; Wang, Zhiming; Wen, Xian-Huan; Dehghani, Kaveh; Chen, Hongquan; Datta-Gupta, Akhil (2017). A Generalized Derivative-Free Rate Allocation Optimization for Water and Gas Flooding Using Streamline-Based Method. Society of Petroleum Engineers. doi:10.2118/187298-MS

Ţene, M., Bosma, S. B., Al Kobaisi, M. S., & Hajibeygi, H. (2017). Projection-based embedded discrete fracture model (pEDFM). Advances in Water Resources, 105, 205-216.

Thiele, Marco R and Batycky, Rod. 2003. Water injection optimization using a streamline-based workflow. Proc., SPE Annual Technical Conference and Exhibition.

Thiele, MR, Batycky, RP, Blunt, MJ et al. 1996. Simulating flow in heterogeneous systems using streamtubes and streamlines. SPE Reservoir Engineering 11 (01): 5-12.

Vasco, D Wr, Yoon, Seongsik, and Datta-Gupta, Akhil. 1998. Integrating dynamic data into high-resolution reservoir models using streamline-based analytic sensitivity coefficients. Proc., SPE Annual Technical Conference and Exhibition.

Watanabe, Shingo, Han, Jichao, Hetz, Gill et al. 2017. Streamline-Based Time-Lapse-Seismic-Data Integration Incorporating Pressure and Saturation Effects. SPE Journal.

Williams, M.A., Keating, J.F., and Barghouty, M.F. 1998. The Stratigraphic Method: A Structured Approach to History Matching Complex Simulation Models. *SPE Reservoir Evaluation & Engineering* 1 (2): 169-176.

Warren, J., Root, P. 1963. The Behavior of Naturally Fractured Reservoirs. SPE Journal, 3(3), 245-255.

Yang, D., Xue, X., & Chen, J. (2018, April 22). High Resolution Hydraulic Fracture Network Modeling Using Flexible Dual Porosity Dual Permeability Framework. Society of Petroleum Engineers. doi:10.2118/190096-MS

Yin, J., Park, H., Datta-Gupta, A., King, J.M., and Choudhary, M.K. 2010. A Hierarchical Streamline-Assisted History Matching Approach With Global and Local Parameter Updates. Paper SPE 132642 presented at the SPE Western Regional Meeting, Anaheim, California, 27-29 May.

Yin, Jichao, Xie, Jiang, Datta-Gupta, Akhil et al. 2011. Improved characterization and performance assessment of shale gas wells by integrating stimulated reservoir volume and production data. Proc., SPE Eastern Regional Meeting.

Yoon, S., Malallah, A.H., Datta-Gupta, A., Vasco, D.W., and Behrens, R.A. 2001. A Multiscale Approach to Production-Data Integration Using Streamline Models. *SPE Journal* 6 (2): 182-192.

Zhang, Y., King, M. J., & Datta-Gupta, A. (2011). Robust Streamline Tracing Using Intercell Fluxes in Locally Refined and Unstructured Grids. Society of Petroleum Engineers. doi:10.2118/140695-MS

APPENDIX A

USER MANUAL MULTI-PURPOSE SOFTWARE (DESTINY) FOR STREAMLINE TRACING, HISTORY MATCHING AND RESERVOIR MANAGEMENT

A.1 Introduction

This is a manual for streamline-based tool called “DESTINY”. The applications in this dissertation have been carried out using it and all new features of streamline-based visualization, history matching, and rate allocation optimization are implemented. The DESTINY has been developed to incorporate with commercial simulators such as Eclipse and CMG. Here, I briefly show how it works and introduce function modules of this software. There is a graphical user interface developed for this tool to generate an input deck to direct executable runs. The keywords and format of input deck are explained here.

A.2 Overview of DESTINY

Figure A.1 shows the DESTINY workflow. It is coordinated with commercial software of Eclipse, CMG, Petrel and Excel VBA. Destiny calls Eclipse or CMG for forward simulations, fetches the information needed for streamline tracing from the simulation results, and traces streamlines.

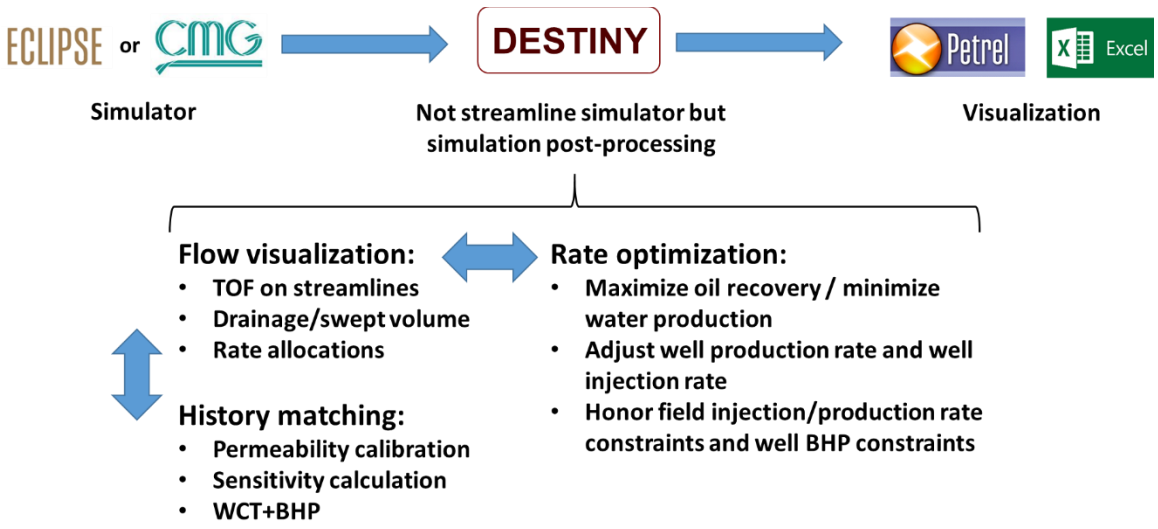

Figure A.1: Overview of DESTINY working environment

The streamlines will then be used for three major purposes: flow visualization, history matching, and rate optimization. Petrel and Excel are used as visualization tools of streamlines and related analytic plots.

Following are some distinctive features of this tool:

- Flow visualization and flood analysis based on industry standard flow simulators
- Streamline based calibration of geological models to BHP and WCT
- Streamlines in a dual porosity dual permeability system via Embedded Discrete Fracture Model

- Gradient free rate allocation optimization for maximizing oil recovery
- User-friendly visualization tools based on Petrel and Excel VBA macros

A.3 Structure of input data

DIP file is an input file for DESTINY where we enter keywords to direct the executions of the software. This section demonstrates keywords sections and gives details about each keyword in input file.

There are 5 keywords sections: simulator, tracing, inversion, output, and rate optimization. The first 4 sections are written in Destiny6.DIP, and the optimization section is written in D6_RateOpt.DIP.

Simulator

The simulator section starts with keyword

SIMULATOR_SET

It is followed by 5 records. And the optional values for each record is given as below.

1. Simulator name: use eclipse, e300, or imex
2. Simulation input deck file name: such as eclipse_model.DATA or imex_model.dat
3. Simulation run control: use RUN or STOP
4. Restart file prefix [optional]: a string of restart file name without file name extension
5. Parallel number [optional]: an integer to indicate how many cores to be used for a forward simulation

Tracing

The tracing section starts with keyword

TRACING_SET

It is followed by 3 records. And the optional values for each record is given as below.

1. Binary files prefix: the binary files refer to the simulation restart files that store the information needed for tracing. If Eclipse is used, its restart files share the same file name prefix with the input deck file; if CMG is used, its restart file prefix may be different than the input deck file name, and needs to be specified accordingly.
2. Tracing mode: streamlines can be traced from either producers or injectors, or from both. This record value can be PRO, INJ, or PRO|INJ.
3. Tracing phase: the streamlines can be traced with single phase flux or the total flux, the record value can be OIL, WAT, GAS, or FLUID

TRACING_STEPS

This keyword is followed by arbitrary number of integer records. The integers defines the simulation steps to be used for streamline tracing. If no record is there, the flow visualization module is turned off. If a record of -1 is followed, all the simulation steps will be used for streamline tracing.

SLN_NUMBER

This keyword is optional. It defines the total number of streamlines to trace. If it is not present, the streamline number is automatically optimized by the software itself.

Inversion

The inversion section starts with keyword

INVERSION_SET

It is followed by 5 records. And the optional values for each record is given as below.

1. Maximum iteration number: an integer defines the maximum number of inversion iterations. If it is none positive, the history matching module is turned off.
2. History matching terms: a string defines which well responses will be considered in the history matching objective function. Its value can be WCT, BHP, or WCT|BHP. The last option will do water cut and bottom hole pressure history matching simultaneously.
3. Damping coefficient: the weighting factor for norm constraint in the objective function (Eq. 3.2). Its value ranges in [0.0, 1.0].
4. Horizontal smoothing coefficient: the weighting factor for the horizontal roughness penalty in the objective function (Eq. 3.2). Its value ranges in [0.0, 1.0].

5. Vertical smoothing coefficient: the weighting factor for the vertical roughness penalty in the objective function (Eq. 3.2). Its value ranges in [0.0, 1.0].

Output

The output section starts with keyword

OUTPUT_SET

It is followed by 11 records. And the optional values for each record is given as below. The first record define the file format for streamline files. And the next 10 records are buttons to indicate whether to output specific information, 0 for no output, and 1 for output.

1. Streamline file format: a string to define which file format is used to store streamlines. Its value can be BINARY, ASCII, and BINARY|ASCII. The binary file format is the same as Petrel streamline binary format, and streamline information is stored in .SLNSPEC file and .SLN#### files
2. Button 1: streamlines in either binary or ASCII format, or both, according to first record
3. Button 2: time of flight on grid blocks in .grdecl file
4. Button 3: partition by wells on grid blocks in .grdecl file
5. Button 4: partition by completion cells on grid blocks in .grdecl file
6. Button 5: well pair rate allocations and injection efficiencies in .csv file
7. Button 6: diffusive time of flight on grid blocks in .grdecl file

8. Button 7: flow capacity map for gas field infill well suggestion in .grdecl file
9. Button 8: dynamic measure map for oil field infill well suggestion in .grdecl file
10. Button 9: well responses in .csv file
11. Button 10: streamline-based sensitivities on grid blocks in .grdecl file

Rate Optimization

The rate optimization section is written in an independent file D6_RateOpt.DIP. Its keywords are listed as below.

OR_OBJ

It is follow by one bool record. If it is true, the objective function is set to maximize the oil recovery estimated by streamline within the total optimization time. If false, this objective function is dismissed.

IE_OBJ

It is follow by one bool record, if it is true, the objective function is set to equalize the injection efficiency. If false, this objective function is dismissed.

TOF_OBJ

It is follow by one bool record, if it is true, the objective function is set to equalize the average time of flight to producer. If false, this objective function is dismissed.

PROD_OPT

If present, rate allocation for producers list in PRODUCERS keyword will be adjusted every optimization step.

INJ_OPT

If present, rate allocation for injectors list in INJECTORS keyword will be adjusted every optimization step.

PRODUCERS

It is followed by 2 columns of records. The first column is the name of producers, the second column defines whether the producer's well scheme can be changed.

INJECTORS

It is followed by 2 columns of records. The first column is the name of injectors, the second column defines whether the injector's well scheme can be changed.

FIELD_PROD_RATE

It is follow by one floating number record whose value defines the field production rate constraint.

NUM_TIME_STEP

It is follow by one integer number record whose value defines the total number of optimization step.

TIME_INTERVAL

It is follow by one floating number record whose value defines the elapsed time for each optimization step.

SINGLE_STEP_ITER_MAX

It is follow by one integer number record whose value defines the maximum number of well rate adjustment iterations within a single optimization step.

FIELD_INJ_RATE

It is follow by one floating number record whose value defines the field injection rate constraint.

MAX_PROD_RATE

It is follow by one floating number record whose value defines the maximum production rate constraint for each producer.

MIN_PROD_RATE

It is follow by one floating number record whose value defines the minimum production rate constraint for each producer.

MAX_INJ_RATE

It is follow by one floating number record whose value defines the maximum injection rate constraint for each injector.

MIN_INJ_RATE

It is follow by one floating number record whose value defines the minimum production rate constraint for each injector.

MAX_RATE_CHANGE

It is follow by one floating number record whose value defines the maximum relative well rate change between two adjacent optimization intervals.

APPENDIX B

THE PREPROCESSOR IMPLEMENTATION FOR EMBEDDED DISCRETE FRACTURE MODELS

Here we present details of the preprocessor for embedded discrete fracture models (EDFMs). In the EDFM approach, fractures are explicitly described in a separate computational domain as 2D planes in addition to the matrix domain. Fractures will be discretized by the cell boundaries in the matrix domain. The discretized fracture grid blocks are then linked with corresponding matrix grid blocks via non-neighbor connections (NNCs), which define additional connections between any grid blocks in finite-difference/volume framework. In our preprocessor, the workflow consists of four steps:

B.1 Matrix domain

First, we need to prepare initial ECLIPSE data sets for the matrix domain, and then run ECLIPSE with NOSIM keyword and generate necessary files (INIT, GRID/EGRID, and .X0000). Grid geometry and final matrix permeabilities within the binary files will be exported as input for the preprocessor.

B.2 Fracture domain

We have a separate external file (EDFM.DATA) in which we specify inputs for fractures. Specifically, we input starting point, angle, length, aperture, and thickness for each fracture. This external file is also an input for the preprocessor.

B.3 Assign NNCs and compute corresponding transmissibilities

Based on the grid geometry, matrix permeabilities, and fracture permeabilities, the preprocessor computes NNCs and corresponding transmissibilities (Li and Lee, 2008), which will be printed in an external file (EDFM_NNC.GRDECL).

B.4 Update the original ECLIPSE data sets

Based on the ECLIPSE data sets that we used for the matrix domain, the preprocessor updates the grid related properties in the data sets. Specifically, grid dimensions will be updated for the additional control volumes (fractures) and also NNCs and transmissibilities will be included in the grid section to perform simulations with embedded discrete fractures. Additional region number will be assigned to the fracture grid blocks, and additional saturation tables describing relative permeabilities and capillary pressures for the fracture media will be added to the original data sets.

B.5 Examples

We have 3 examples to demonstrate our implementation (**Tab B.1** and **Fig. B.1**). A simple 5x5x1 grid is used for the matrix domain.

The first example is the simplest case in which we have a single fracture discretized in 3 grid blocks (**Fig. B.1 (a)**). The grid dimension is updates as 5x7x1. Here we have inactive grid blocks at 6^{th} row (J=6) to avoid improper connections between fracture grid blocks and active matrix grid blocks in 5^{th} row. Also, grid blocks except for the fracture

grid blocks in the 7th row (I,J,K=4,7,1 and 5,7,1) are inactivated as they will not be used in the simulation. The fracture grid blocks are connected with matrix grid blocks using NNCs as illustrated in **Fig. B.1 (a)** and the number of active grid blocks is 28 (=25 for matrix + 3 for fracture grid blocks).

The second example has two horizontal fractures. Each fracture has the same geometry as the fracture in example 1. The grid dimension is updated as 5x9x1. The 6th row and 8th row are inactive grid blocks, and grid blocks other than fractures in the 7th and 9th rows are also inactive. NNCs are used to describe fracture-matrix connections (**Fig. B.1 (b)**). The number of grid blocks in this case is 31 (=25 for matrix + 2x3 for two fractures). As seen in these two examples, we expand grid dimension in J direction depending upon the number of fractures. It is informative to mention that we need special treatments for a long fracture. That is, as a result of discretization, the number of grid blocks for a long fracture may exceed NX. In such cases, we expand J-direction further (+2) for the long fracture and separate them, then connect edges of the separated fracture using an additional NNC as illustrated as a red arrow in **Fig. B.2**.

The third example is similar to the second example except for a fracture intersection. Here we have a fracture-fracture NNC (red colored in **Fig B.1(c)**) in addition to NNCs for fracture-matrix, and the number of grid blocks is 33 (=25 for matrix + 3 for fracture1 + 5 for fracture2).

Table B.1: List of example cases and their grid information

	Grid Dimension (original=5x5x1)			#Active Grid blocks (original=25)	NNCs (matrix-fracture)	NNCs (fracture - fracture)
	NX	NY	NZ			
Case 1	5	7	1	28	3	0
Case 2	5	9	1	31	6	0
Case 3	5	9	1	33	6	1

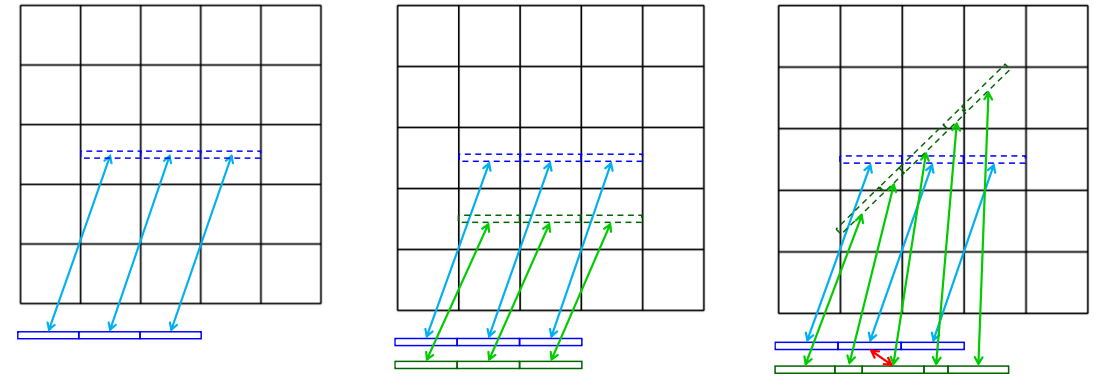

(a) Case 1: One horizontal fracture

(b) Case 2: Two horizontal fractures

(c) Case 3: Two intersecting fractures

Figure B.1: Illustration of EDFM examples

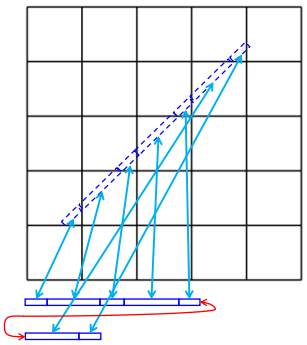

Figure B.2: Illustration of the treatment for a long fracture